Electronic Supplementary Material (ESI) for ChemComm.

Steric Control of Sorting Regimes in Self-Assembled Cages

Samuel E. Walker,[a] Stephanie A. Boer,[a,b] Thomas Malcomson,[c] Martin J. Paterson,[d] Kellie L. Tuck [a] and David R. Turner *[a]

[a] School of Chemistry, Monash University, Clayton, VIC 3800, Australia.

[b] Australian Synchrotron, ANSTO, 800 Blackburn Road, Clayton, VIC 3168, Australia.

[c] Department of Chemistry, Manchester University, Manchester, M13 9PL, United Kingdom.

[d] Institute of Chemical Sciences, Heriot-Watt University, Edinburgh, EH14 4AS, United Kingdom.

Supporting Information

Materials and instrumentation

Reagents were purchased from commercial vendors and used as received, with no further purification. Ligands H_2**G** and H_2**L** were synthesised as previously reported and H_2**I**, H_2**A** and H_2**V** were synthesised using a similar method.[1]

^{1}H and ^{13}C{^{1}H} NMR spectra were recorded at 298 K on a Bruker Avance III NMR spectrometer equipped with a 14.1 T magnet and 5 mm TCI cryoprobe, operating at 600.27 MHz (^{1}H) and 92.15 MHz 150.95 MHz (^{13}C). Chemical shifts (δ) are reported in ppm and were referenced to the residual solvent.

Measurement was performed by the Monash Analytical Platform using an Agilent 6540 UHD Accurate Mass Q-TOF fitted with an Agilent Jet Stream Source. ESI conditions were optimised to obtain the best signal; N_2 drying gas at 300 °C and flow rate of 10 L/min, nebuliser 45 psi, sheath gas temperature 350 °C, 10 L/min, capillary voltage 3000 V, nozzle voltage 1300 V, and fragmentor voltage 100 V, and skimmer 65 V.

HPLC was performed on an Agilent Infinity 1220 LC using an Agilent C18 column of 3.9 x 150 mm dimensions with 5 µm particle size at a flow rate of 1 mL/minute of 100% acetonitrile. The output was measured at wavelengths of 220, 254 and 280 nm and the data were processed with Agilent Open Labs CDS Chemstation Editor software.

Circular dichroism (CD) spectra were collected in the range 200-350 nm at room temperature using a Jasco J-815 circular dichroism spectrophotometer. Spectra were obtained at a scan rate of 100 nm min^{-1} using a bandwidth of 1 nm and a D.I.T of 2 s.

Synthesis of ligands

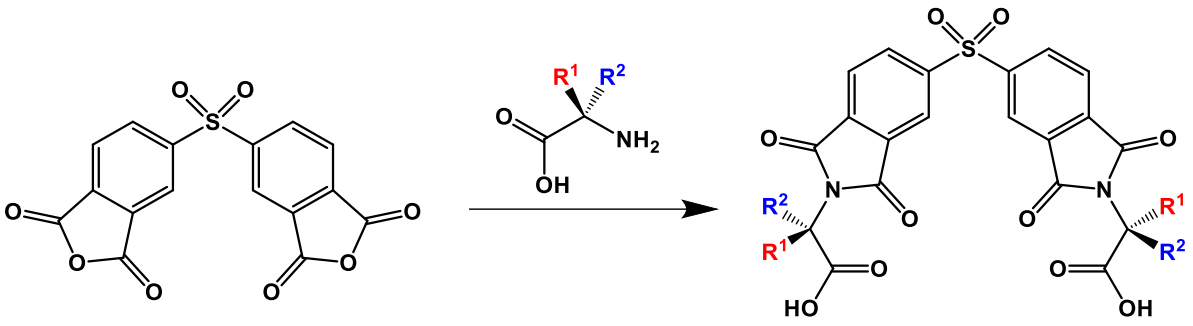

H_2**G**: $R^1 = R^2 = H$
H_2**I**: $R^1 = R^2 = CH_3$
H_2**A**: $R^1 = H$, $R^2 = CH_3$
(S)-H_2**L**: $R^1 = H$, $R^2 = CH_2CH(CH_3)_2$
(*R*)-H_2**L**: $R^1 = CH_2CH(CH_3)_2$, $R^2 = H$
H_2**V**: $R^1 = CH(CH_3)_2$, $R^2 = CH_3$

Scheme S1. – General synthetic scheme for the formation of the ligands used throughout. The dianhydride species is reacted with an excess of amino acid to form the diimide ligands.

*Synthesis of H_2**G**, (S)-H_2**L** and (R)-H_2**L***

Prepared using previously recorded procedure.[1]

*Synthesis of H_2**I***

3,3',4,4'-diphenylsulfone tetracarboxylic dianhydride (220 mg, 0.61 mmol) and 2-aminoisobutyric acid (158 mg, 1.54 mmol, 2.5 eq) were dissolved in 20 mL glacial acetic acid. The mixture was heated at 100 °C for 48 hours before being added dropwise over ice. The white precipitate was collected *via* vacuum filtration and washed with copious DI water to give a white solid, yield 0.18 g, 63 %. ^{1}H NMR (600 MHz, DMSO-d_6) δ 1.70 (s, 12H), 8.07 (d, J = 7.9 Hz, 2H), 8.49 (d, J = 1.5 Hz, 2H), 8.53 (dd, J = 7.9, 1.6 Hz, 2H), 12.98 (s, 2H). ^{13}C NMR (151 MHz, DMSO-d_6) δ 24.55, 60.74, 122.90, 125.04, 132.94, 134.82, 136.04, 145.74, 166.76, 166.90, 174.01. ESI MS (negative) 527.0755, predicted H**I**$^-$ 527.0760.

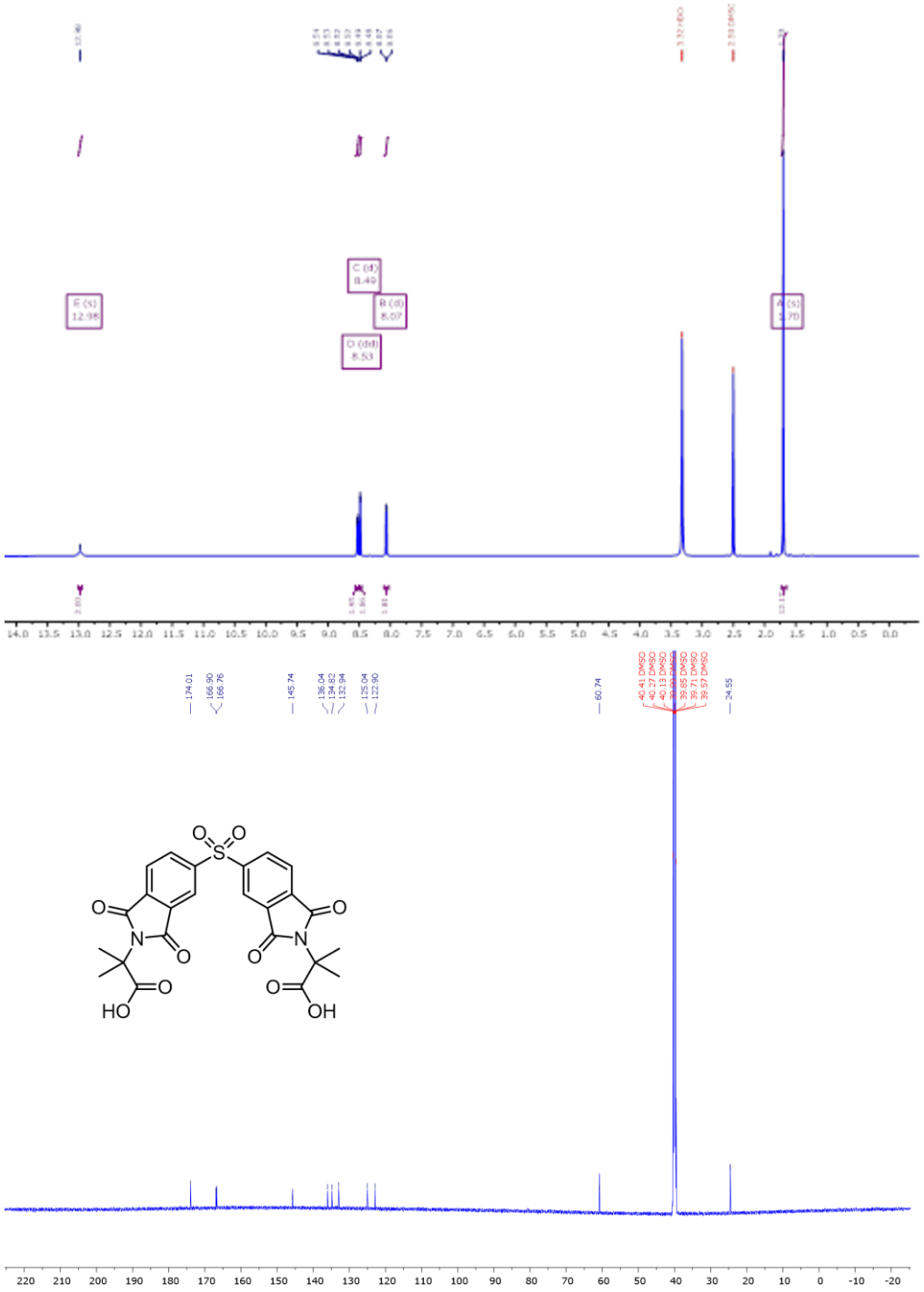

Figure S1. – ^{1}H and ^{13}C NMR spectra of H_2**I**.

*Synthesis of H_2**A***

3,3',4,4'-diphenylsulfone tetracarboxylic dianhydride (1.00 g, 2.79 mmol) and L-alanine (1.43 g, 6.98 mmol, 2.5 eq) were dissolved in 20 mL glacial acetic acid. The mixture was heated at 100 °C for 48 hours before being added dropwise over ice. The white precipitate was collected *via* vacuum filtration and washed with copious DI water to give a white solid, yield 1.45 g, 75.9 %. ^{1}H NMR (600 MHz, DMSO-d_6) δ 1.52 (d, *J* = 7.3 Hz, 6H), 4.89 (q, *J* = 7.3 Hz, 2H), 8.12 (dd, *J* = 7.7, 0.9 Hz, 2H), 8.54 – 8.59 (m, 4H), 13.12 (s, 2H). ^{13}C NMR (151 MHz, DMSO-d6) δ 15.06, 47.85, 123.28, 125.33, 133.14, 134.98, 136.18, 145.82, 165.93, 166.10, 171.15. ESI MS (negative) 499.0311, predicted H**A**$^{-}$ 499.0447.

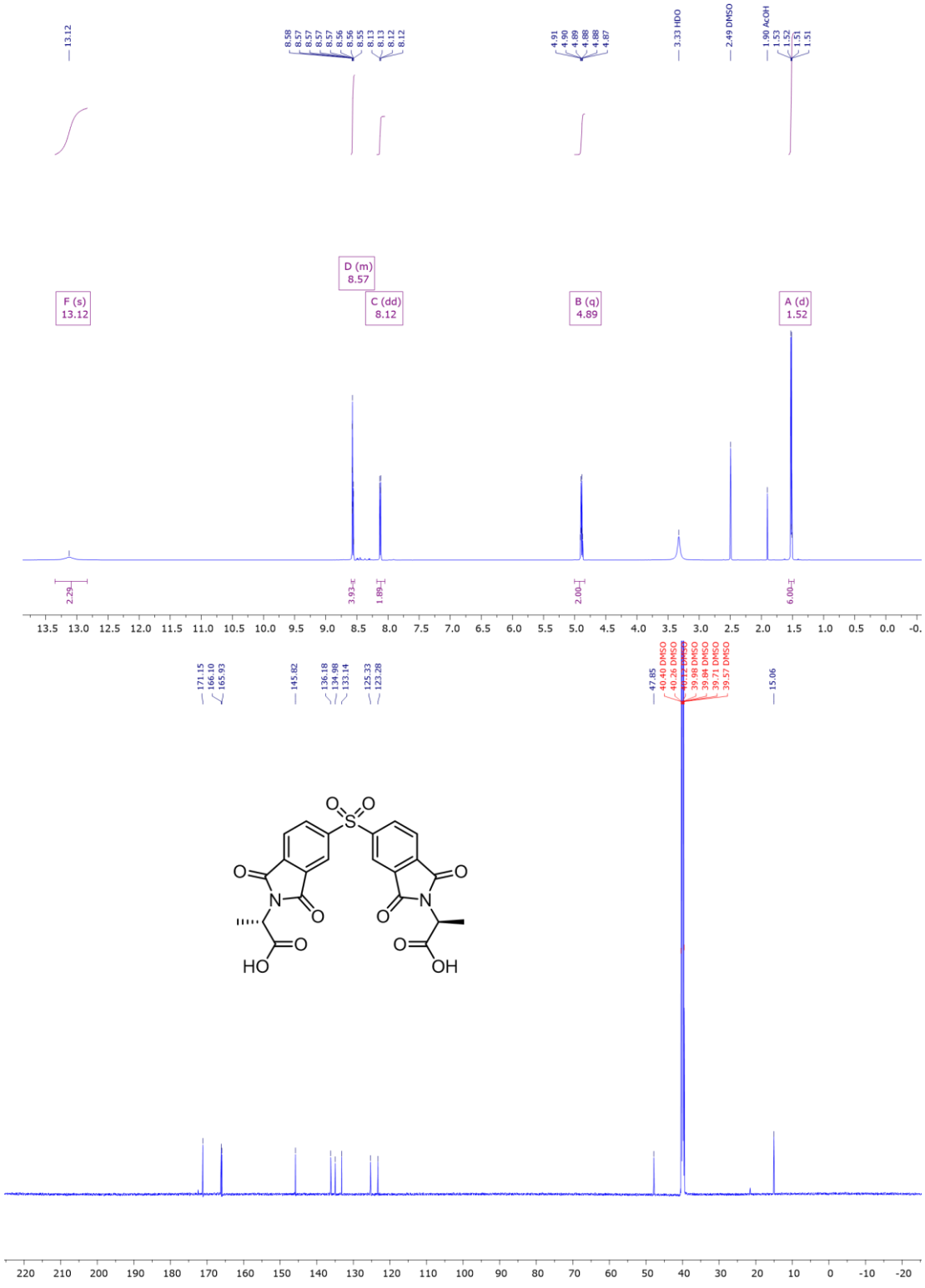

Figure S2. – The ^{1}H and ^{13}C NMR spectra of H_2**A**.

*Synthesis of H_2**V***

3,3',4,4'-diphenylsulfone tetracarboxylic dianhydride (220 mg, 0.61 mmol) and L-α-methyl valine (200 mg, 1.54 mmol, 2.5 eq) were dissolved in 20 mL glacial acetic acid. The mixture was heated at 100 °C for 48 hours before being added dropwise over ice. The white precipitate was collected *via* vacuum filtration and washed with copious DI water to give a white solid, yield 60 mg, 17 % (unoptimised). ^{1}H NMR (600 MHz, DMSO-d_6) δ 0.88 (d, J = 6.9 Hz, 6H), 0.99 (d, J = 6.7 Hz, 6H), 1.65 (s, 6H), 2.81 (hept, J = 6.8 Hz, 1H), 8.07 (d, J = 7.9 Hz, 2H), 8.48 (d, J = 1.5 Hz, 2H), 8.54 (dd, J = 7.9, 1.6 Hz, 2H), 12.98 (s, 2H). ^{13}C NMR (151 MHz, DMSO-d6) δ 18.58, 18.82, 20.17, 32.64, 67.18, 123.04, 125.10, 132.69, 134.91, 135.74, 145.78, 167.04, 167.22, 172.10. ESI MS (negative) 583.1403, predicted H**V**$^{-}$ 583.1386.

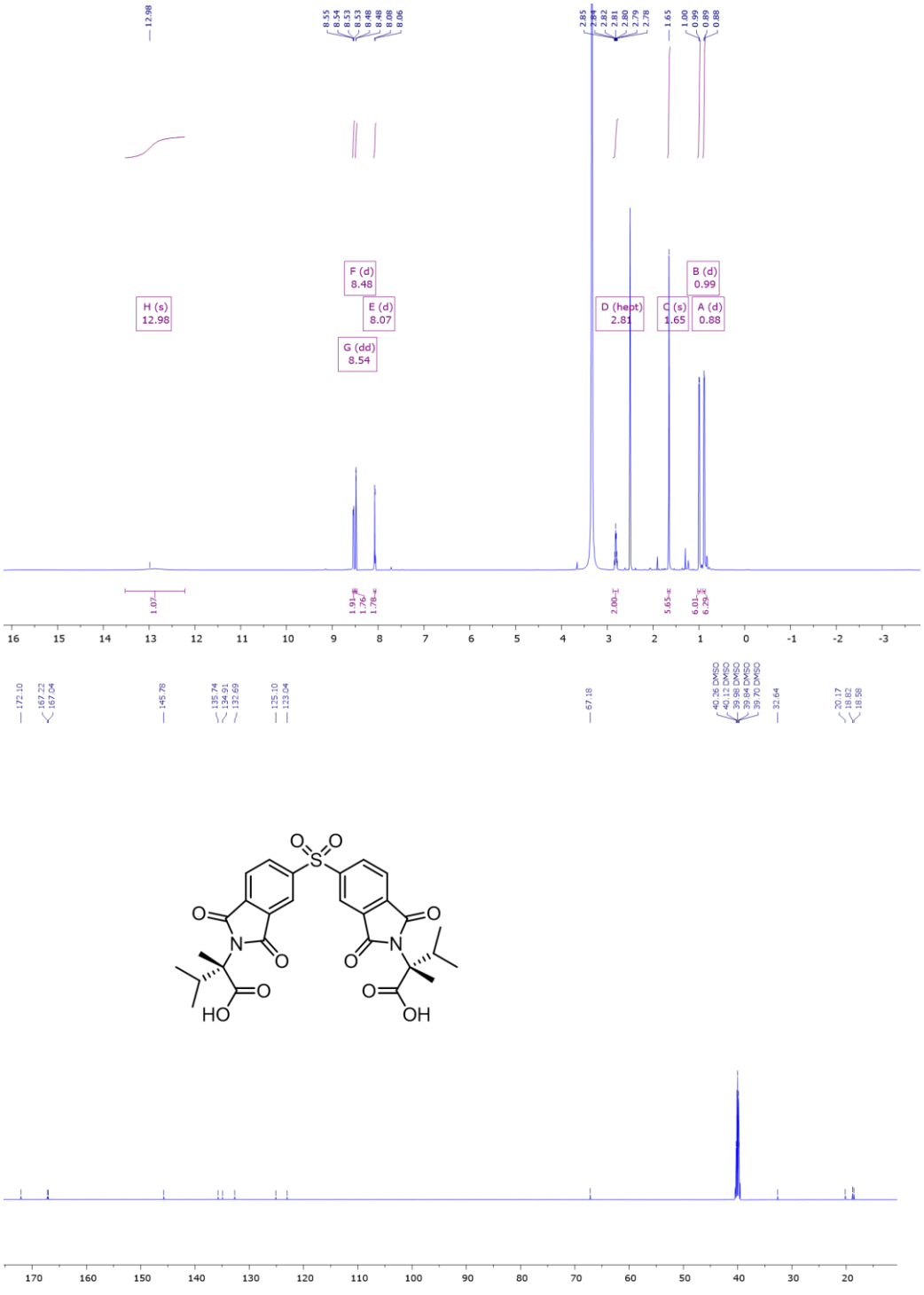

Figure S3. – The ^{1}H and ^{13}C NMR spectra of H_2**V**.

Synthesis of homoleptic coordination cages

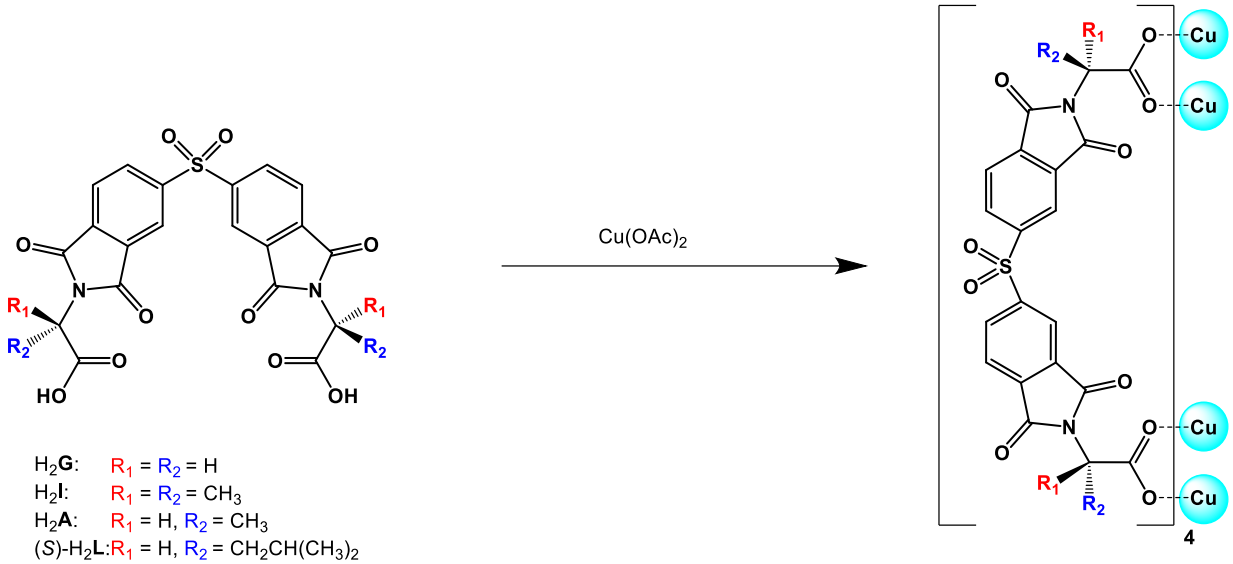

H_2**G**: $R_1 = R_2 = H$
H_2**I**: $R_1 = R_2 = CH_3$
H_2**A**: $R_1 = H$, $R_2 = CH_3$
(*S*)-H_2**L**: $R_1 = H$, $R_2 = CH_2CH(CH_3)_2$
(*R*)-H_2**L**: $R_1 = CH_2CH(CH_3)_2$, $R_2 = H$

Scheme S2. - The five homochiral ligands react with copper(II) acetate in either acetonitrile and dimethylacetamide (H_2**G**, H_2**I**, H_2**V**) or 100% acetonitrile (H_2**A**, (*S*)-H_2**L**), (*R*)-H_2**L**) to form homoleptic coordination cages with two copper paddlewheel nodes linked by four ligands.

Synthesis of ***G*$_4$**

H_2**G** (70 mg, 0.149 mmol) is dissolved in 1 mL dimethylacetamide, and $Cu(OAc)_2$ (27 mg, 0.075 mmol) dissolved in 5 mL acetonitrile. 160 µL of the H_2**G** solution is added to 800 µL of the $Cu(OAc)_2$ solution, and the solution made up to 6 mL with acetonitrile. Analysis by HPLC and mass spectrometry (see Figure S4) after addition of the ligand to the metal shows immediate complexation to form the **G**$_4$ complex as a 1 mM solution (quantitative yield).

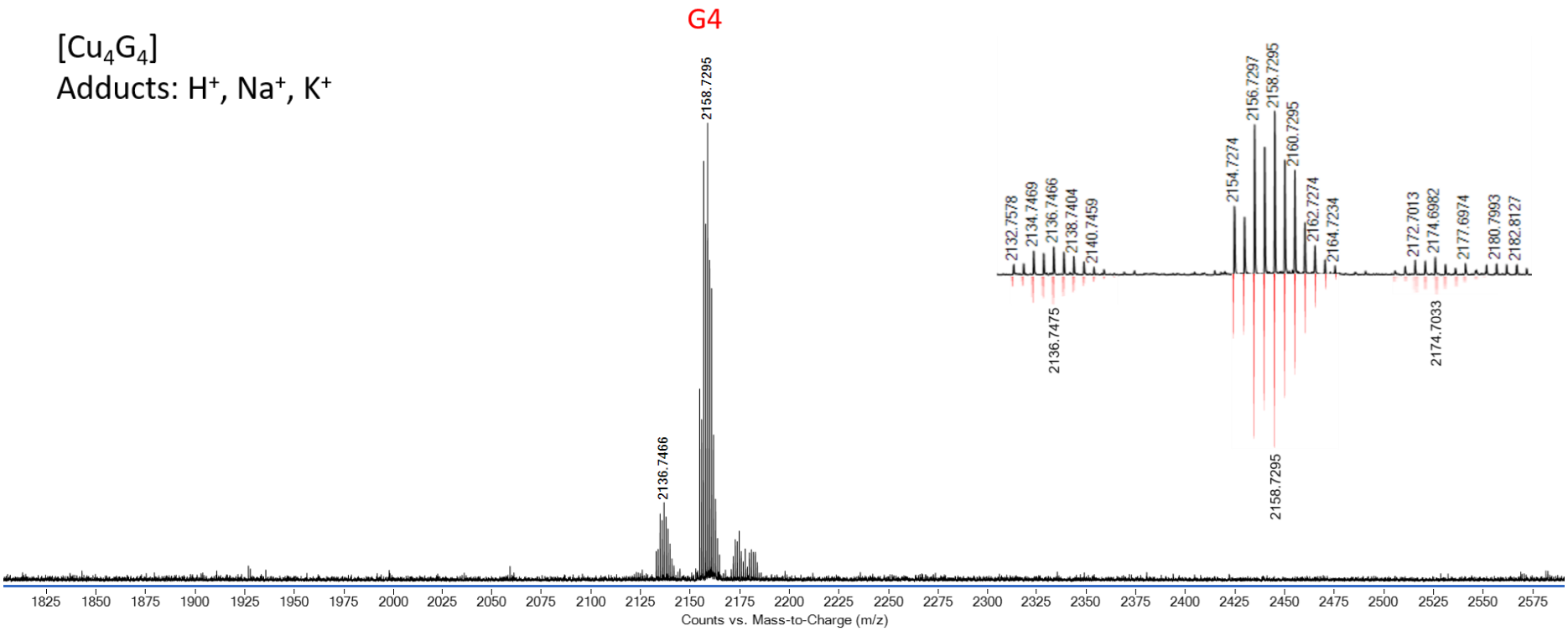

Figure S4. – MS analysis of the reaction mixture of H_2**G** with copper(II) acetate gave rise only to signals originating from **G**$_4$ as the H^+, Na^+ and K^+ adduct. Inlaid is a zoom of the three signals corresponding to the three adducts, with the matching predicted isotope patterns displayed in red.

Synthesis of $\mathbf{I_4}$

$H_2\mathbf{I}$ (79 mg, 0.149 mmol) was dissolved in 1 mL dimethylacetamide, and $Cu(OAc)_2$ (27 mg, 0.075 mmol) dissolved in 5 mL acetonitrile. 160 µL of the $H_2\mathbf{I}$ solution was added to 800 µL of the $Cu(OAc)_2$ solution, and the solution made up to 6 mL with acetonitrile. Analysis by HPLC after addition of the ligand to the metal shows immediate complexation to form the $\mathbf{I_4}$ complex, in an approximately 34% yield. Mass spectrometry was used to confirm the presence of the species in solution (Figures S5-12.) and SCXRD analysis provided clear evidence of the coordination cage formation of $\mathbf{I_4}$. Crystallisation was achieved after 3 days of 1 mL of the above described reaction mixture sitting at room temperature, yielding large clear blue cubic crystals.

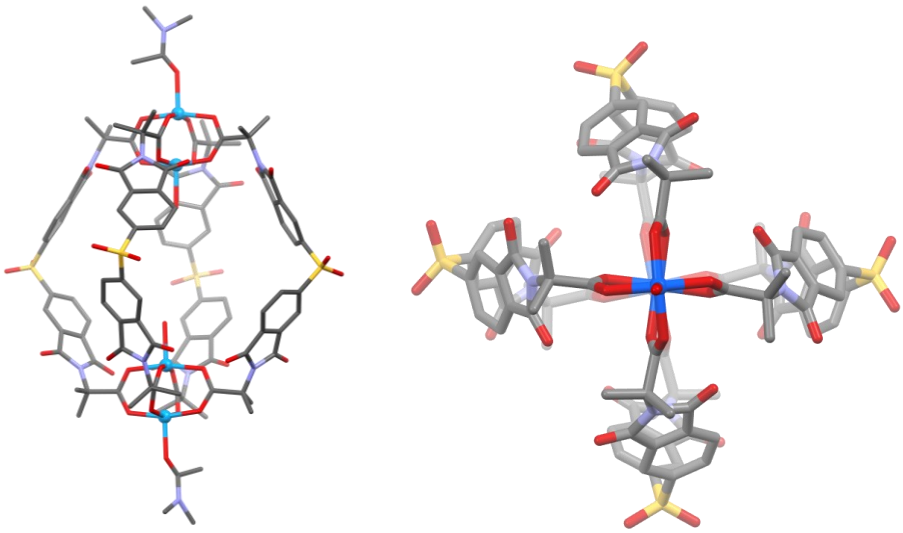

Figure S5. – The molecular structure of $[Cu_4\mathbf{I_4}(H_2O)(DMA)_3]\cdot MeCN$ ($\mathbf{I_4}$) as determined by X-ray crystallographic studies. Left: Four of ligand **I** link the two Cu_2 paddlewheel nodes to form the lantern-type cage architecture. Right: Looking along the Cu_2 – Cu_2 axis shows the mesocate conformation that this species takes due to the lack of chiral functionalities to drive formation of a helicate.

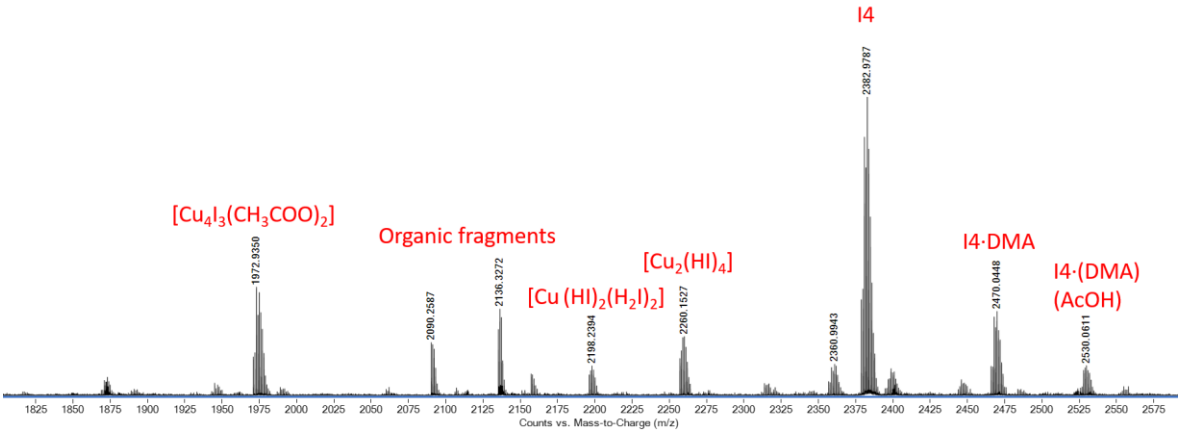

Figure S6. - MS analysis of the reaction mixture of H_2**I** with copper(II) acetate gave rise to signals originating **I**$_4$ as the H^+, Na^+ and K^+ adducts and smaller, partially formed fragments of **I**$_4$.

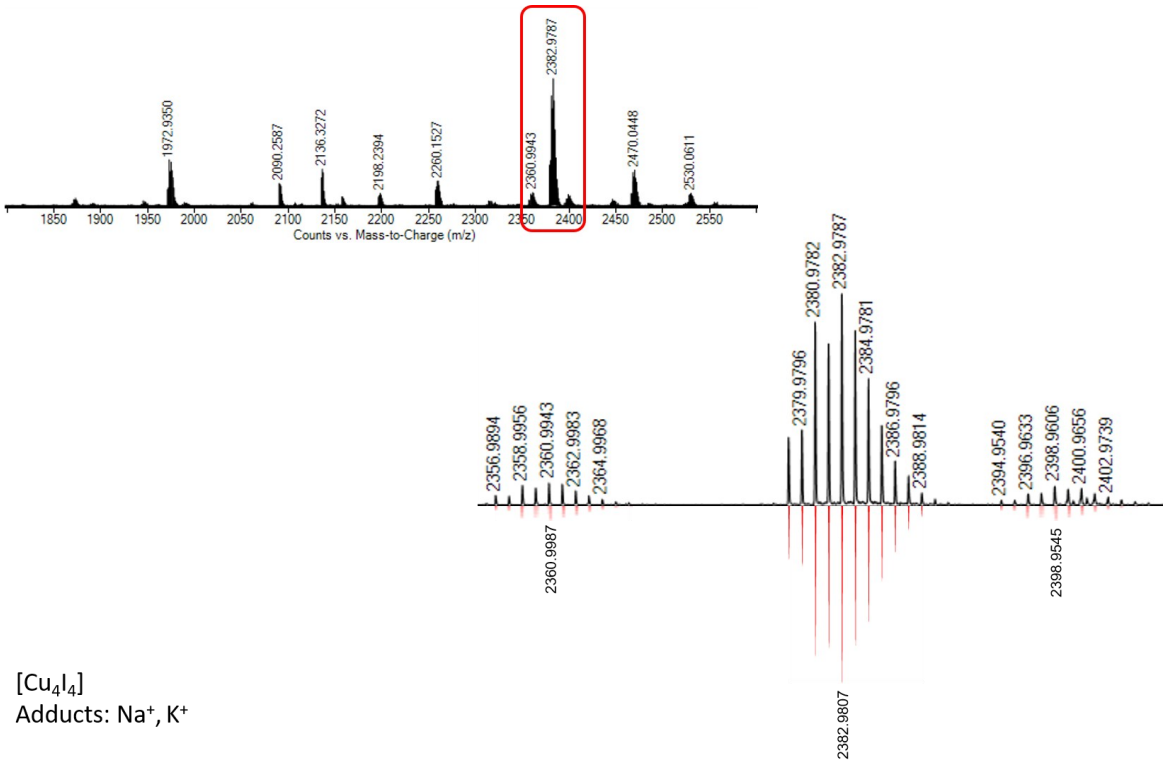

Figure S7. – A zoom of the three signals in the MS analysis of the reaction mixture of H_2**I** with copper(II) acetate that originate from **I**$_4$ as the H^+, Na^+ and K^+ adducts.

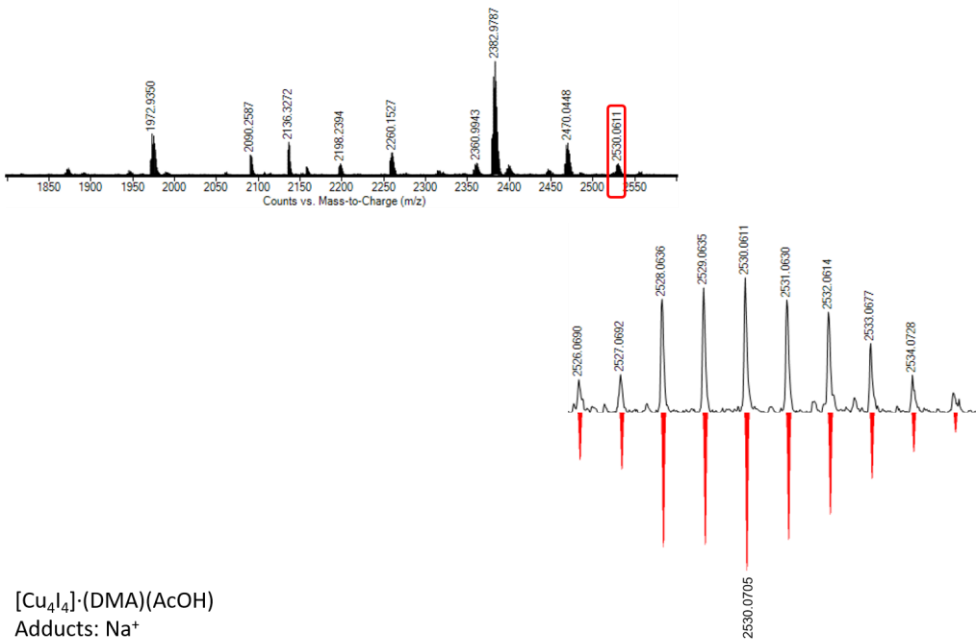

Figure S8. - A zoom of the signal in the MS analysis of the reaction mixture of H_2**I** with copper(II) acetate that originate from **I**$_4$·(DMA)(AcOH) as the Na^+ and adduct.

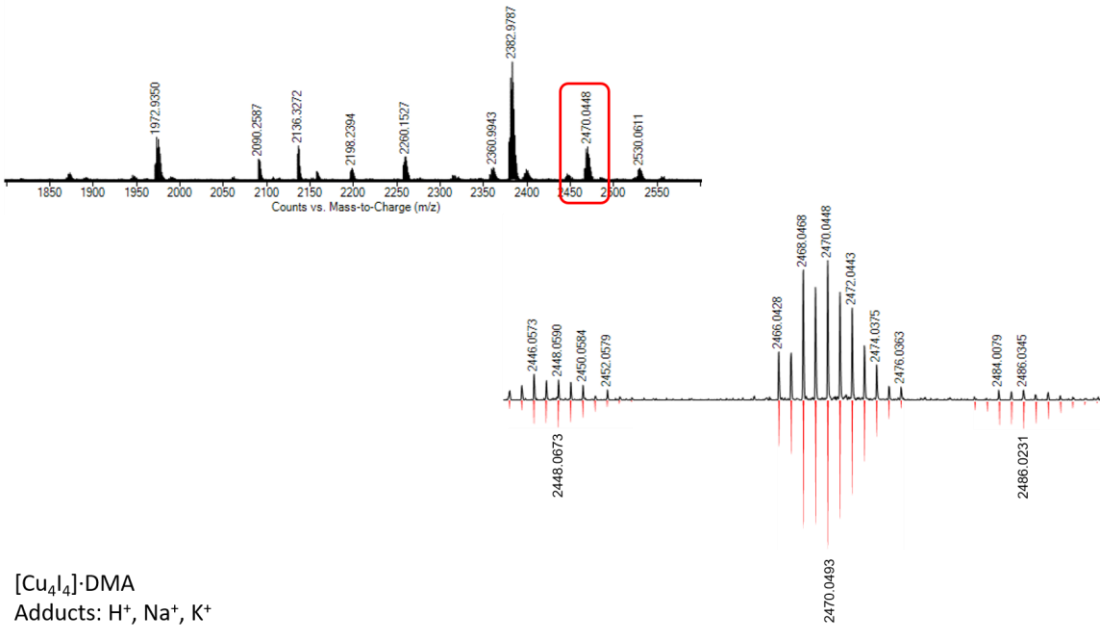

Figure S9. - A zoom of the three signals in the MS analysis of the reaction mixture of H_2**I** with copper(II) acetate that originate from **I**$_4$·(DMA) as the H^+, Na^+ and K^+ adducts.

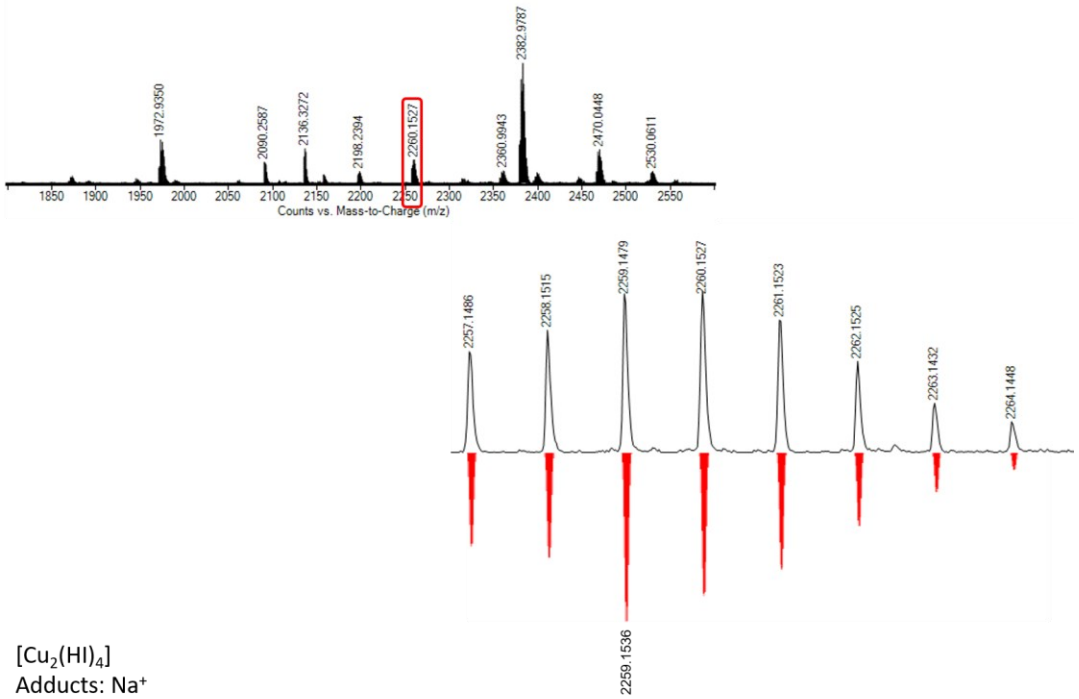

Figure S10. - A zoom of the signal in the MS analysis of the reaction mixture of H_2**I** with copper(II) acetate that originate from $[Cu_2(HI)_4]$ as the Na^+ adduct.

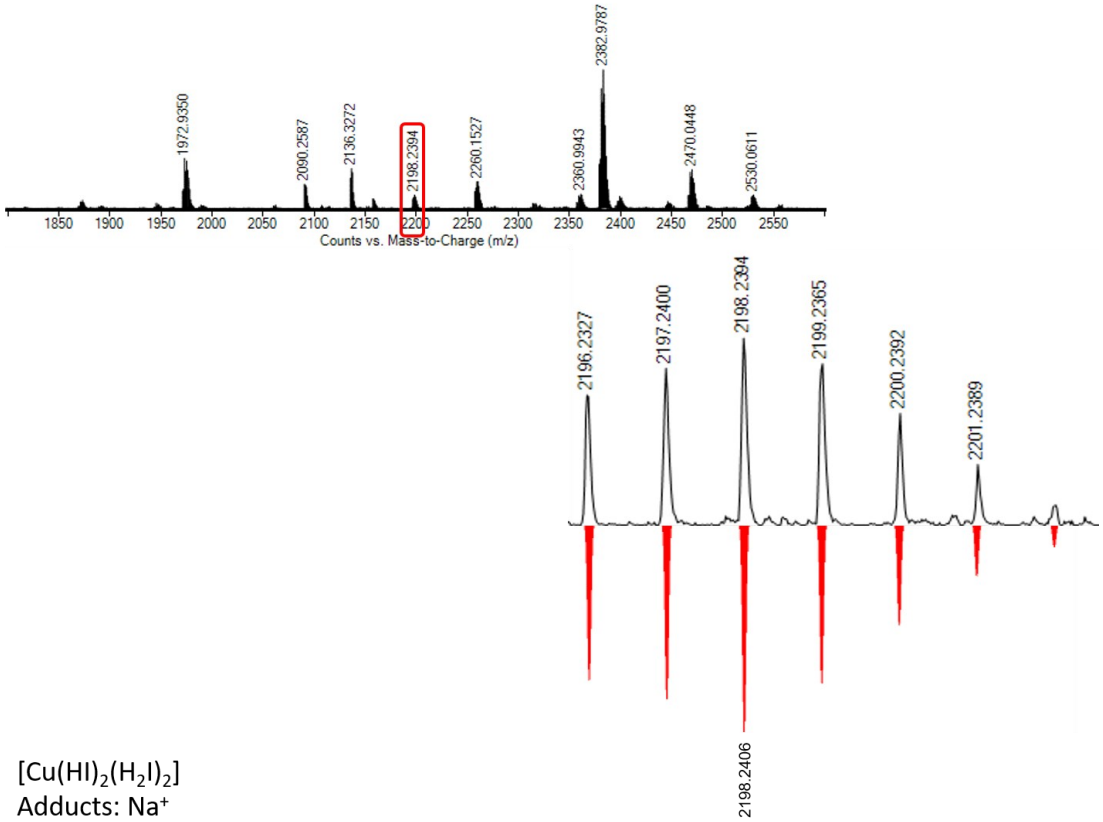

Figure S11. - A zoom of the signal in the MS analysis of the reaction mixture of H_2**I** with copper(II) acetate that originate from $[Cu(HI)_2(H_2I)_2]$ as the Na^+ adduct.

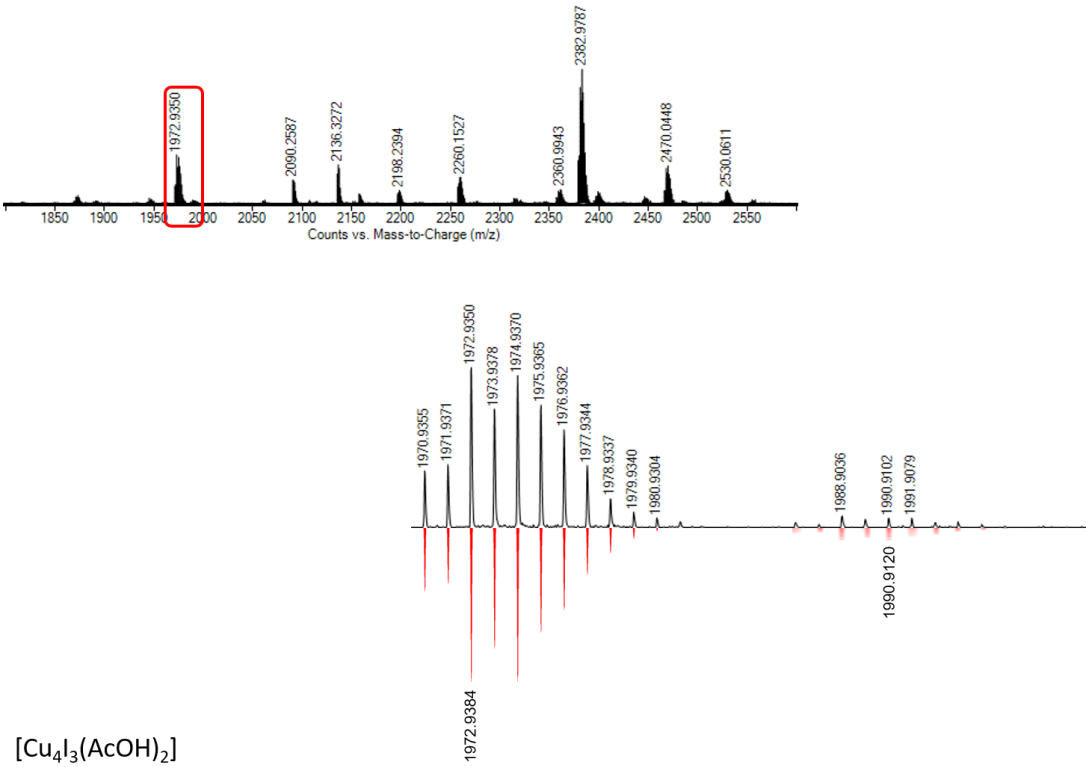

$[Cu_4I_3(AcOH)_2]$
Adducts: Na^+, K^+

Figure S12. - A zoom of the two signals in the MS analysis of the reaction mixture of H_2**I** with copper(II) acetate that originate from $[Cu_4(\mathbf{I})_3(AcOH)_2]$ as the Na^+ and K^+ adducts.

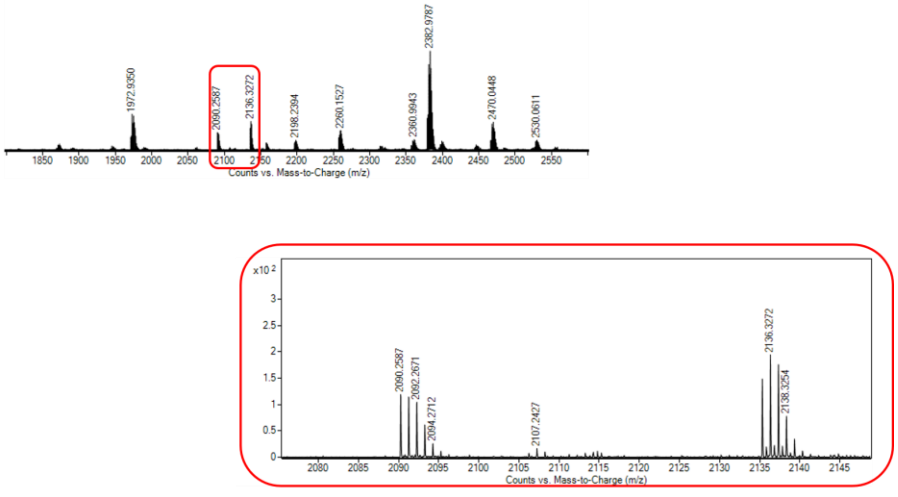

Isotope pattern inconsistent with copper containing complexes

Figure S13. – The remaining unassigned signals in the MS analysis of the reaction mixture could not be assigned to a logical species, however the isotope pattern is not consistent with any copper containing complexes.

Synthesis of ***A*****$_4$**

H_2**A** (74 mg, 0.149 mmol) was dissolved in 1 mL acetonitrile, and $Cu(OAc)_2$ (27 mg, 0.075 mmol) dissolved in 5 mL acetonitrile. 160 µL of the H_2**A** solution was added to 800 µL of the $Cu(OAc)_2$ solution, and the solution made up to 6 mL with acetonitrile. Analysis by HPLC and mass spectrometry after addition of the ligand to the metal shows immediate complexation to form the **A$_4$** complex as a 1 mM solution (quantitative yield by HPLC, not isolated as a solid). Crystallisation was achieved by diffusion of methanol (1 mL) into an acetonitrile solution of **A$_4$** (1 mM, 1 mL). Formation of clear, blue crystals occurred overnight of sufficient quality for SC-XRD analysis.

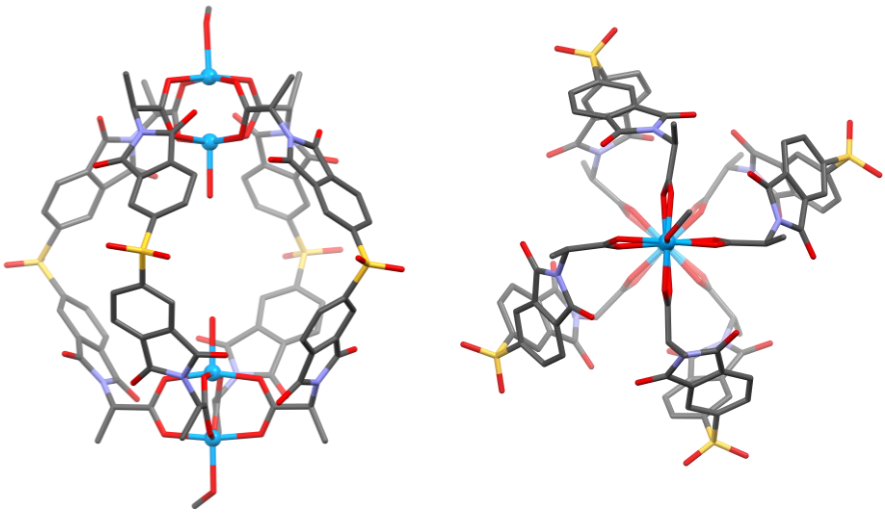

Figure S14. – The molecular structure of $[Cu_4$**A**$_4(H_2O)_2(MeOH)_2]\cdot 3(MeCN)\cdot 1.66(MeOH)$ (**A**$_4$) as determined by X-ray crystallographic studies. Left: Four of ligand **A** link the two Cu_2 paddlewheel nodes to form the lantern-type cage architecture. Right: Looking along the Cu_2 – Cu_2 axis shows the helicate conformation that this species takes due to the presence of chiral functionalities which drive formation of the helix.

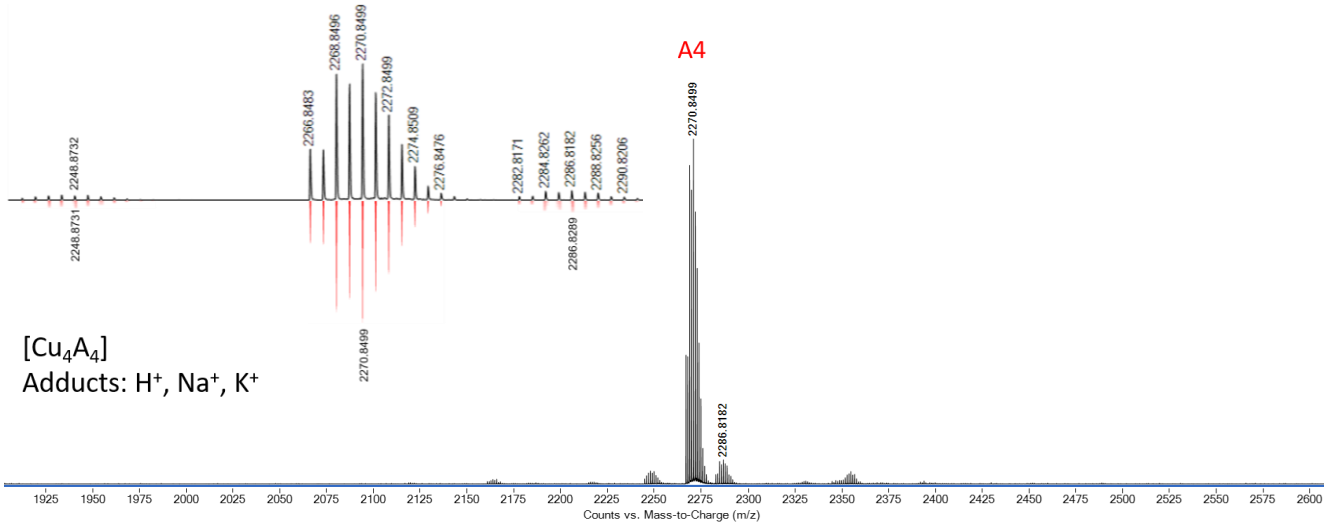

Figure S15. - MS analysis of the reaction mixture of (*S*)-H_2**A** with copper(II) acetate gave rise only to signals originating from **A**$_4$ as the H^+, Na^+ and K^+ adduct. Inlaid is a zoom of the three signals corresponding to the three adducts, with the matching predicted isotope patterns displayed in red.

*Synthesis of M-**L4** and P-**L4***

As previously reported, (*S*)-H_2**L** or (*R*)-H_2**L** (87 mg, 0.149 mmol), to form the M or P helicates, is dissolved in 1 mL acetonitrile, and $Cu(OAc)_2$ (27 mg, 0.075 mmol) dissolved in 5 mL acetonitrile. 160 µL of the H_2**L** solution is added to 800 µL of the $Cu(OAc)_2$ solution, and the solution made up to 6 mL with acetonitrile. Analysis by HPLC and mass spectrometry after addition of the ligand to the metal shows immediate complexation to form the **L4** complex as a 1 mM solution (quantitative yield).

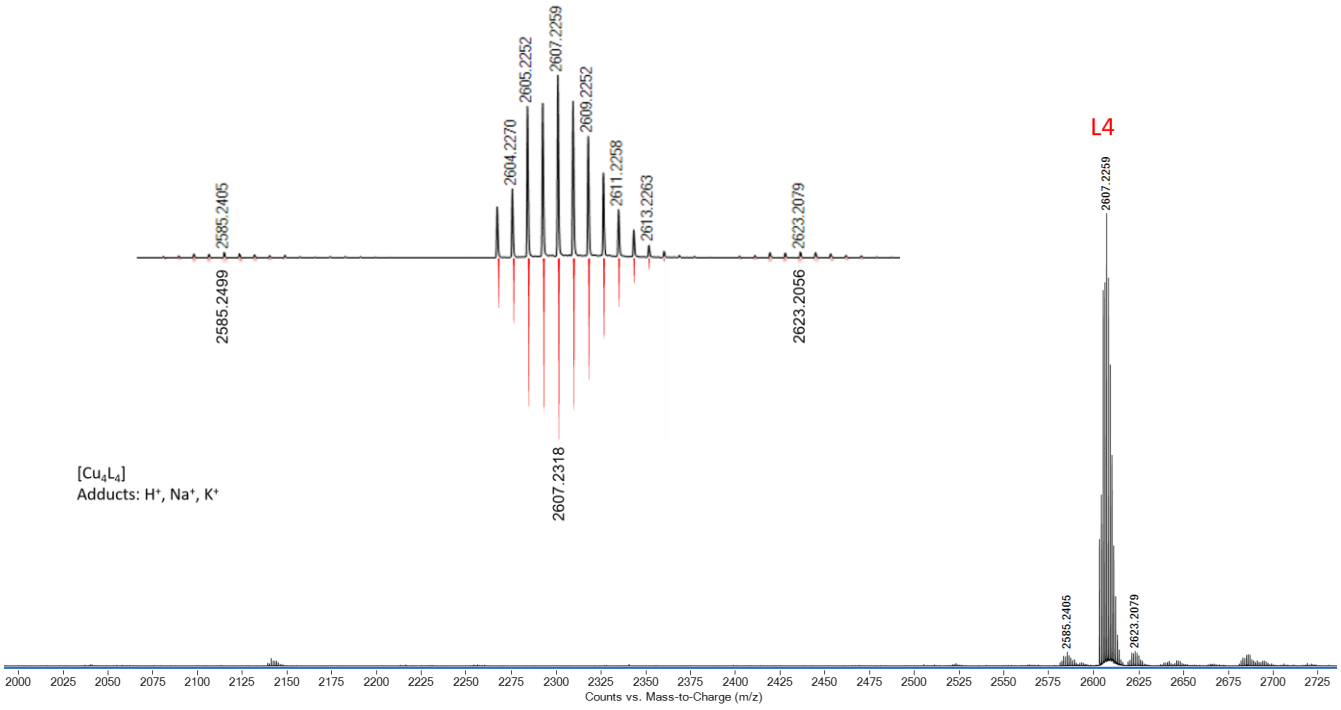

Figure S16. - MS analysis of the reaction mixture of H_2**L** with copper(II) acetate gave rise only to signals originating from **L4** as the H^+, Na^+ and K^+ adduct. Inlaid is a zoom of the three signals corresponding to the three adducts, with the matching predicted isotope patterns displayed in red.

Synthesis of ***V₄***

H_2**V** (87 mg, 0.149 mmol) was dissolved in 1 mL dimethylacetamide, and $Cu(OAc)_2$ (27 mg, 0.075 mmol) dissolved in 5 mL acetonitrile. 160 µL of the H_2**V** solution was added to 800 µL of the $Cu(OAc)_2$ solution, and the solution made up to 6 mL with acetonitrile. Analysis by HPLC and mass spectrometry after addition of the ligand to the metal shows immediate complexation to form the **V₄** complex in low yields, with fragments of the complex also seen in mass spectrometry.

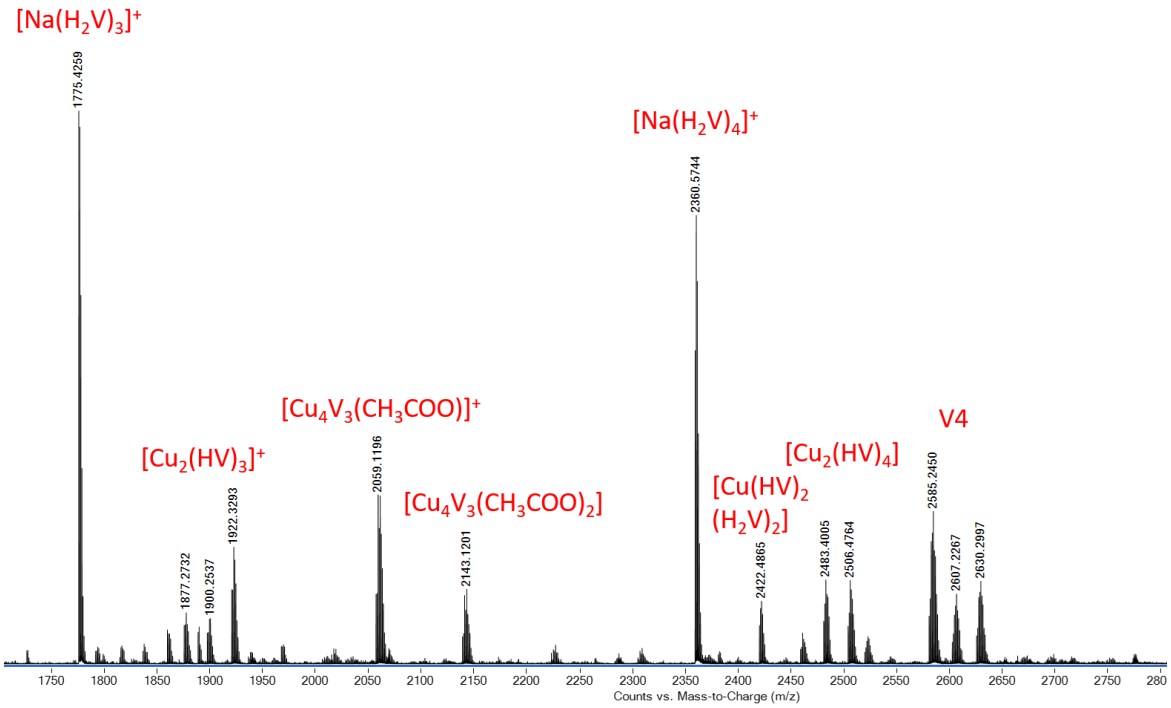

Figure S17. - MS analysis of the reaction mixture of H_2**V** with copper(II) acetate gave rise to signals originating **V₄** as the H^+, Na^+ and $NMe_2H_2^+$ adducts and smaller, partially formed fragments of **V₄**.

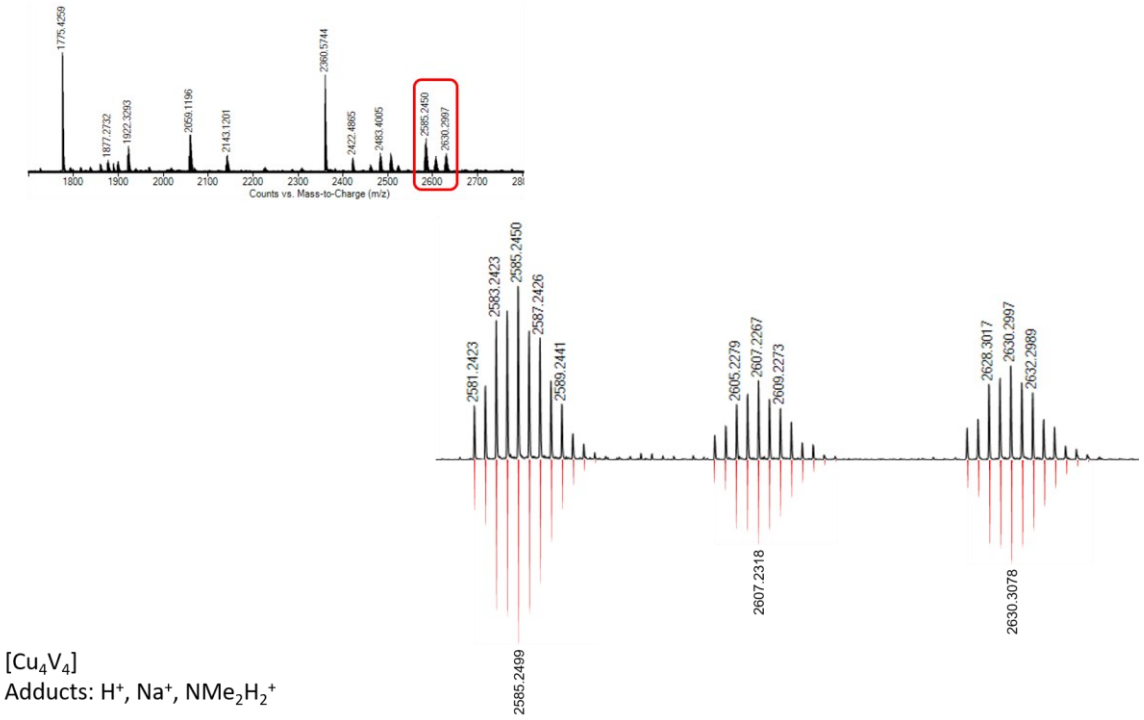

Figure S18. – A zoom of the three signals in the MS analysis of the reaction mixture of H_2**V** with copper(II) acetate that originate from [Cu_4**V**$_4$] as the H^+, Na^+ and $NMe_2H_2^+$ adducts.

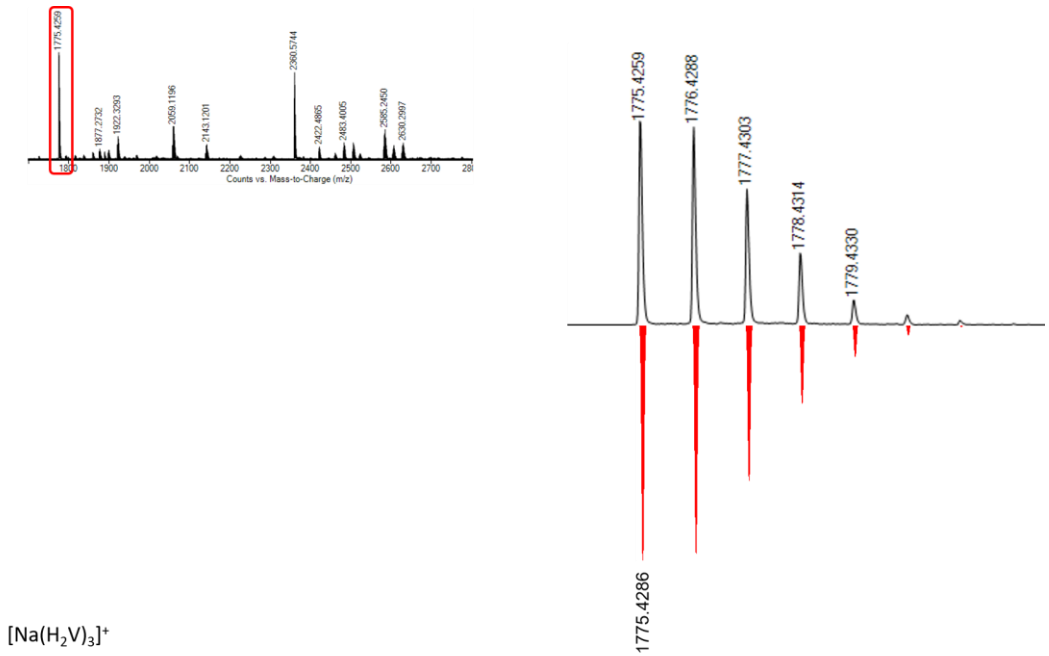

Figure S19. - A zoom of the signal in the MS analysis of the reaction mixture of H_2**V** with copper(II) acetate that originate from [$Na(H_2$**V**$)_3]^+$.

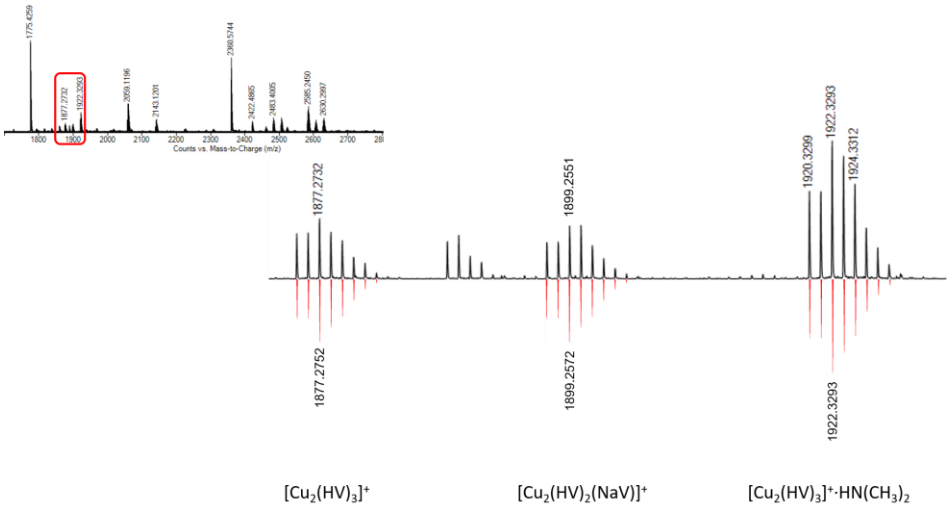

Figure S20. - A zoom of the three signals in the MS analysis of the reaction mixture of H_2**V** with copper(II) acetate that originate from $[Cu_2(H\mathbf{V})_3]^+$, $[Cu_2(H\mathbf{V})_2(Na\mathbf{V})]^+$ and $[Cu_2(H\mathbf{V})_3]^+\cdot HNMe_2$.

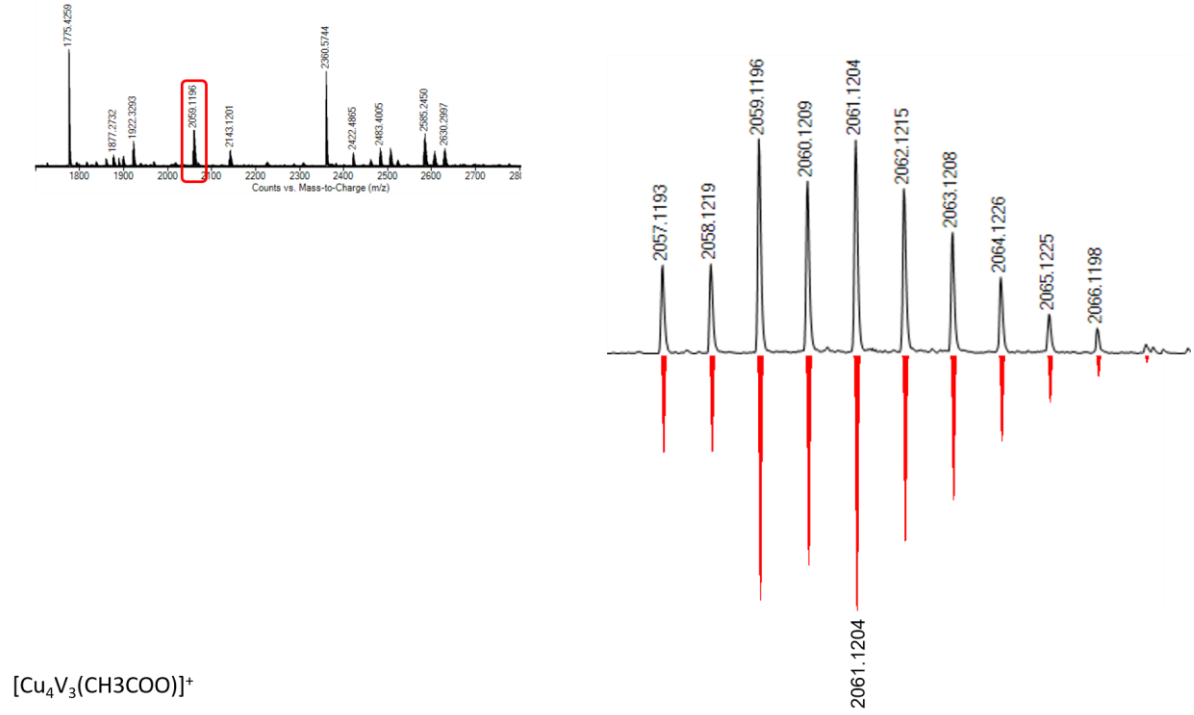

Figure S21. - A zoom of the signal in the MS analysis of the reaction mixture of H_2**V** with copper(II) acetate that originate from $[Cu_4\mathbf{V}_3(CH_3COO)]^+$.

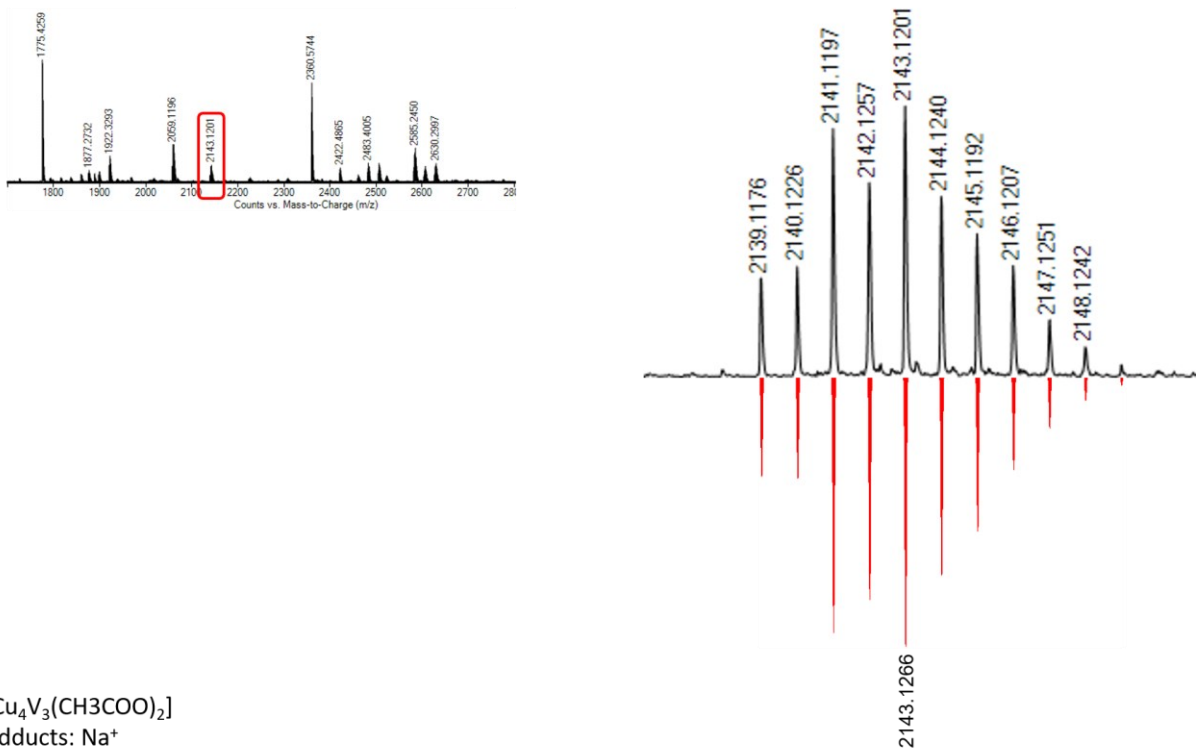

Figure S22. – A zoom of the signal in the MS analysis of the reaction mixture of H_2**V** with copper(II) acetate that originate from $[Cu_4\mathbf{V}_3(CH_3COO)_2]$ as the Na^+ adduct.

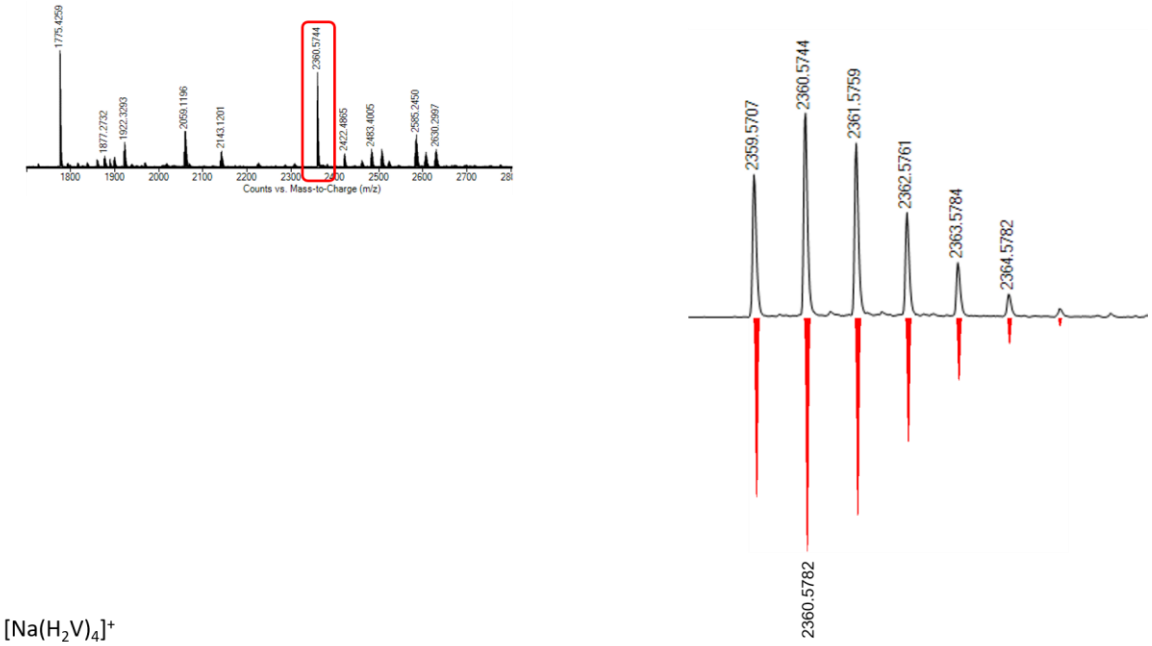

Figure S23. - A zoom of the signal in the MS analysis of the reaction mixture of H_2**V** with copper(II) acetate that originate from $[Na(H_2\mathbf{V})_4]^+$.

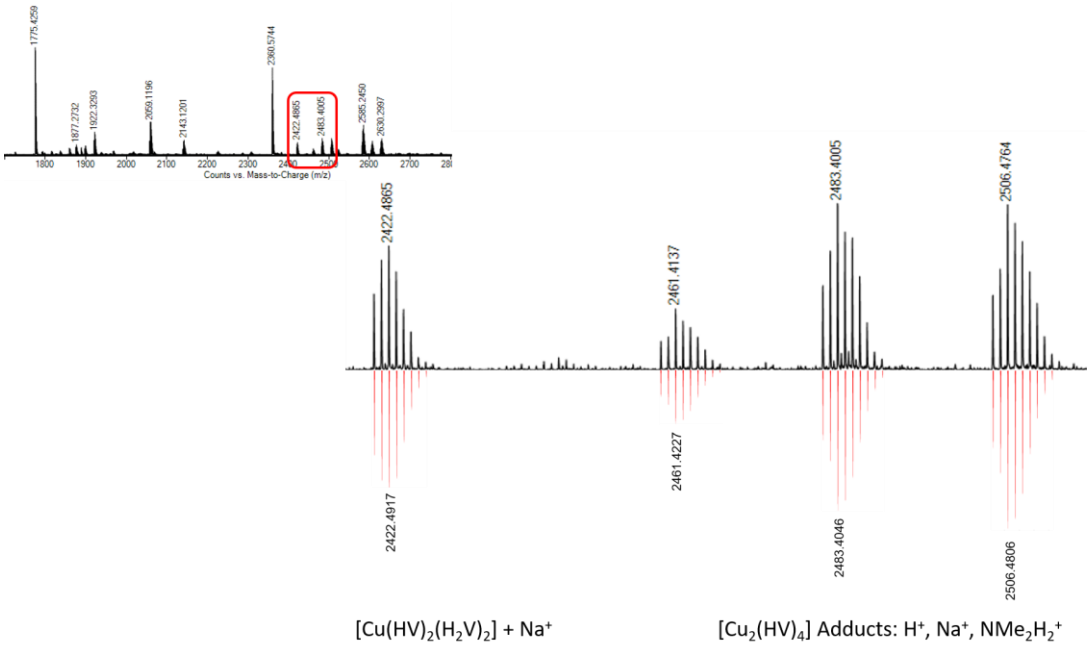

Figure S24. - A zoom of the four signals in the MS analysis of the reaction mixture of H_2**V** with copper(II) acetate that originate from [Cu(H**V**)$_2$(H_2**V**)$_2$] as the Na^+ adduct and [Cu_2(H**V**)$_4$] as the H^+, Na^+ and $NMe_2H_2^+$ adducts.

Synthesis of heteroleptic coordination cages

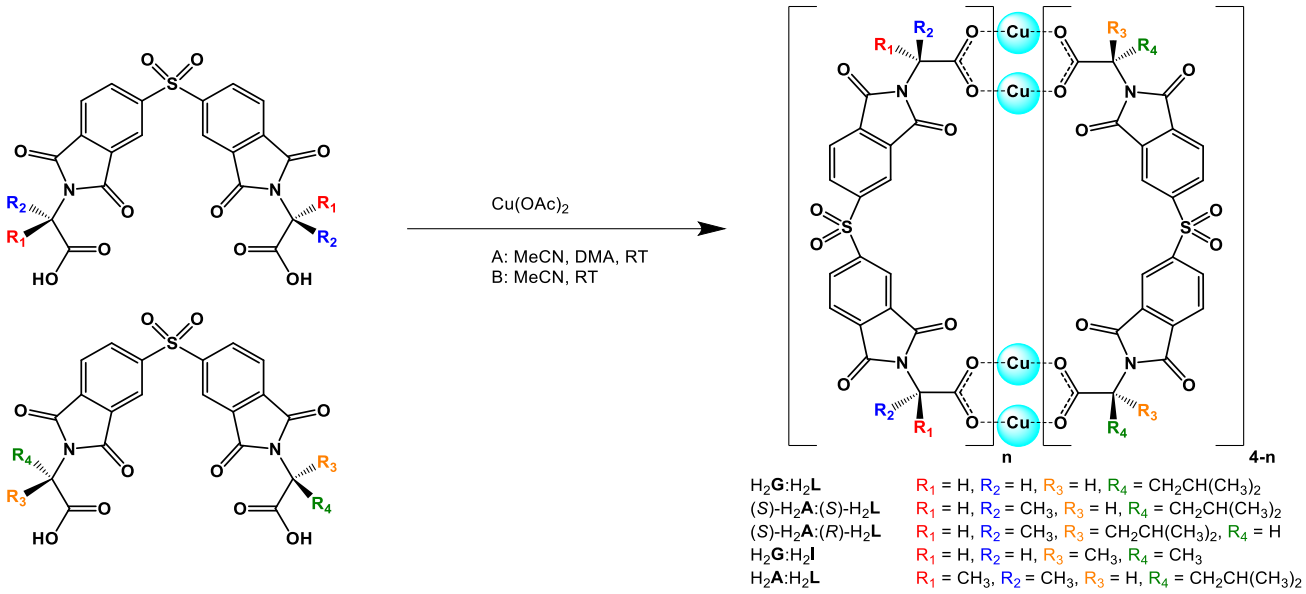

Scheme S3. - A mixture of two different homochiral ligands react with copper(II) acetate to form heteroleptic species in which both ligands are incorporated into the structure of the cage.

*Synthesis of heteroleptic coordination cages with **G** and (S)-**L***

H_2**G** (70 mg, 0.149 mmol) was dissolved in 1 mL dimethylacetamide, (*S*)-H_2**L** (87 mg, 0.149 mmol) was dissolved in 1 mL acetonitrile, and $Cu(OAc)_2$ (27 mg, 0.075 mmol) dissolved in 5 mL acetonitrile. 80 µL of the H_2**G** solution and 80 µL of the (*S*)-H_2**L** solution were mixed, and to this mixture was added 800 µL of the $Cu(OAc)_2$ solution. The solution was made up to 6 mL with acetonitrile. Analysis after addition of the ligand to the metal suggested immediate complexation to form the $\mathbf{G}_n\mathbf{L}_{4-n}$ (n=0-4) complexes as a solution with a cumulative coordination cage concentration of 1 mM (quantitative yield).

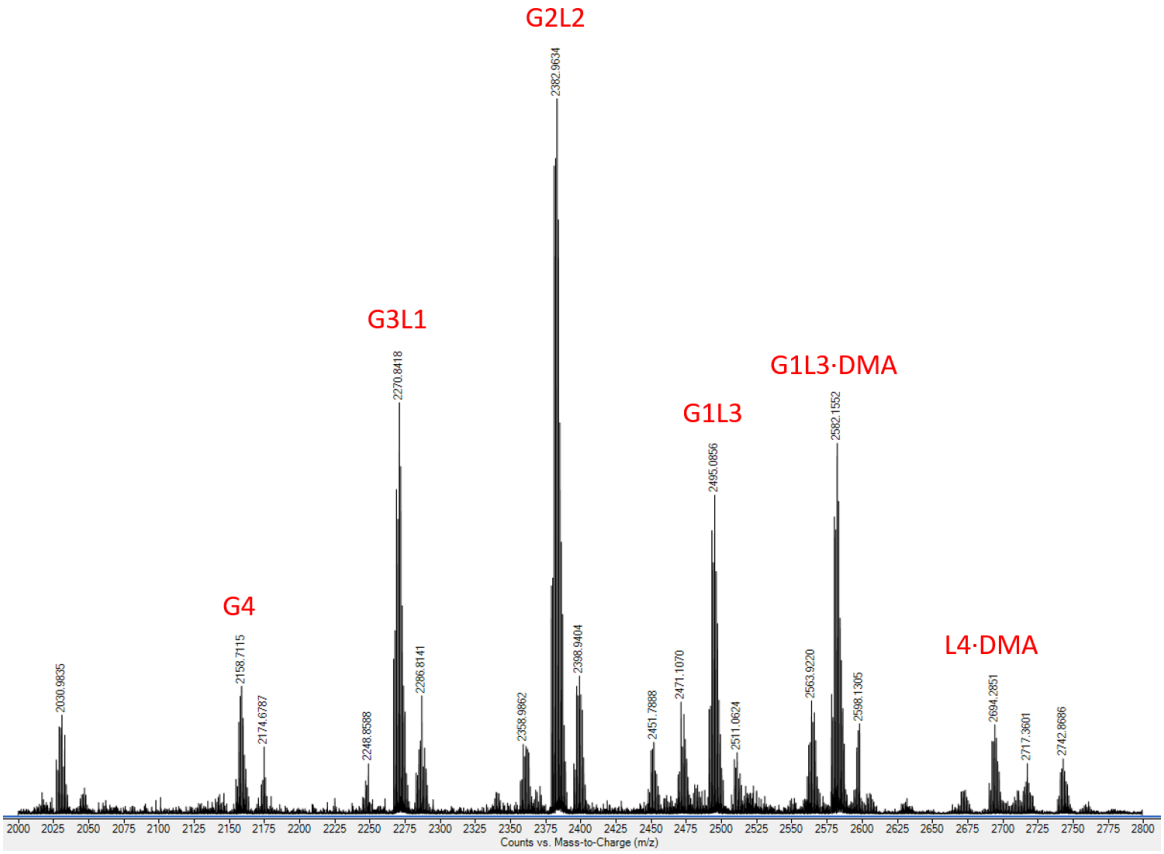

Figure S25. – MS analysis of the reaction mixture of H_2**G** and H_2**L** with copper(II) acetate gave rise to signals originating from the homoleptic species $\mathbf{G_4}$ and $\mathbf{L_4}$ and the heteroleptic species $\mathbf{G_3L_1}$, $\mathbf{G_2L_2}$ and $\mathbf{G_1L_3}$.

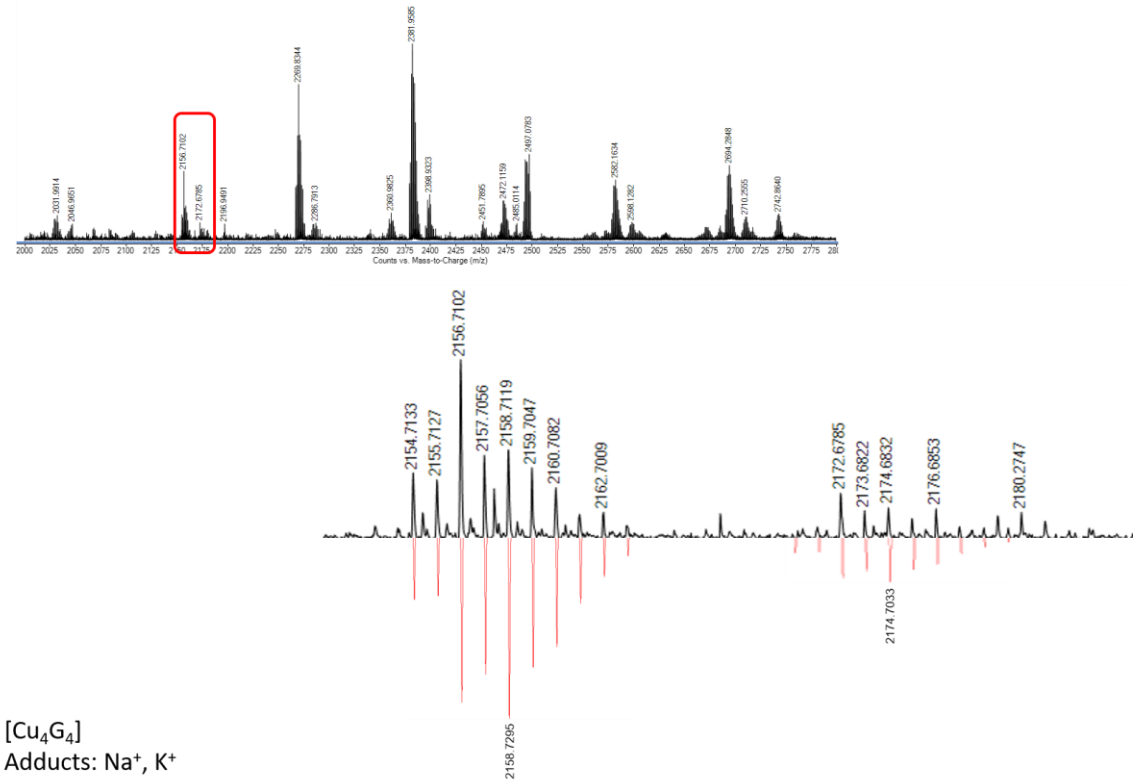

Figure S26. - A zoom of the signals in the MS analysis of the reaction mixture of H_2**G** and H_2**L** with copper(II) acetate that originate from **G₄** as the Na^+ and K^+ adducts.

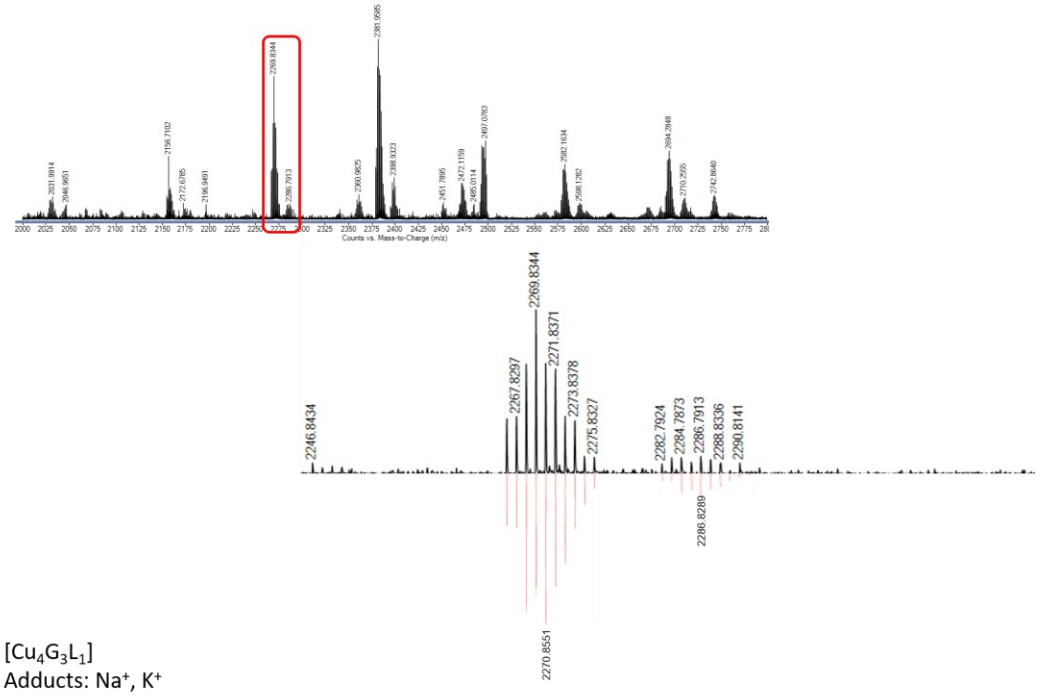

Figure S27. - A zoom of the signals in the MS analysis of the reaction mixture of H_2**G** and H_2**L** with copper(II) acetate that originate from **G₃L₁** as the Na^+ and K^+ adducts.

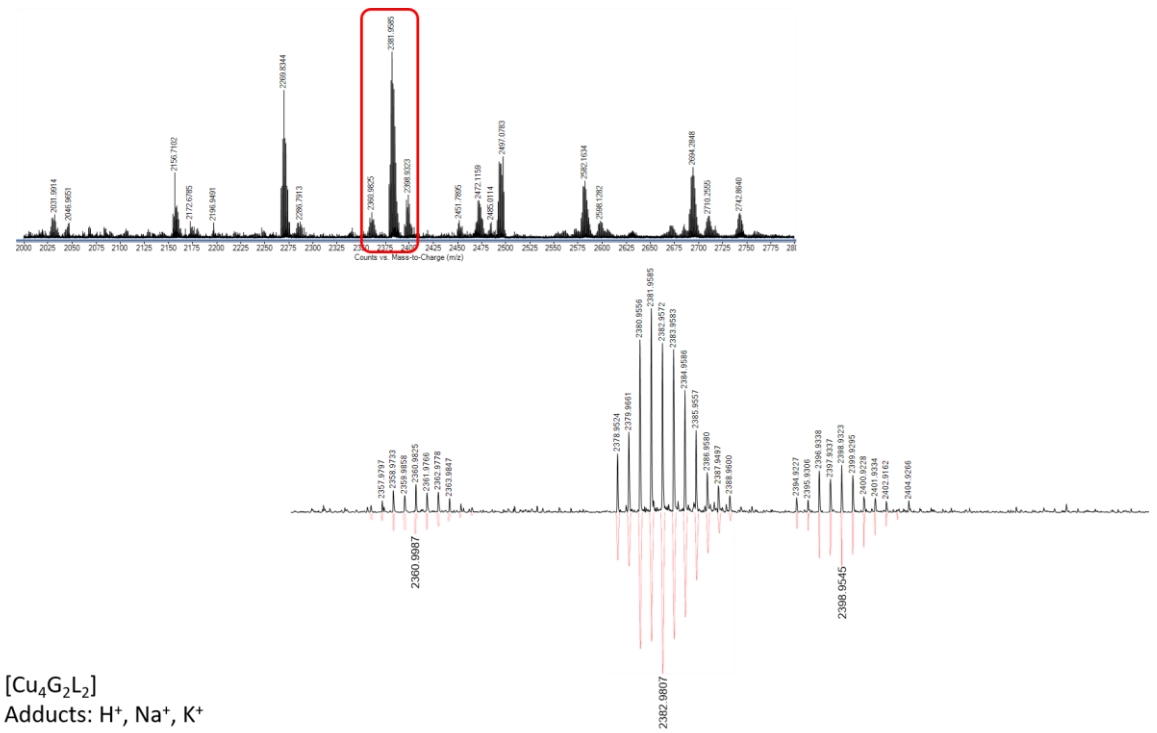

$[Cu_4G_2L_2]$
Adducts: H^+, Na^+, K^+

Figure S28. - A zoom of the signals in the MS analysis of the reaction mixture of H_2**G** and H_2**L** with copper(II) acetate that originate from **G_2L_2** as the H^+, Na^+ and K^+ adducts.

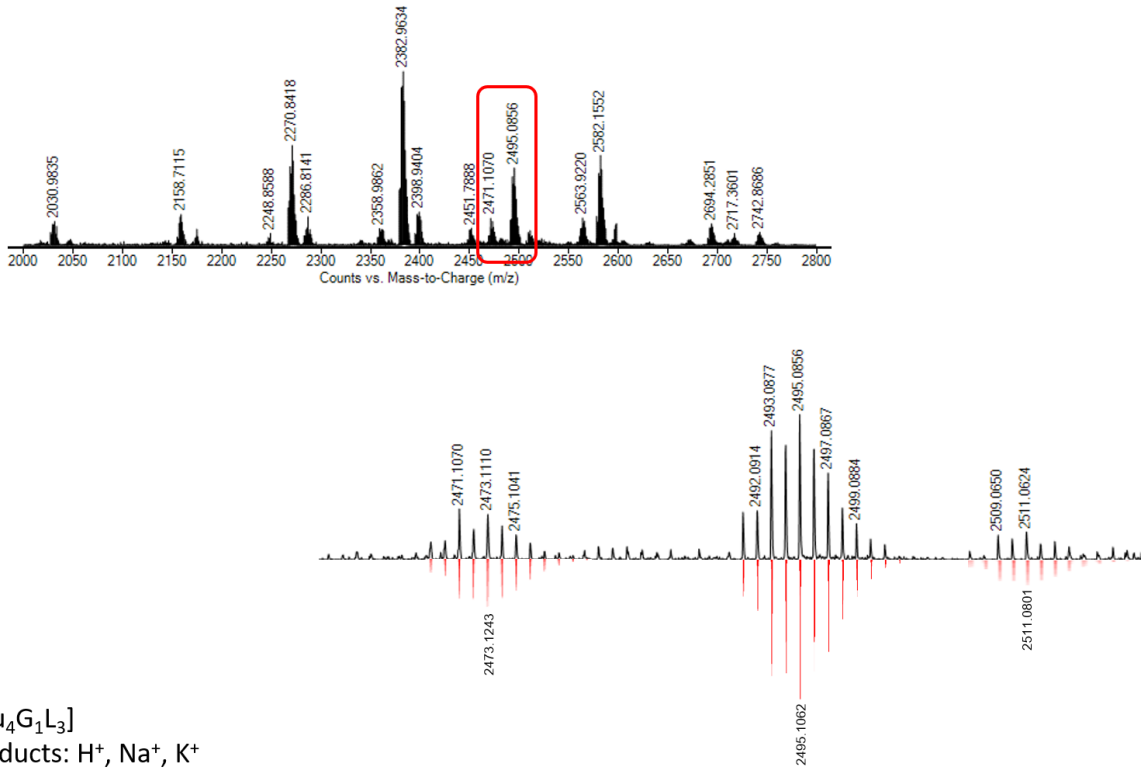

$[Cu_4G_1L_3]$
Adducts: H^+, Na^+, K^+

Figure S29. - A zoom of the signals in the MS analysis of the reaction mixture of H_2**G** and H_2**L** with copper(II) acetate that originate from **G_1L_3** as the H^+, Na^+ and K^+ adducts.

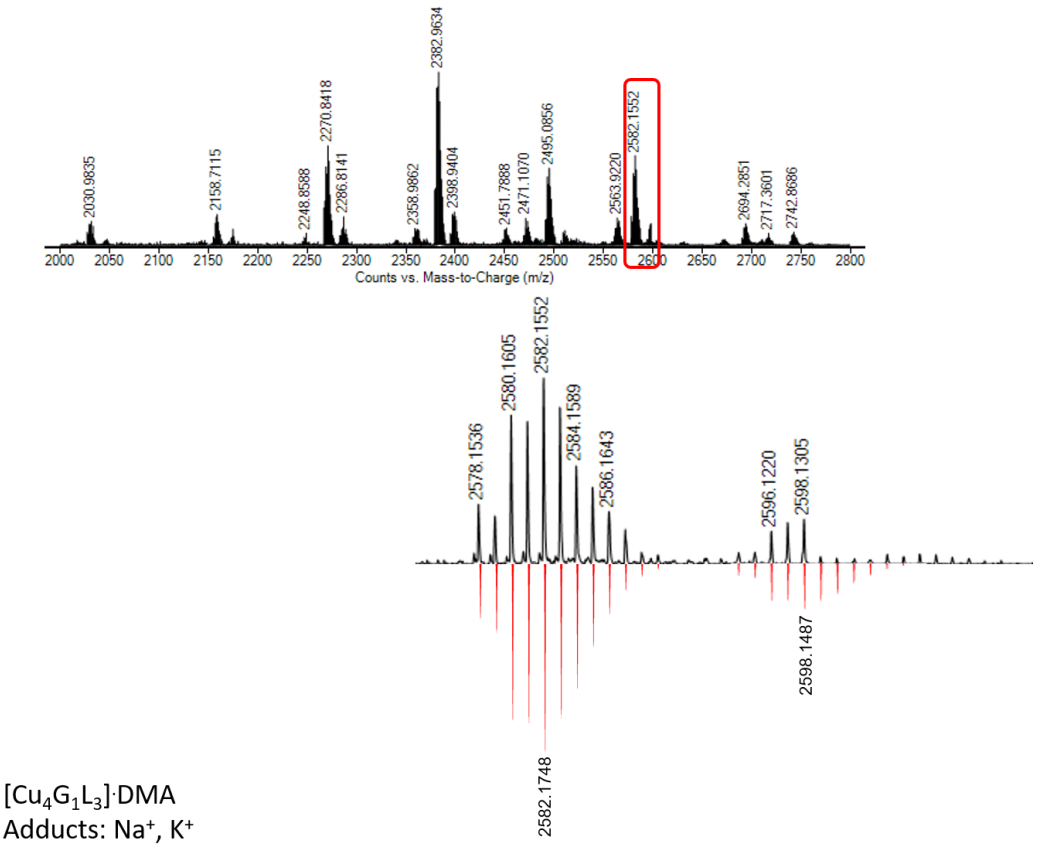

Figure S30. - A zoom of the signals in the MS analysis of the reaction mixture of H_2**G** and H_2**L** with copper(II) acetate that originate from **G_2L_2**·(DMA) as the Na^+ and K^+ adducts.

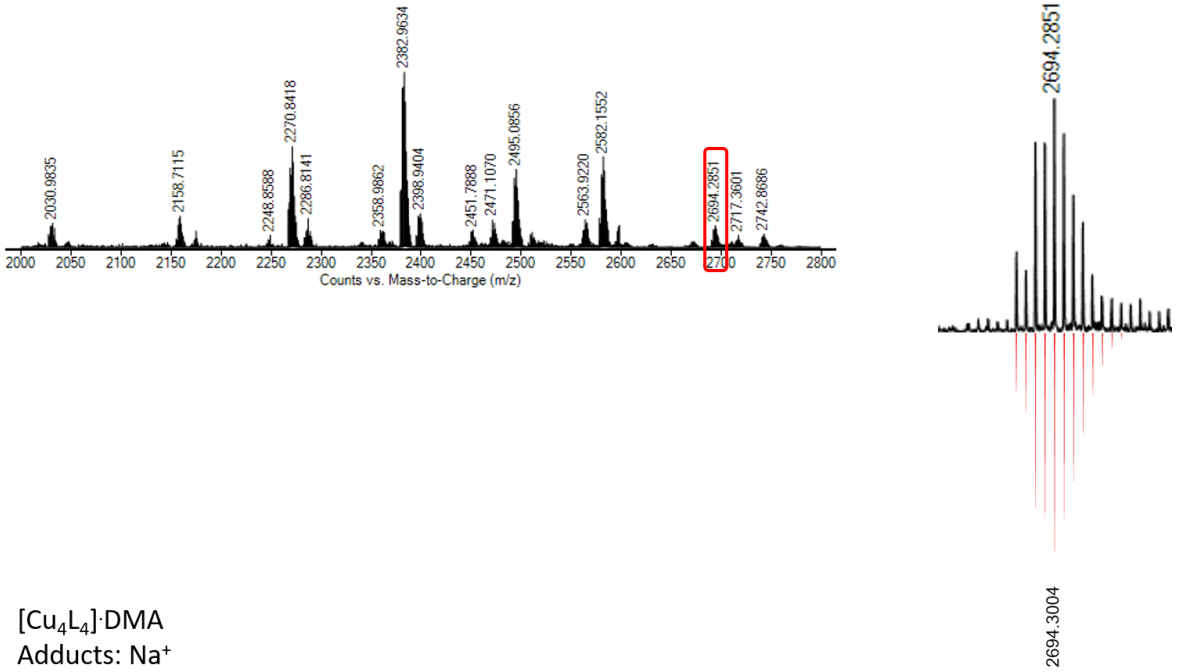

Figure S31. - A zoom of the signals in the MS analysis of the reaction mixture of H_2**G** and H_2**L** with copper(II) acetate that originate from **L_4**·(DMA) as the Na^+ adduct.

*Synthesis of heteroleptic coordination cages with **I** and (R)-**L***

H_2**I** (79 mg, 0.149 mmol) was dissolved in 1 mL acetonitrile, (*R*)-H_2**L** (87 mg, 0.149 mmol) was dissolved in 1 mL acetonitrile, and $Cu(OAc)_2$ (27 mg, 0.075 mmol) dissolved in 5 mL acetonitrile. 80 µL of the H_2**I** solution and 80 µL of the (*R*)-H_2**L** solution were mixed, and to this mixture is added 800 µL of the $Cu(OAc)_2$ solution. The solution is made up to 6 mL with acetonitrile. Analysis after addition of the ligand to the metal suggested immediate complexation to form the $\mathbf{I_n}$(*R*)-$\mathbf{L_{4-n}}$ (n=0,1,2) complexes as a solution with a cumulative coordination cage concentration of 1 mM (quantitative yield).

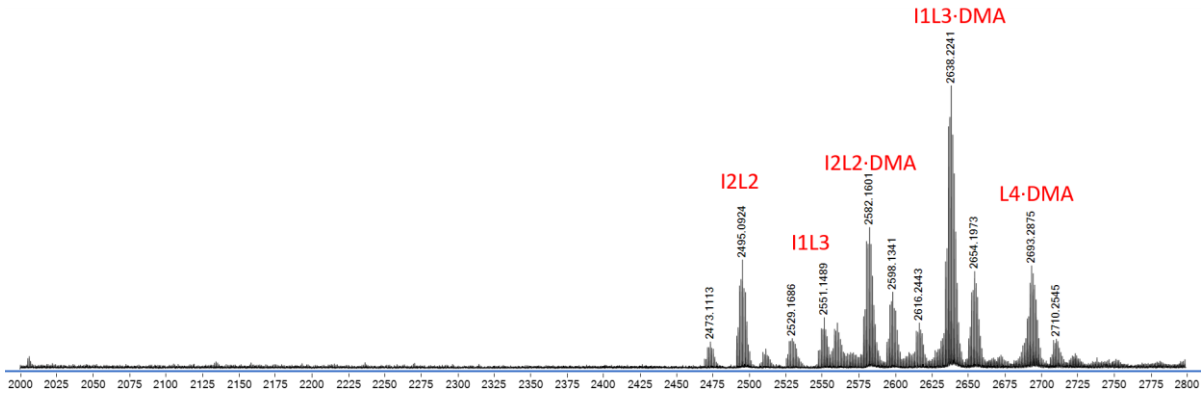

Figure S32. – MS analysis of the reaction mixture of H_2**I** and H_2**L** with copper(II) acetate gave rise to signals originating from the homoleptic species $\mathbf{L_4}$ and the heteroleptic species $\mathbf{I_2L_2}$ and $\mathbf{I_1L_3}$.

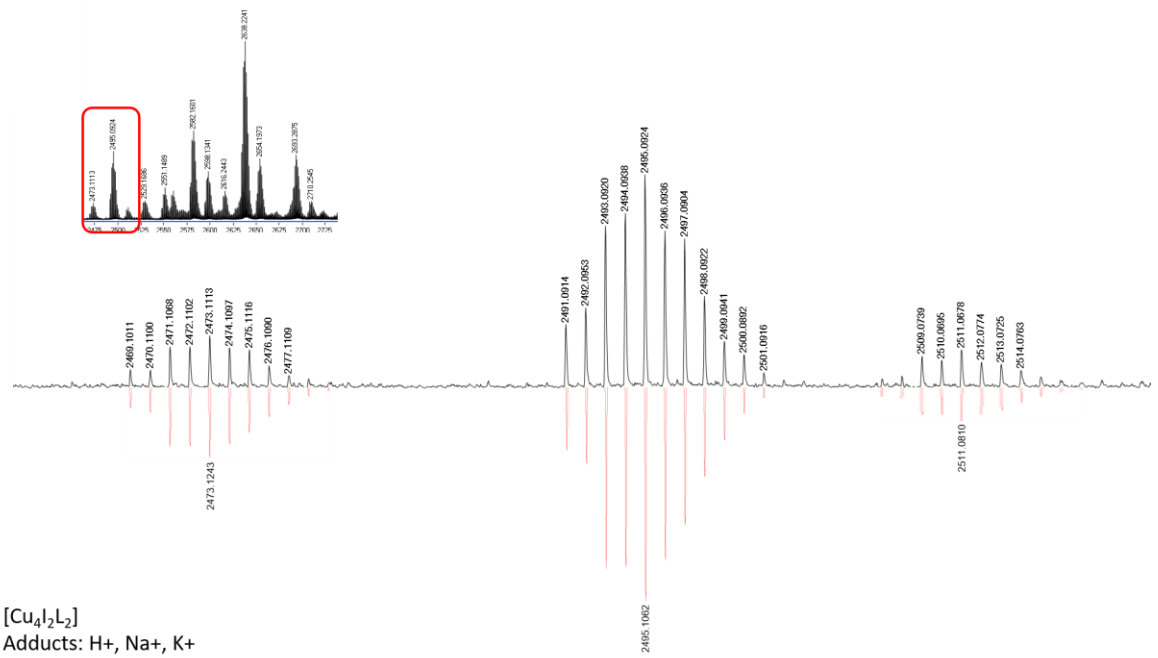

Figure S33. – A zoom of the signals in the MS analysis of the reaction mixture of H_2**I** and H_2**L** with copper(II) acetate that originate from $\mathbf{I_2L_2}$ as the H^+, Na^+ and K^+ adducts.

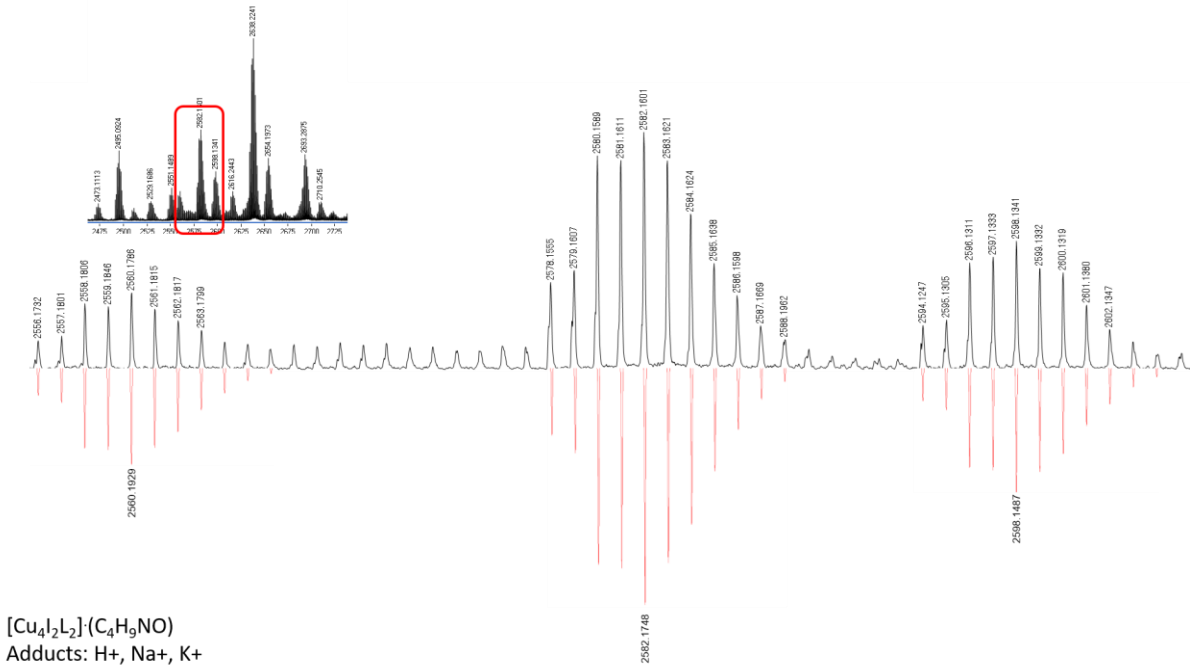

Figure S34. – A zoom of the signals in the MS analysis of the reaction mixture of H_2**I** and H_2**L** with copper(II) acetate that originate from $\mathbf{I_2L_2}$·(DMA) as the H^+, Na^+ and K^+ adducts.

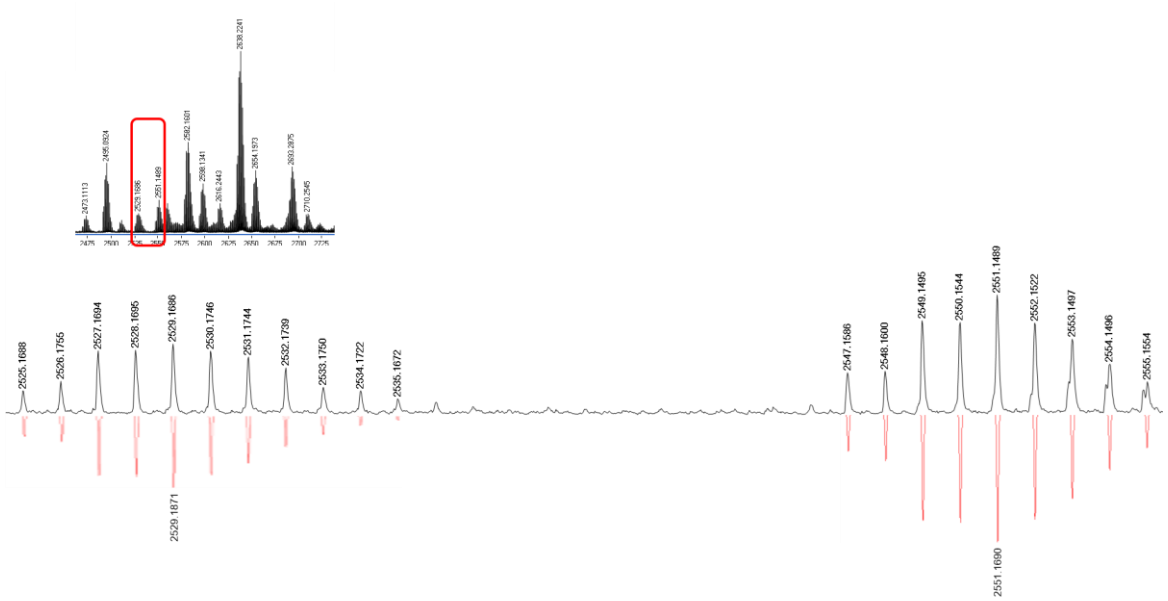

$[Cu_4I_1L_3]$
Adducts: H^+, Na^+

Figure S35. – A zoom of the signals in the MS analysis of the reaction mixture of H_2**I** and H_2**L** with copper(II) acetate that originate from $\mathbf{I_1L_3}$ as the H^+ and Na^+ adducts.

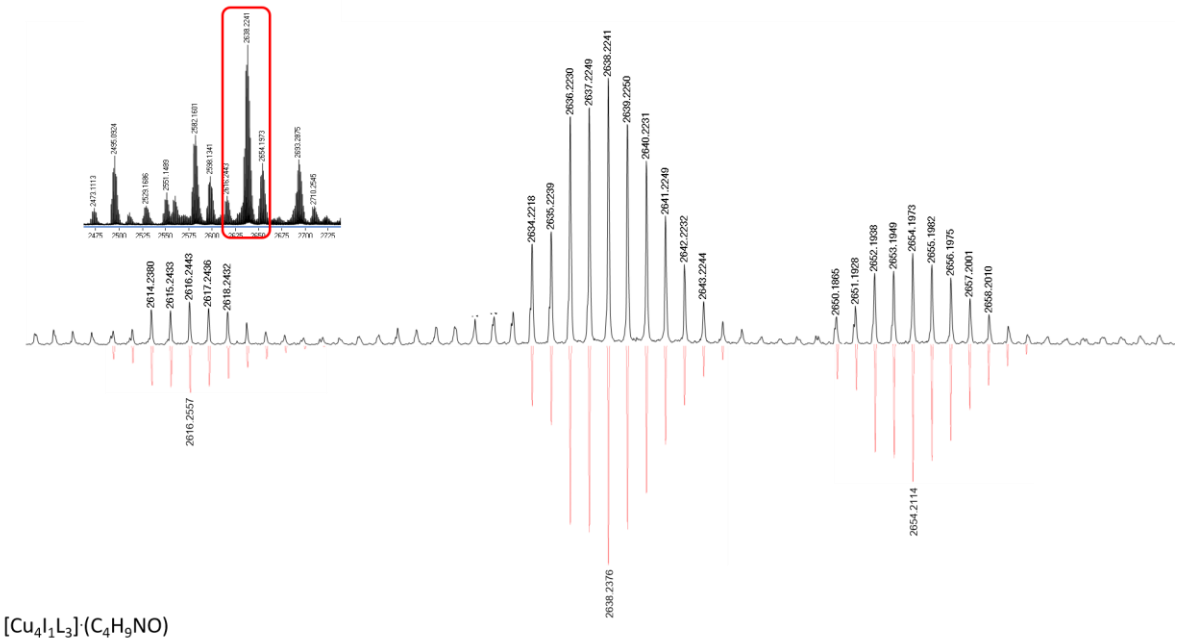

$[Cu_4I_1L_3]\cdot(C_4H_9NO)$
Adducts: H^+, Na^+, K^+

Figure S36. - A zoom of the signals in the MS analysis of the reaction mixture of H_2**I** and H_2**L** with copper(II) acetate that originate from $\mathbf{I_1L_3}\cdot$(DMA) as the H^+, Na^+ and K^+ adducts.

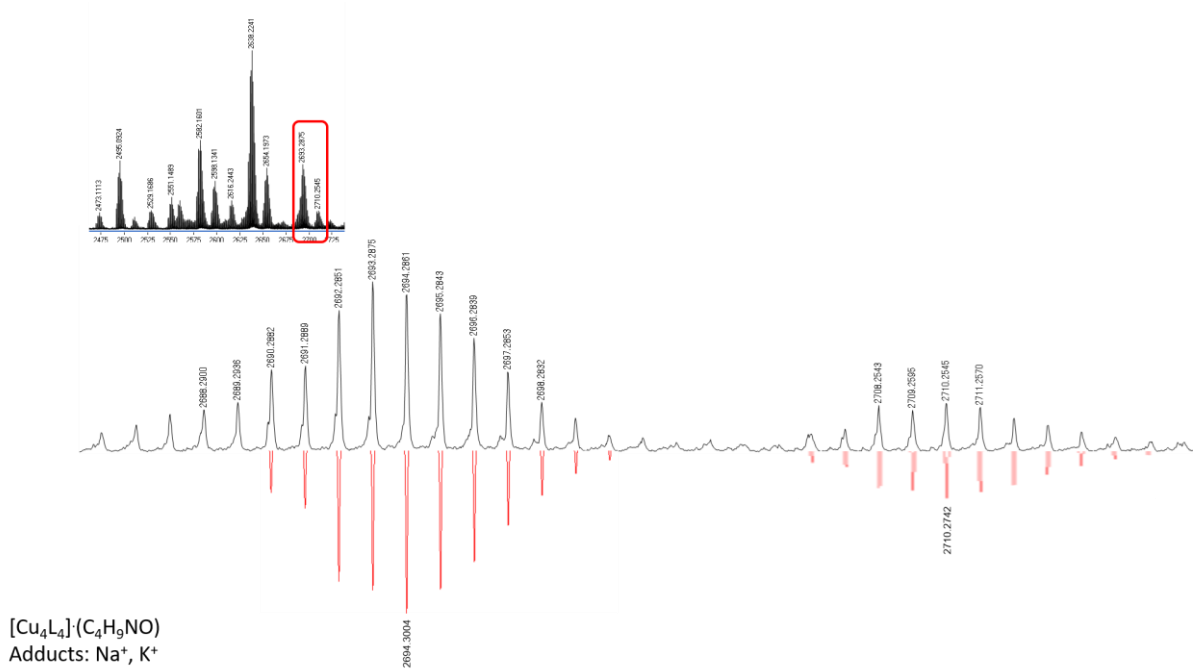

Figure S37. - A zoom of the signals in the MS analysis of the reaction mixture of H_2**I** and H_2**L** with copper(II) acetate that originate from **L**$_4$·(DMA) as the Na^+ and K^+ adducts.

*Synthesis of heteroleptic coordination cages with (S)-**A** and (S)-**L***

(*S*)-H_2**A** (74 mg, 0.149 mmol) was dissolved in 1 mL acetonitrile, (*S*)-H_2**L** (87 mg, 0.149 mmol) was dissolved in 1 mL acetonitrile, and $Cu(OAc)_2$ (27 mg, 0.075 mmol) dissolved in 5 mL acetonitrile. 80 µL of the H_2**A** solution and 80 µL of the (*S*)-H_2**L** solution are mixed, and to this mixture is added 800 µL of the $Cu(OAc)_2$ solution. The solution was made up to 6 mL with acetonitrile. Analysis after addition of the ligand to the metal suggests immediate complexation to form the (*S*)-$\mathbf{A_n}$(*R*)-$\mathbf{L_{4-n}}$ (n=0-4) complexes as a solution with a cumulative coordination cage concentration of 1 mM (quantitative yield).

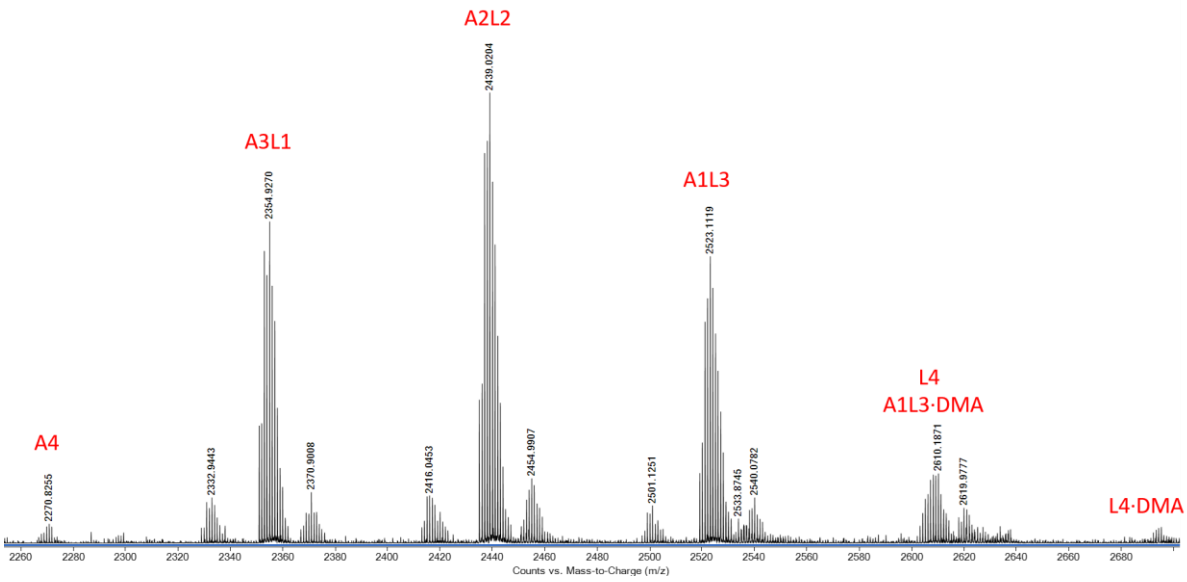

Figure S38. – MS analysis of the reaction mixture of H_2**A** and H_2**L** with copper(II) acetate gave rise to signals originating from the homoleptic species $\mathbf{A_4}$ and $\mathbf{L_4}$ and the heteroleptic species $\mathbf{A_3L_1}$, $\mathbf{A_2L_2}$ and $\mathbf{A_1L_3}$.

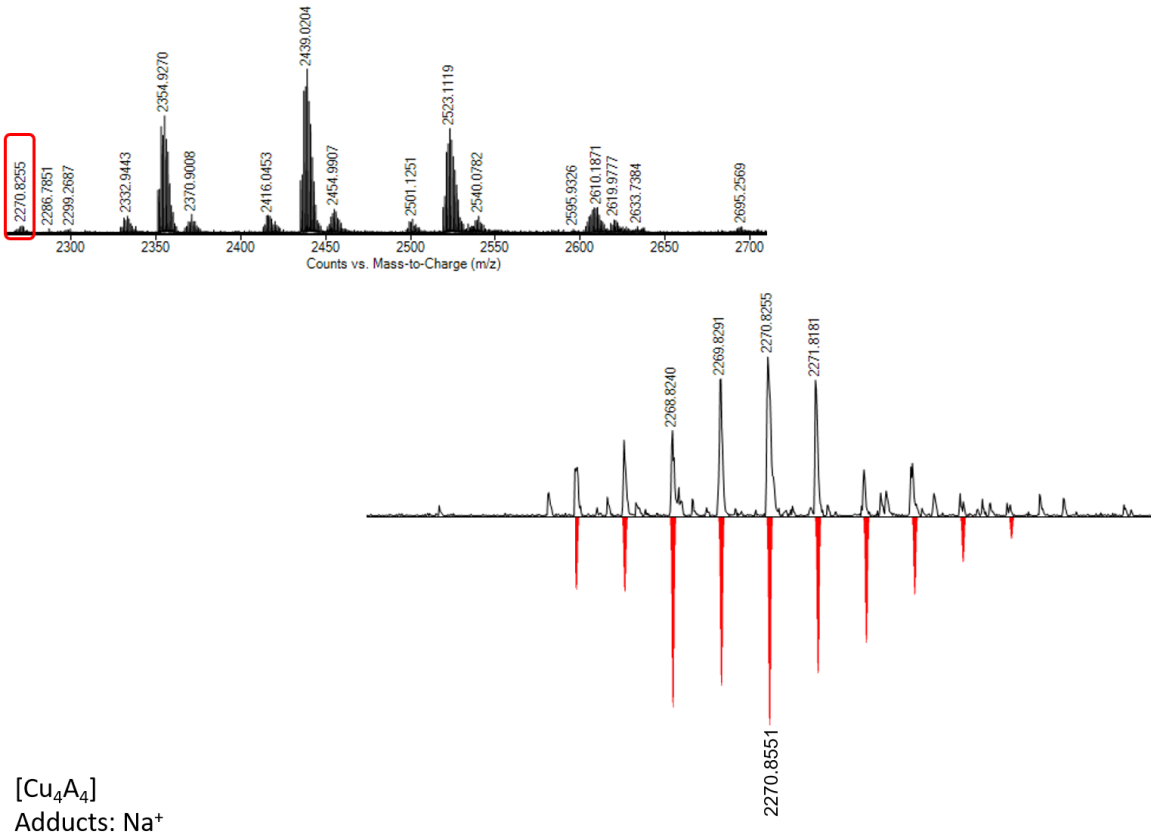

Figure S39. - A zoom of the signals in the MS analysis of the reaction mixture of H_2**A** and H_2**L** with copper(II) acetate that originate from $\mathbf{A_4}$·(DMA) as the Na^+ adduct.

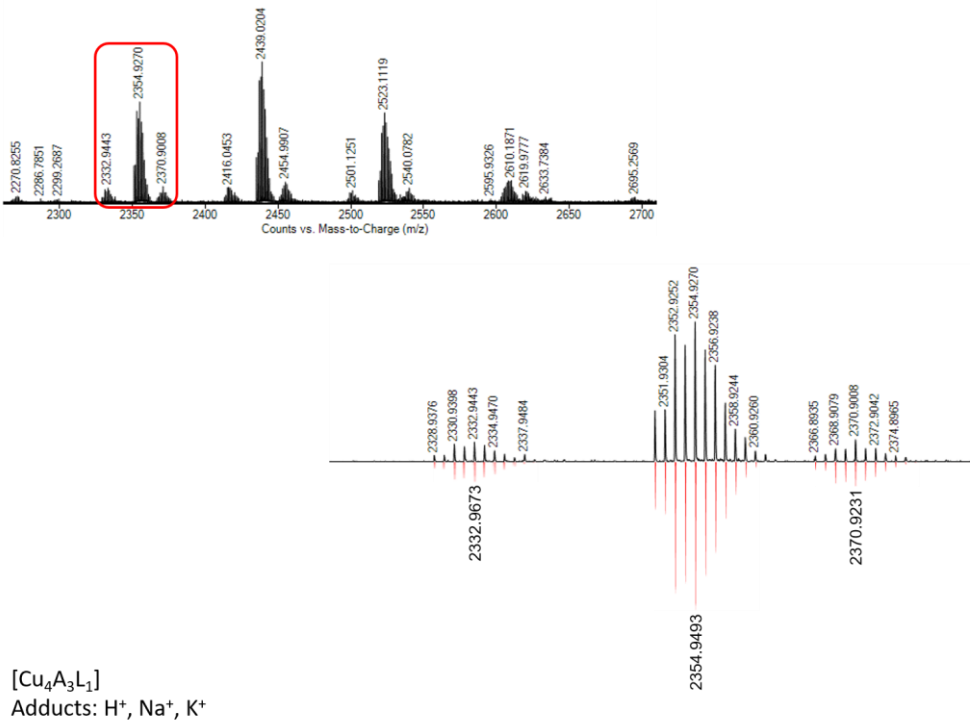

Figure S40. - A zoom of the signals in the MS analysis of the reaction mixture of H_2**A** and H_2**L** with copper(II) acetate that originate from $\mathbf{A_3L_1}$ as the H^+, Na^+ and K^+ adducts.

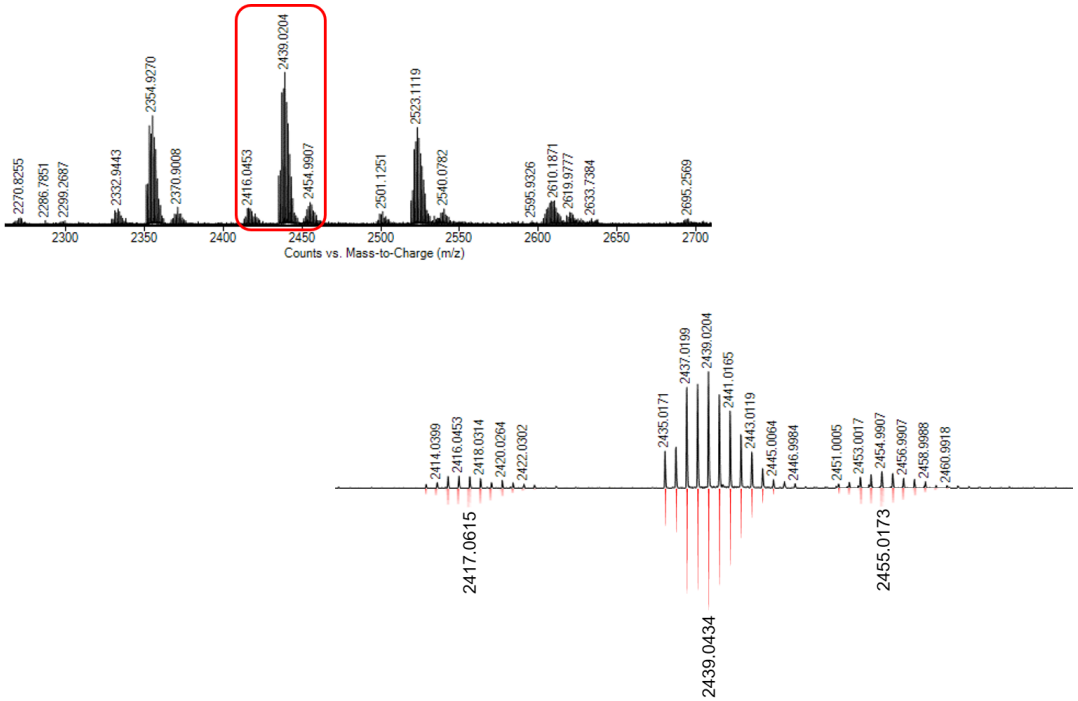

$[Cu_4A_2L_2]$
Adducts: H^+, Na^+, K^+

Figure S41. - A zoom of the signals in the MS analysis of the reaction mixture of H_2**A** and H_2**L** with copper(II) acetate that originate from $\mathbf{A_2L_2}$ as the H^+, Na^+ and K^+ adducts.

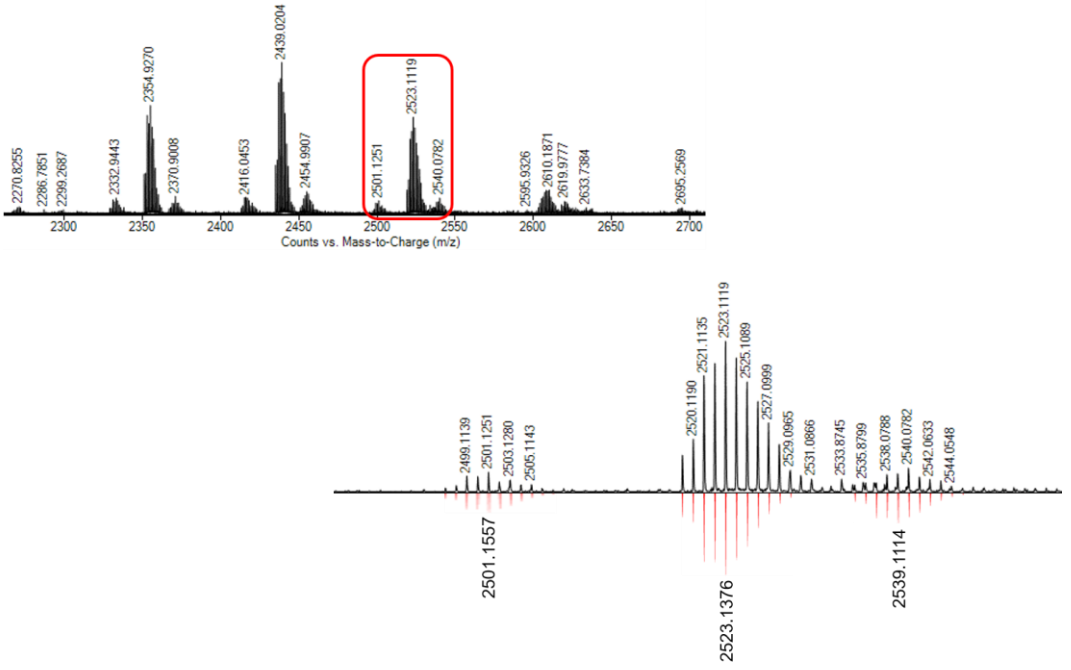

$[Cu_4A_1L_3]$
Adducts: H^+, Na^+, K^+

Figure S42. - A zoom of the signals in the MS analysis of the reaction mixture of H_2**A** and H_2**L** with copper(II) acetate that originate from $\mathbf{A_1L_3}$ as the H^+, Na^+ and K^+ adducts.

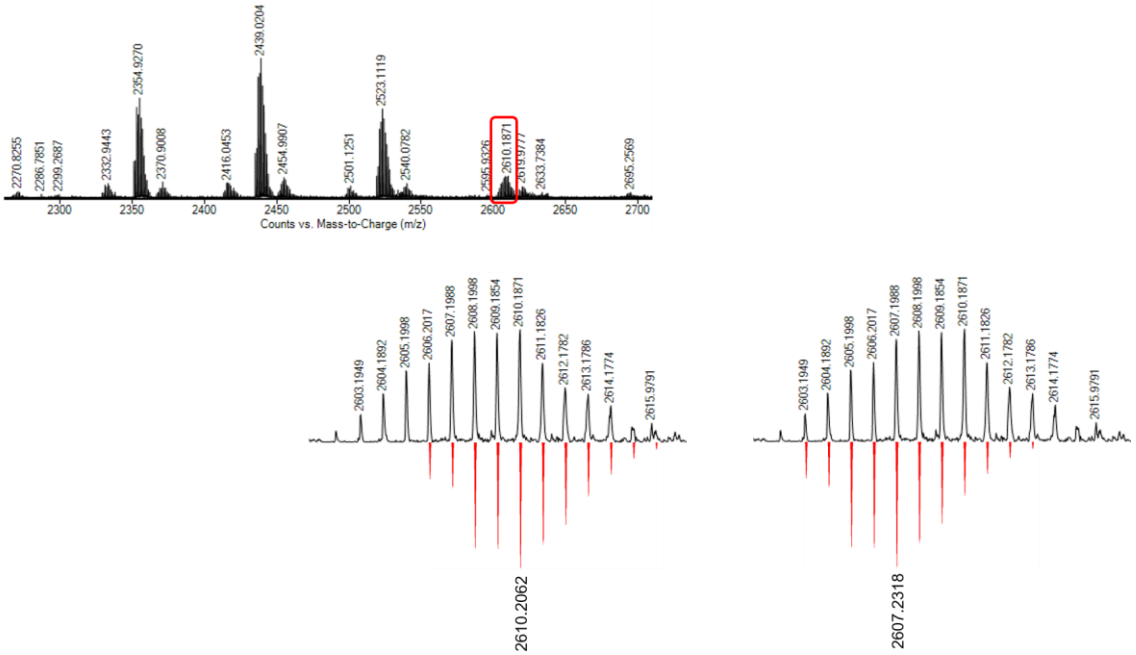

$[Cu_4A_1L_3]$·DMA and $[Cu_4L_4]$
Adducts: Na^+,

Figure S43. - A zoom of the signals in the MS analysis of the reaction mixture of H_2**A** and H_2**L** with copper(II) acetate that originate from $\mathbf{A_1L_3}$·(DMA) and $\mathbf{L_4}$ as the Na^+ adducts.

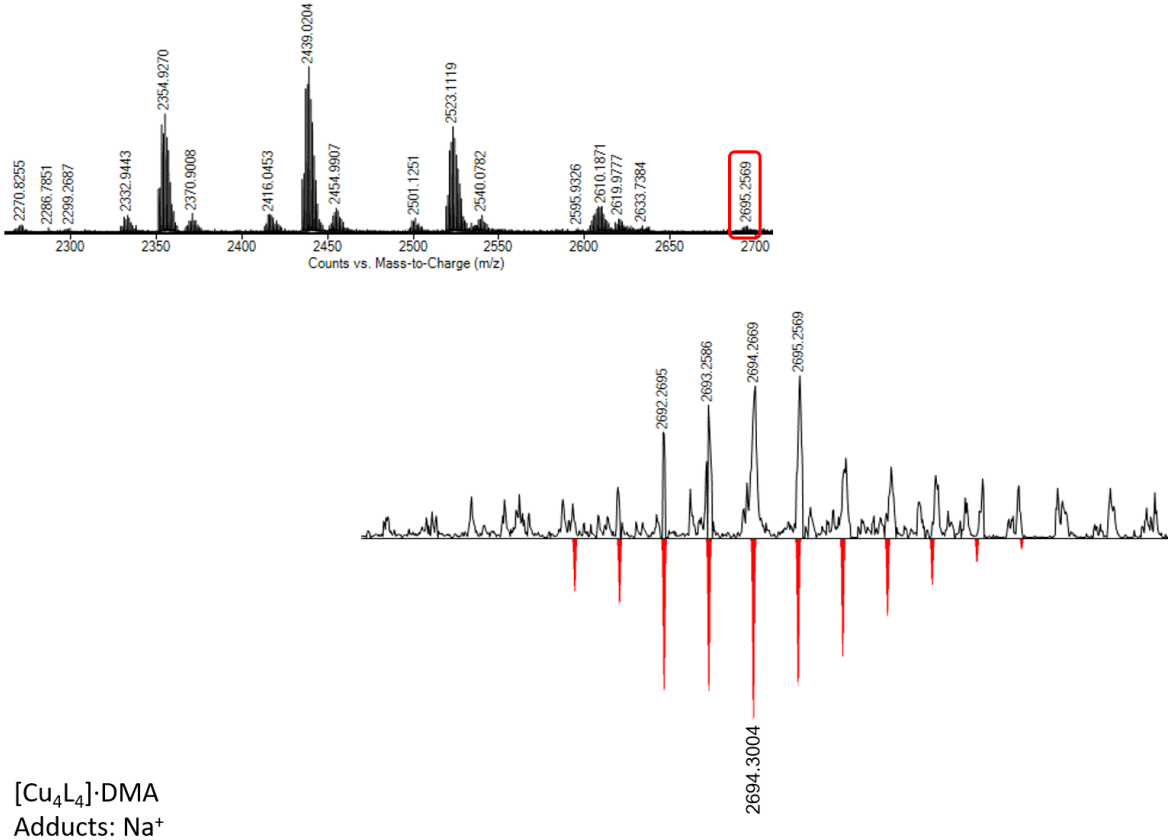

$[Cu_4L_4]$·DMA
Adducts: Na^+

Figure S44. - A zoom of the signals in the MS analysis of the reaction mixture of H_2**A** and H_2**L** with copper(II) acetate that originate from $\mathbf{A_1L_3}$·(DMA) and $\mathbf{L_4}$ as the Na^+ adducts.

*Synthesis of heteroleptic coordination cages with (S)-**A** and (R)-**L***

(*S*)-H_2**A** (74 mg, 0.149 mmol) is dissolved in 1 mL acetonitrile, (*R*)-H_2**L** (87 mg, 0.149 mmol) was dissolved in 1 mL acetonitrile, and $Cu(OAc)_2$ (27 mg, 0.075 mmol) dissolved in 5 mL acetonitrile. 80 µL of the H_2**A** solution and 80 µL of the (*R*)-H_2**L** solution were mixed, and to this mixture is added 800 µL of the $Cu(OAc)_2$ solution. The solution was made up to 6 mL with acetonitrile. Analysis after addition of the ligand to the metal suggests immediate complexation to form the (*S*)-$\mathbf{A_n}$(*R*)-$\mathbf{L_{4-n}}$ (n=0,1,3,4) complexes as a solution with a cumulative coordination cage concentration of 1 mM (quantitative yield).

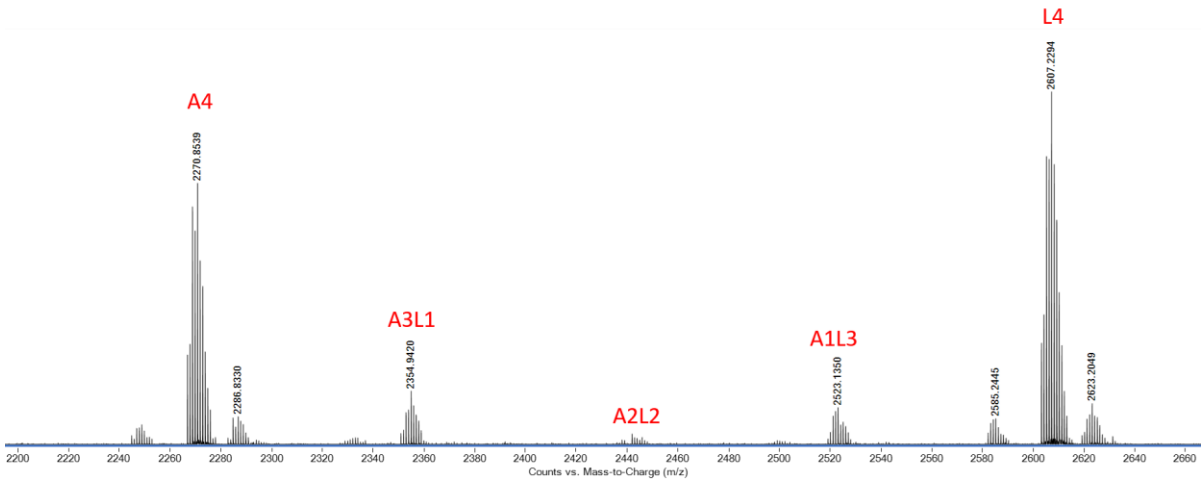

Figure S45. - MS analysis of the reaction mixture of (*S*)-H_2**A** and (*R*)-H_2**L** with copper(II) acetate gave rise to signals originating from the homoleptic species $\mathbf{A_4}$ and $\mathbf{L_4}$ and the heteroleptic species $\mathbf{A_3L_1}$ and $\mathbf{A_1L_3}$.

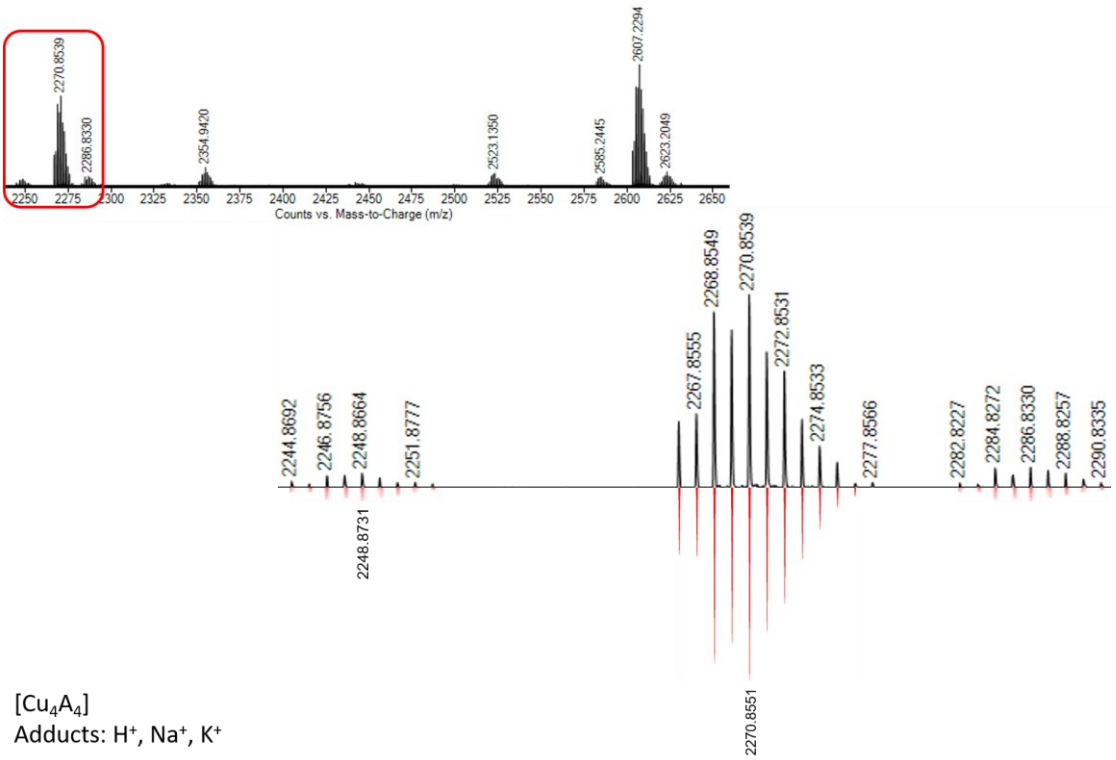

$[Cu_4A_4]$
Adducts: H^+, Na^+, K^+

Figure S46. - A zoom of the signals in the MS analysis of the reaction mixture of (*S*)-H_2**A** and (*R*)-H_2**L** with copper(II) acetate that originate from $\mathbf{A_4}$ as the H^+, Na^+ and K^+ adducts.

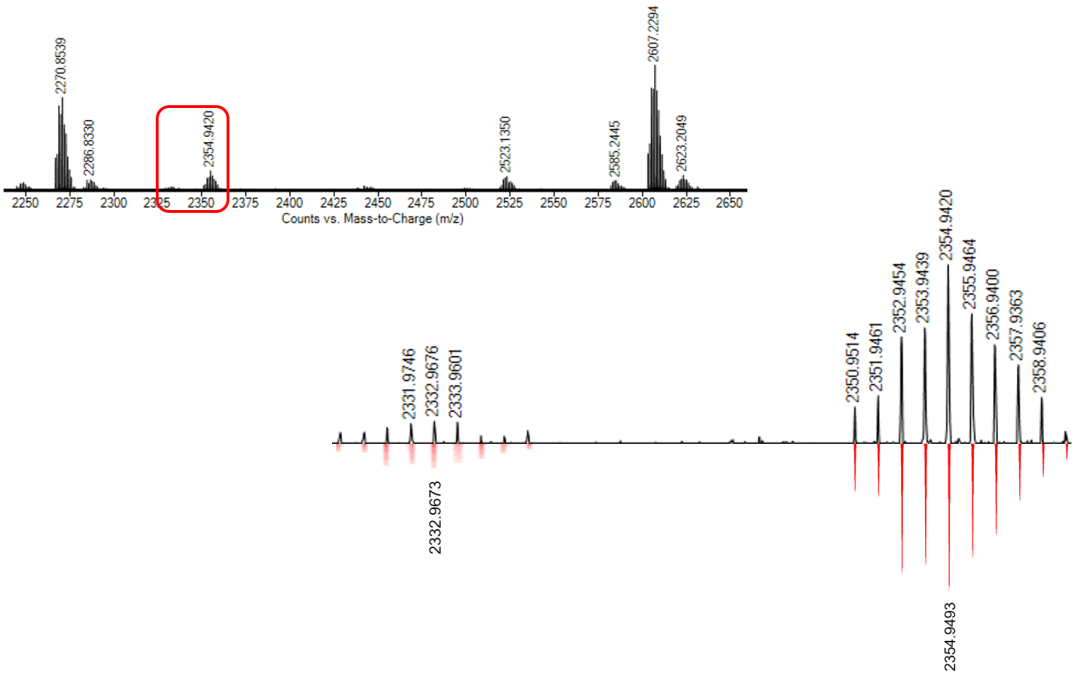

$[Cu_4A_3L_1]$
Adducts: H^+, Na^+

Figure S47. - A zoom of the signals in the MS analysis of the reaction mixture of (*S*)-H_2**A** and (*R*)-H_2**L** with copper(II) acetate that originate from $\mathbf{A_3L_1}$ as the H^+ and Na^+ adducts.

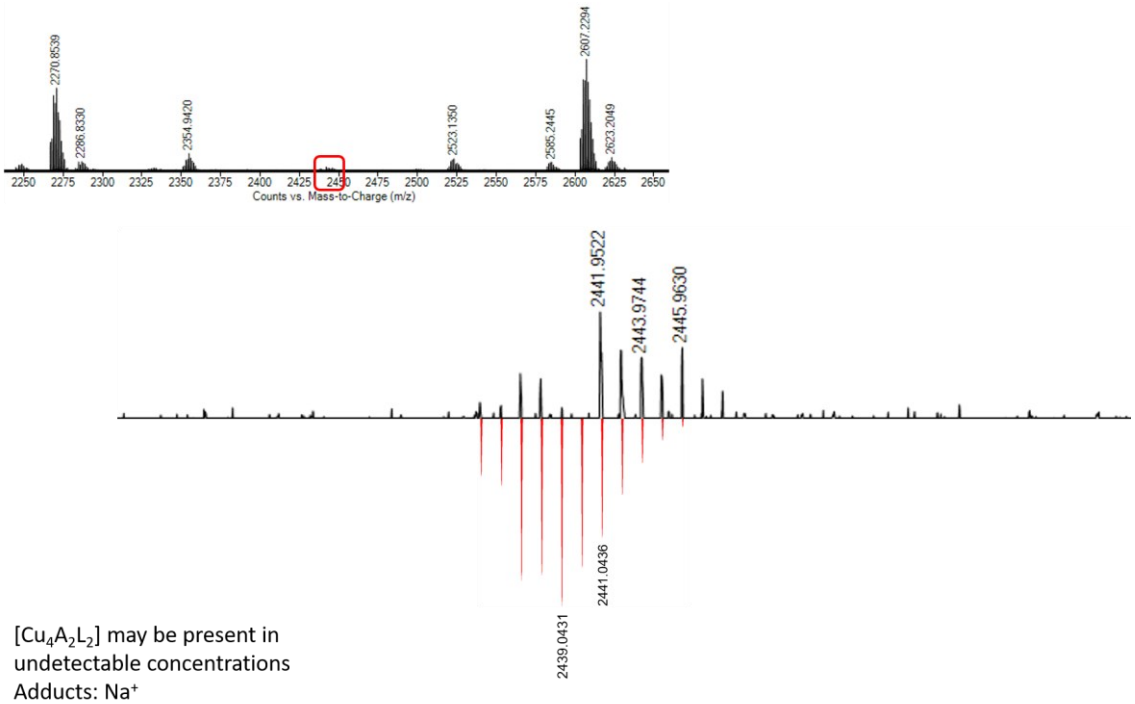

Figure S48. – The predicted MS spectrum of A2L2 overlaid over the region in which it would be expected to be observed in the reaction mixture of (*S*)-H_2**A** and (*R*)-H_2**L** with copper(II) acetate.

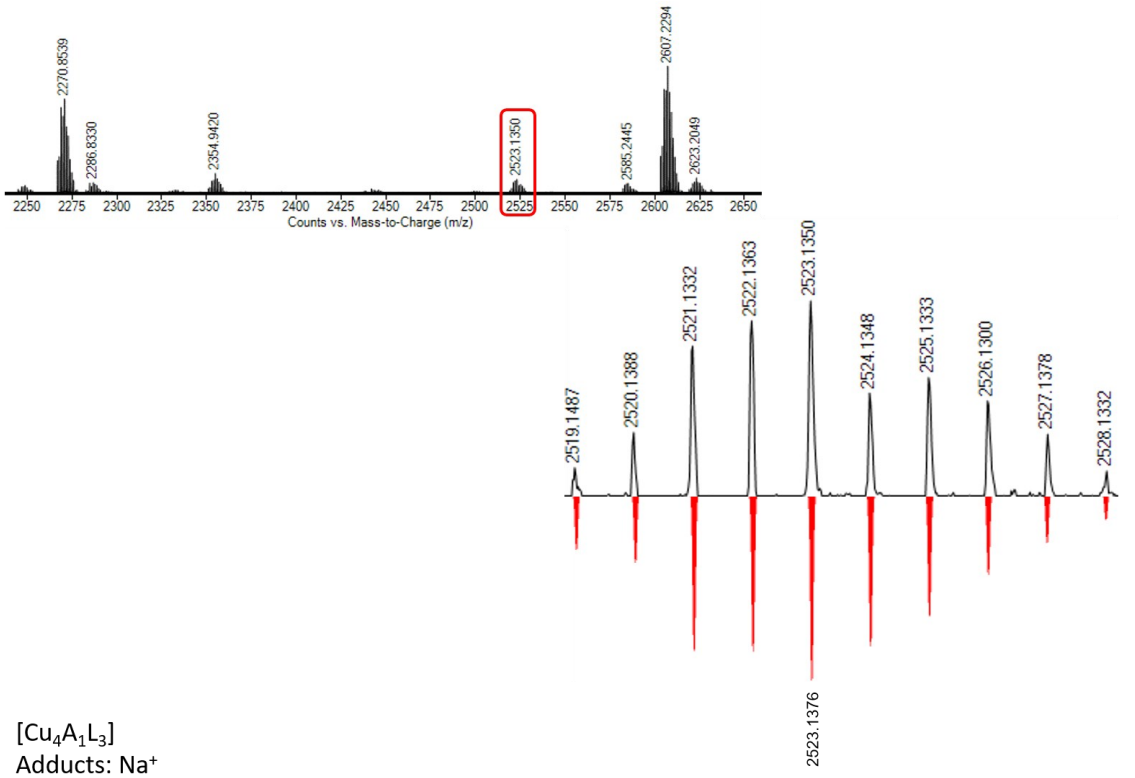

Figure S49. - A zoom of the signals in the MS analysis of the reaction mixture of (*S*)-H_2**A** and (*R*)-H_2**L** with copper(II) acetate that originate from $\mathbf{A_1L_3}$ as the Na^+ adduct.

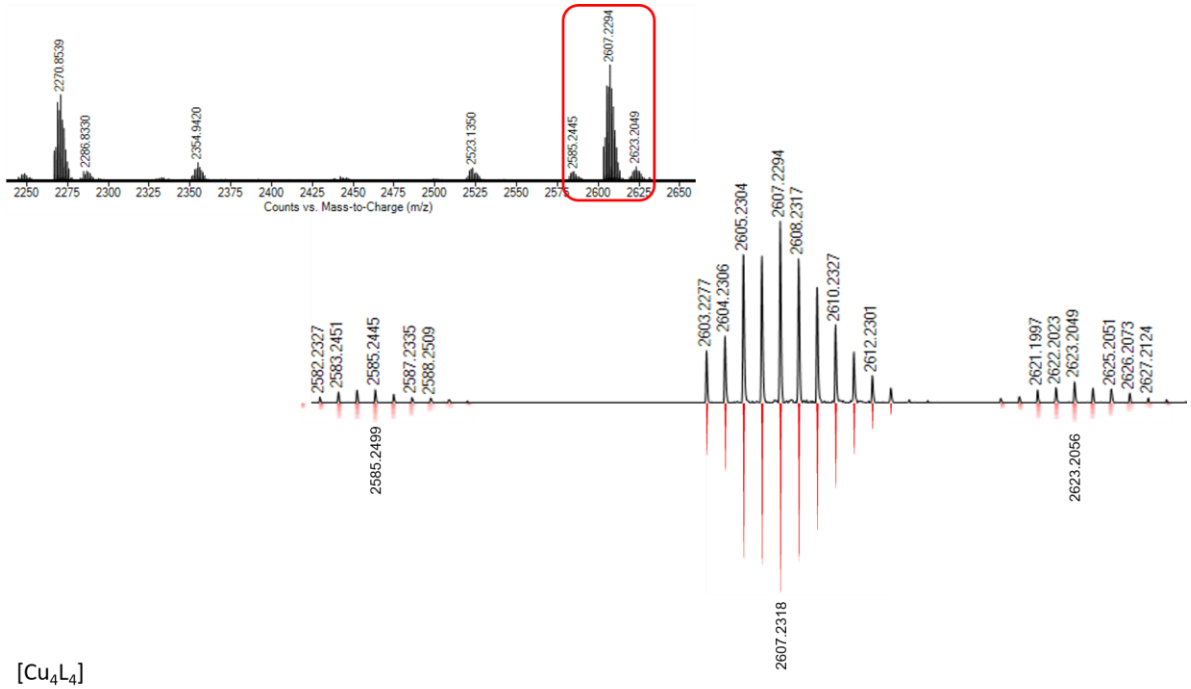

$[Cu_4L_4]$
Adducts: H^+, Na^+, K^+

Figure S50. - A zoom of the signals in the MS analysis of the reaction mixture of (*S*)-H_2**A** and (*R*)-H_2**L** with copper(II) acetate that originate from $\mathbf{L_4}$ as the H^+, Na^+ and K^+ adducts.

Synthesis of ***G*$_2$*I*$_2$**

H_2**G** (70 mg, 0.149 mmol) was dissolved in 1 mL dimethylacetamide, H_2**I** (79 mg, 0.149 mmol) is dissolved in 1 mL dimethylacetamide, and $Cu(OAc)_2$ (27 mg, 0.075 mmol) dissolved in 5 mL acetonitrile. 80 µL of the H_2**G** solution and 80 µL of the H_2**I** solution were mixed, and to this mixture was added 800 µL of the $Cu(OAc)_2$ solution. The solution was made up to 6 mL with acetonitrile. Analysis by HPLC after addition of the ligand to the metal shows immediate complexation to form the **G**$_2$**I**$_2$ complex as a 1 mM solution (quantitative yield). After 3 days of being left to sit at room temperature, large blue cubic crystals were deposited onto the wall of the vial in which the reaction mixture was stored. SCXRD studies confirmed these crystals to consist of **G**$_2$**I**$_2$ (Figure S51).

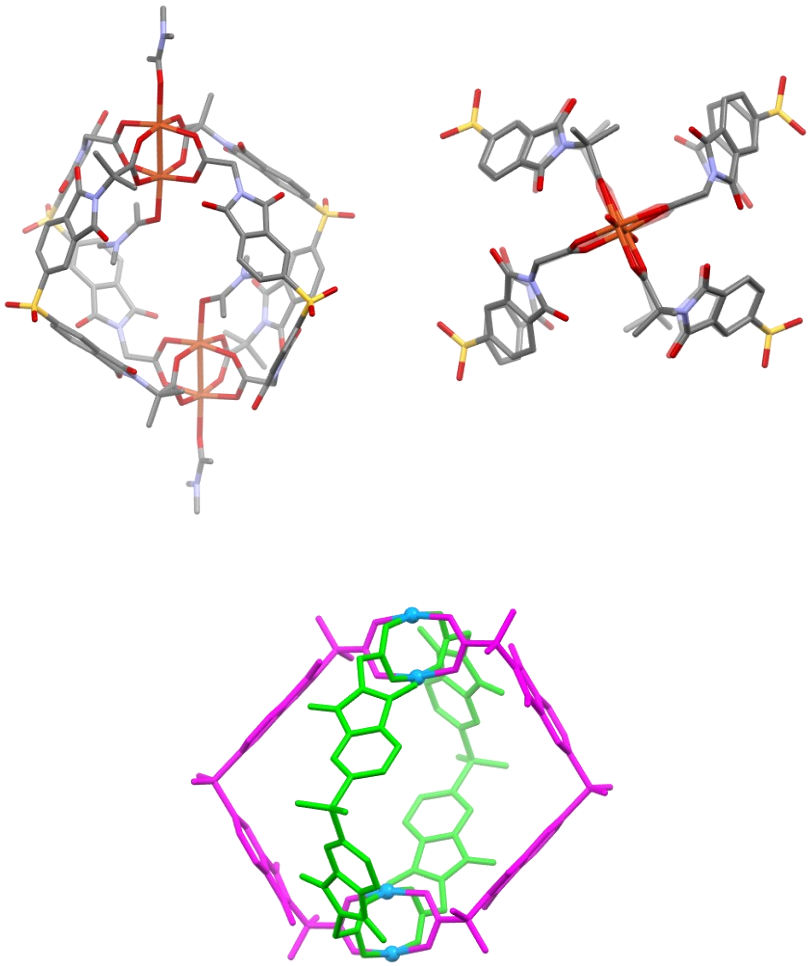

Figure S51. - The molecular structure of $[Cu_4$**G**$_2$**I**$_2(DMA)_{2.5}(OH_2)_{1.5}]\cdot 6.66(DMA)\cdot 3(H_2O)$ (**G**$_2$**I**$_2$) as determined by X-ray crystallographic studies. Left: Two of ligand **G** and two of ligand **I** link the two Cu_2 paddlewheel nodes in a *trans* fashion relative to ligands of the same type to form the lantern-type cage architecture. Right: Looking along the Cu_2 – Cu_2 axis shows the mesocate conformation that this species takes due to the presence of chiral functionalities which drive formation of the helix. Bottom: The coordination cage **G**$_2$**I**$_2$ with **G** ligands coloured magenta and **I** ligands coloured green.

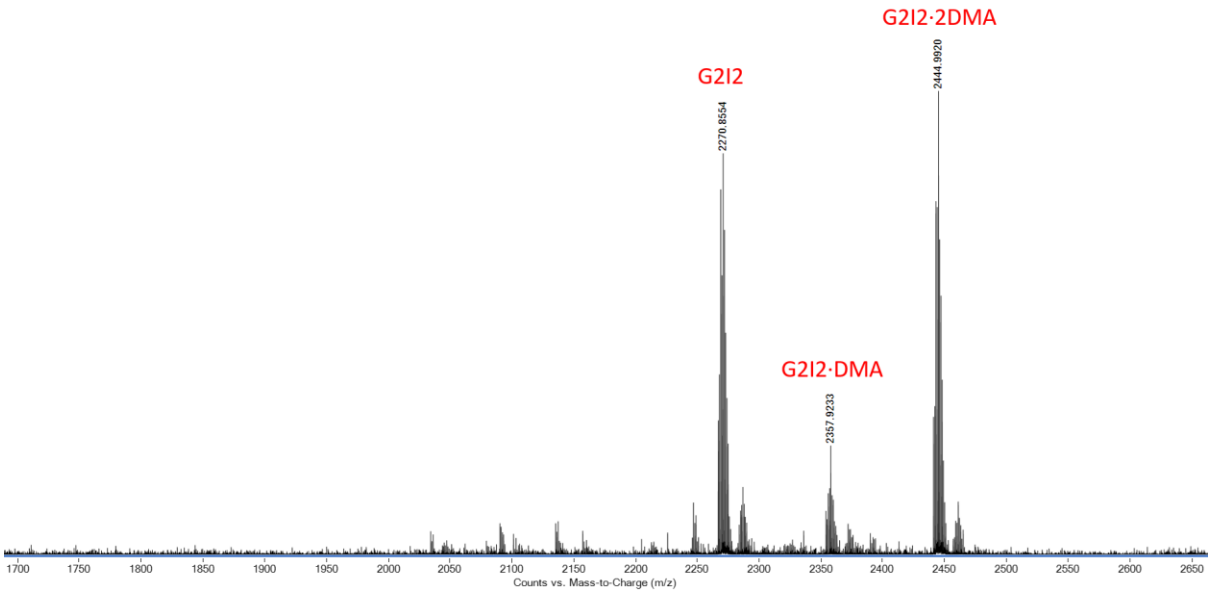

Figure S52. – MS analysis of the reaction mixture of H_2**A** and H_2**L** with copper(II) acetate gave rise to signals originating from only the heteroleptic species **G_2I_2**.

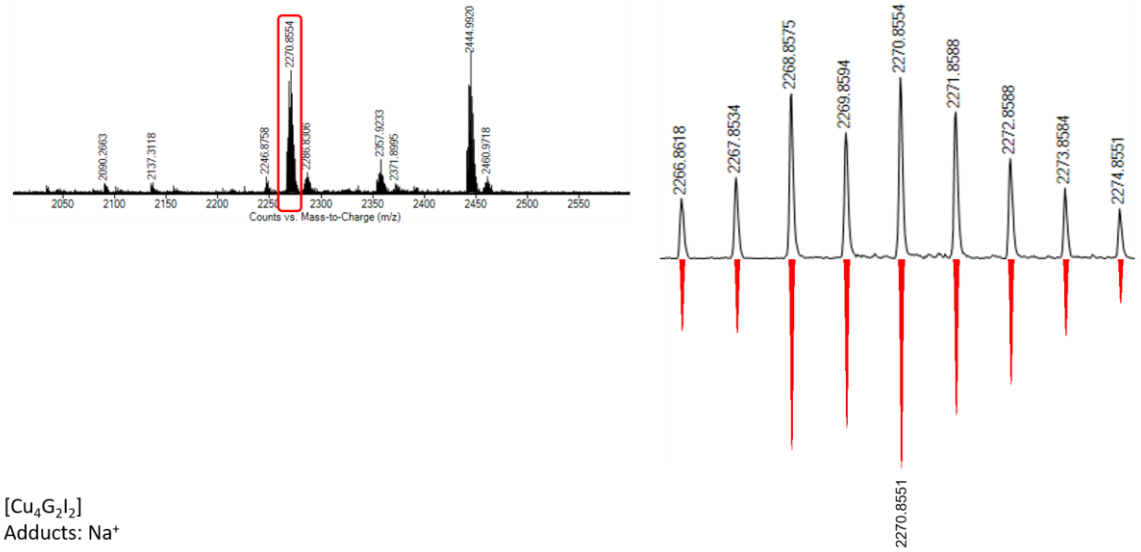

Figure S53. - A zoom of the signals in the MS analysis of the reaction mixture of H_2**G** and H_2**I** with copper(II) acetate that originate from **G_2I_2** as the Na^+ adducts.

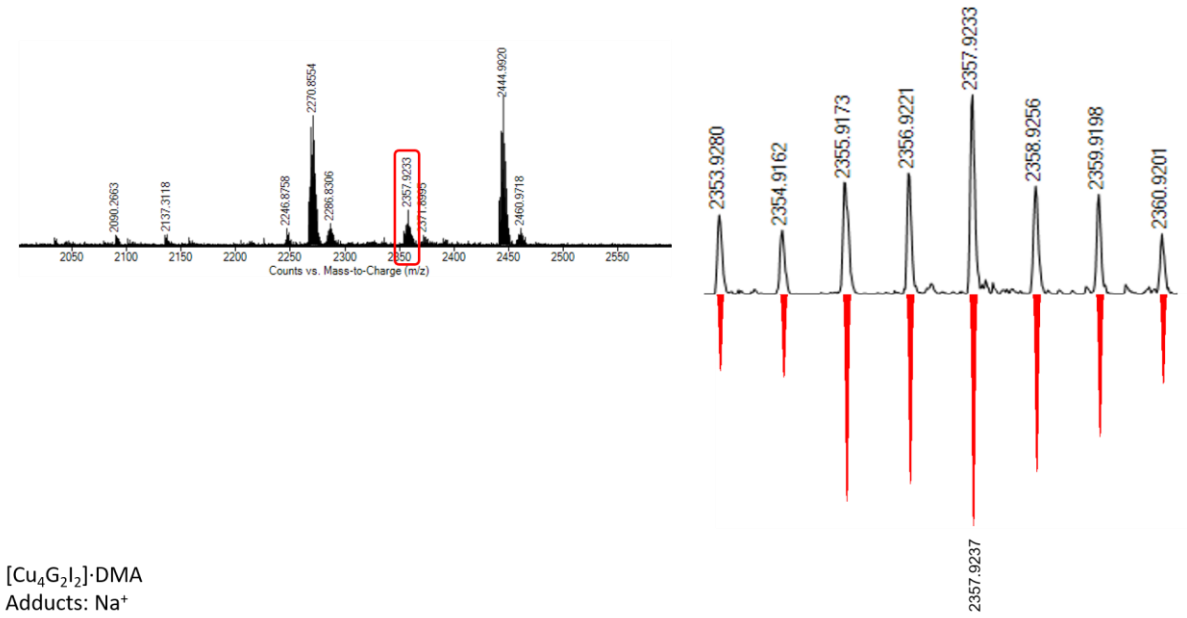

Figure S54. - A zoom of the signals in the MS analysis of the reaction mixture of H_2**G** and H_2**I** with copper(II) acetate that originate from **G_2I_2**·DMA as the Na^+ adducts.

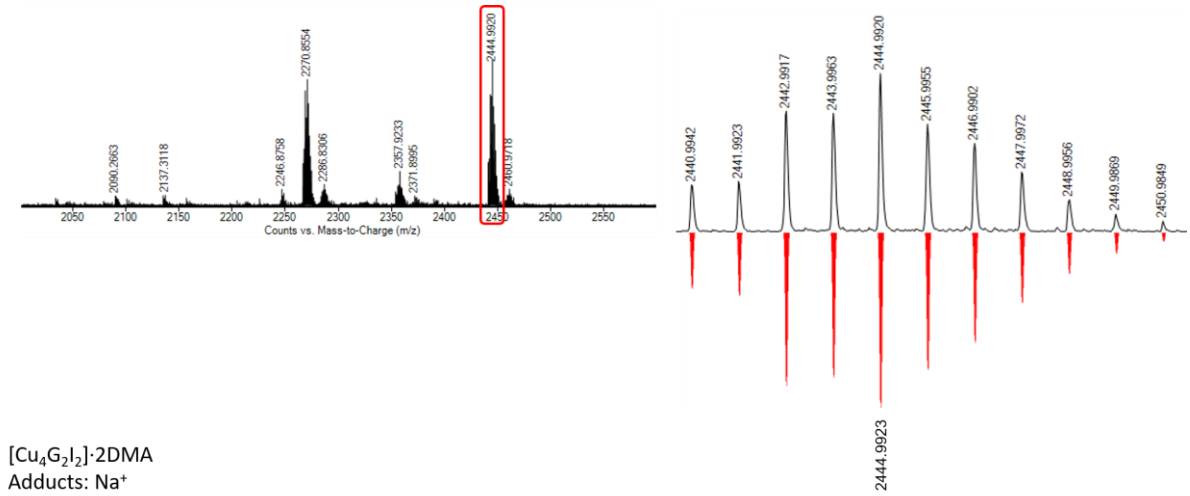

Figure S55. - A zoom of the signals in the MS analysis of the reaction mixture of H_2**G** and H_2**I** with copper(II) acetate that originate from **G_2I_2**·2DMA as the Na^+ adducts.

Synthesis of ***G_2V_2***

H_2**G** (70 mg, 0.149 mmol) was dissolved in 1 mL dimethylacetamide, H_2**V** (87 mg, 0.149 mmol) is dissolved in 1 mL dimethylacetamide, and $Cu(OAc)_2$ (27 mg, 0.075 mmol) dissolved in 5 mL acetonitrile. 80 µL of the H_2**G** solution and 80 µL of the H_2**V** solution were mixed, and to this mixture was added 800 µL of the $Cu(OAc)_2$ solution. The solution was made up to 6 mL with acetonitrile. Analysis by HPLC and mass spectrometry after addition of the ligand to the metal shows immediate complexation to form the **G_2V_2** complex as a 1 mM solution (quantitative yield).

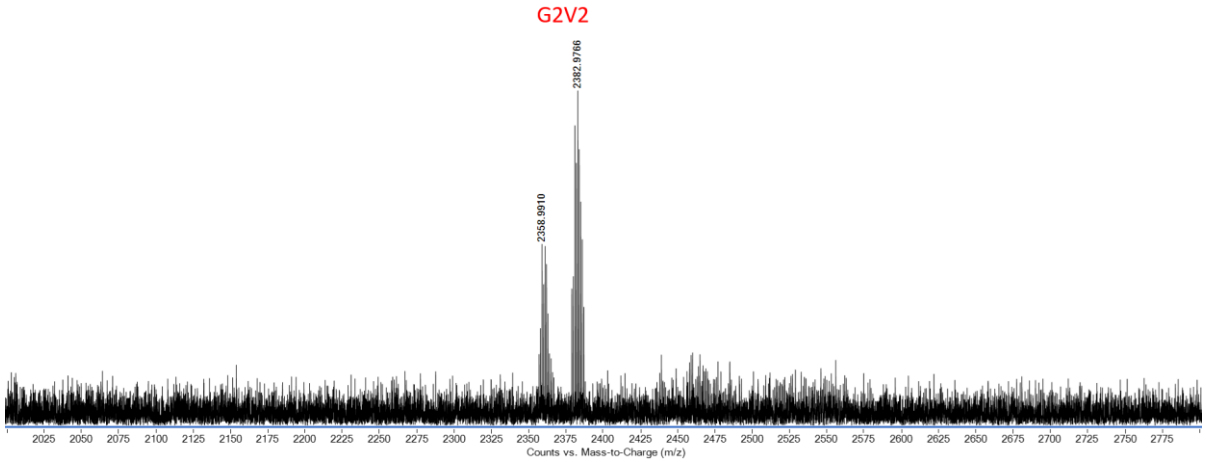

Figure S56. - MS analysis of the reaction mixture of H_2**A** and H_2**L** with copper(II) acetate gave rise to signals originating from only the heteroleptic species **G_2V_2**.

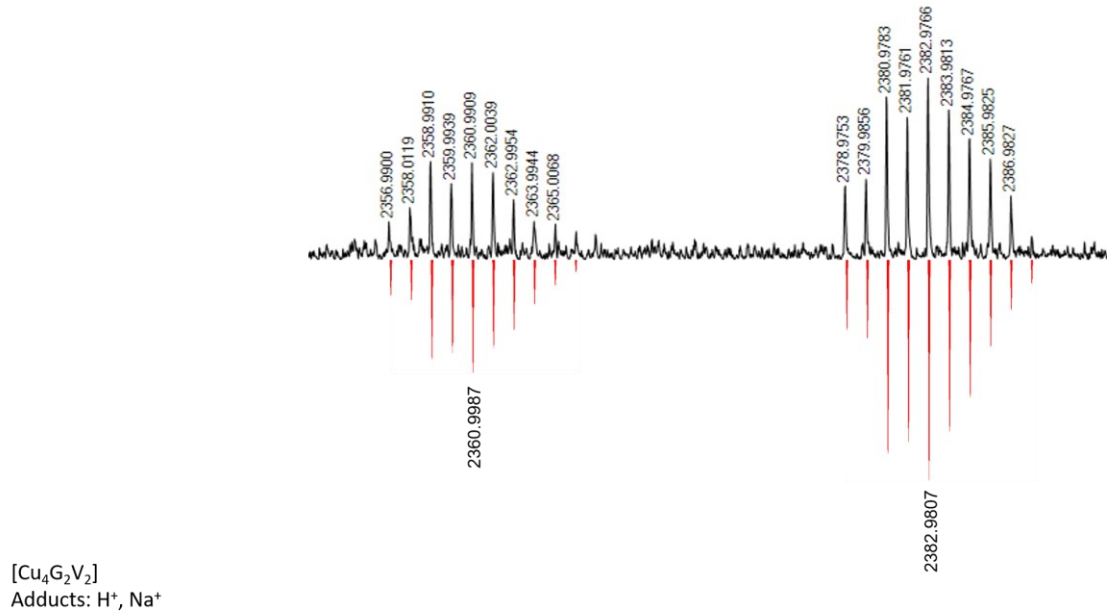

Figure S57. - A zoom of the signals in the MS analysis of the reaction mixture of H_2**G** and H_2**I** with copper(II) acetate that originate from **G_2I_2** as the H^+ and Na^+ adducts.

HPLC analysis

Ligand exchange reaction between homoleptic cages $\mathbf{A}_4$ and $\mathbf{L}_4$

1 mM solutions of $\mathbf{A}_4$ and $\mathbf{L}_4$ were prepared and 50 µL aliquots of each added to a vial containing 900 µL acetonitrile. Immediately upon addition, the vial was capped and shaken and a 10 µL aliquot injected into the HPLC for analysis. 10 µL aliquots were taken and analysed by HPLC every 10 minutes until the ligand exchange reaction reached equilibrium (Figure 2).

Reactions between homoleptic cages and homoleptic cages with free ligand

A 1 mM solution of homoleptic cage $\mathbf{A}_4$ and a 4 mM solution of $H_2\mathbf{L}$ was prepared as previously described. 50 µL of each were mixed by adding to 900 µL acetonitrile to make a 1 mL reaction mixture. Aliquots of 10 µL of this reaction mixture were injected into the HPLC every 10 minutes and the distribution of species present was analysed by the differences in retention time and absorption at 254 nm.

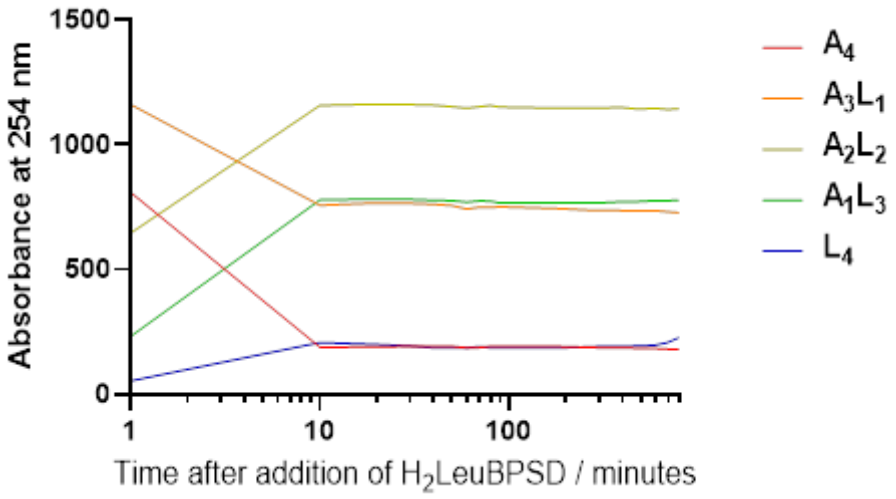

Figure S58. - Ligand exchange to form a statistical mixture from a solution containing $\mathbf{A}_4$ and $H_2\mathbf{L}$ occurred within 10 minutes.

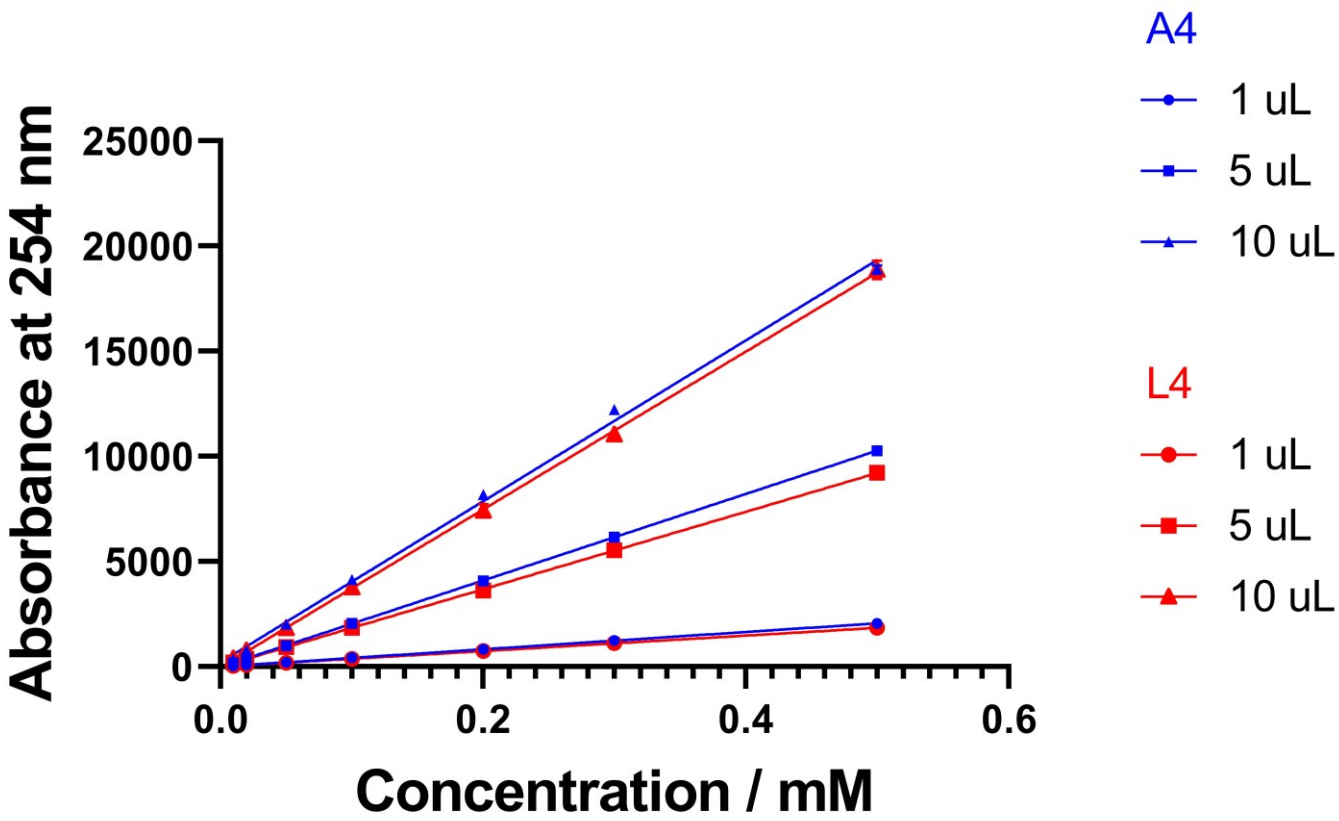

Figure S59. – Concentration curves for **A_4** and **L_4** with the absorbance measured using the HPLC with different injection volumes. The gradients (38877±687 and 37424±400 respectively) are similar enough that we can approximate signals of equivalent intensity from each species to correspond to equivalent concentrations.

HPLC control experiments

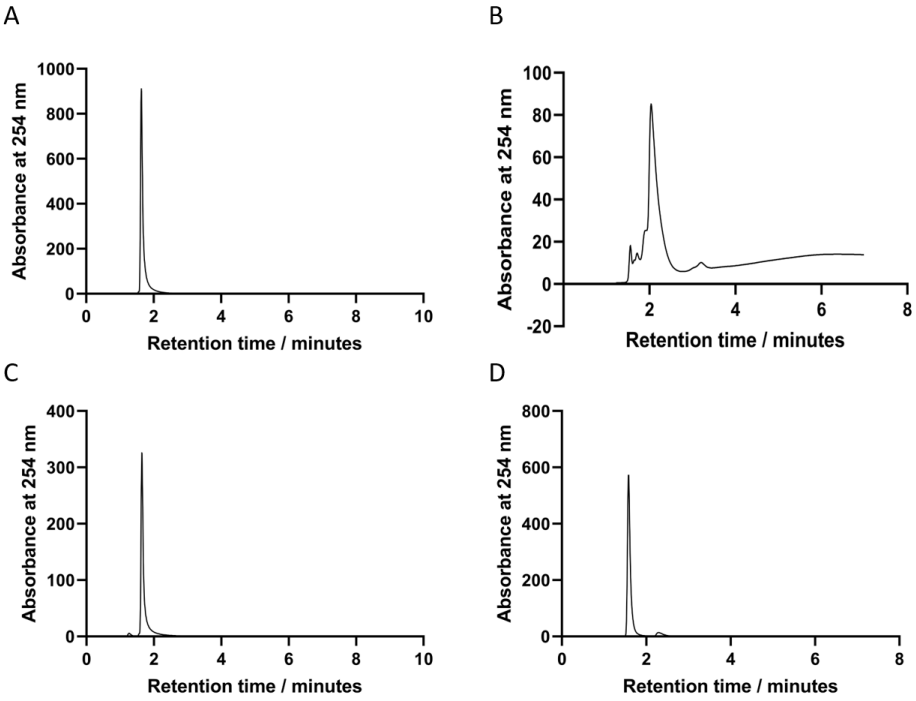

Figure S60. – The HPLC traces of H_2**G** with a mobile phase of 70 % water/30 % acetonitrile/0.1 % formic acid (A) and with 100 % acetonitrile (B), and H_2**G** and $Cu(OAc)_2$ with a mobile phase of 70 % water/30 % acetonitrile/0.1 % formic acid (C) and with 100 % acetonitrile (D).

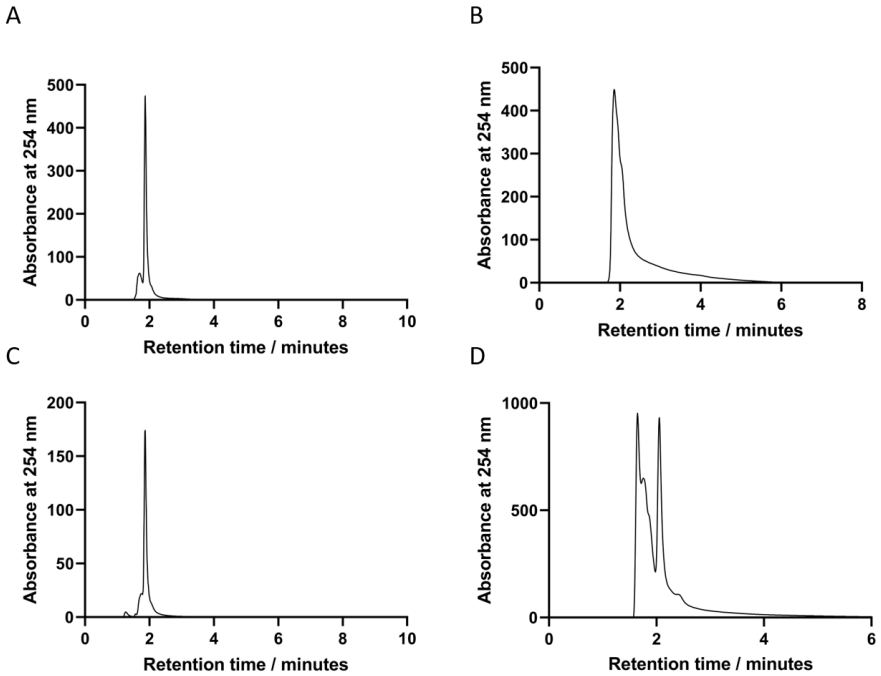

Figure S61. - The HPLC traces of H_2**I** with a mobile phase of 70 % water/30 % acetonitrile/0.1 % formic acid (A) and with 100 % acetonitrile (B), and H_2**I** and $Cu(OAc)_2$ with a mobile phase of 70 % water/30 % acetonitrile/0.1 % formic acid (C) and with 100 % acetonitrile (D).

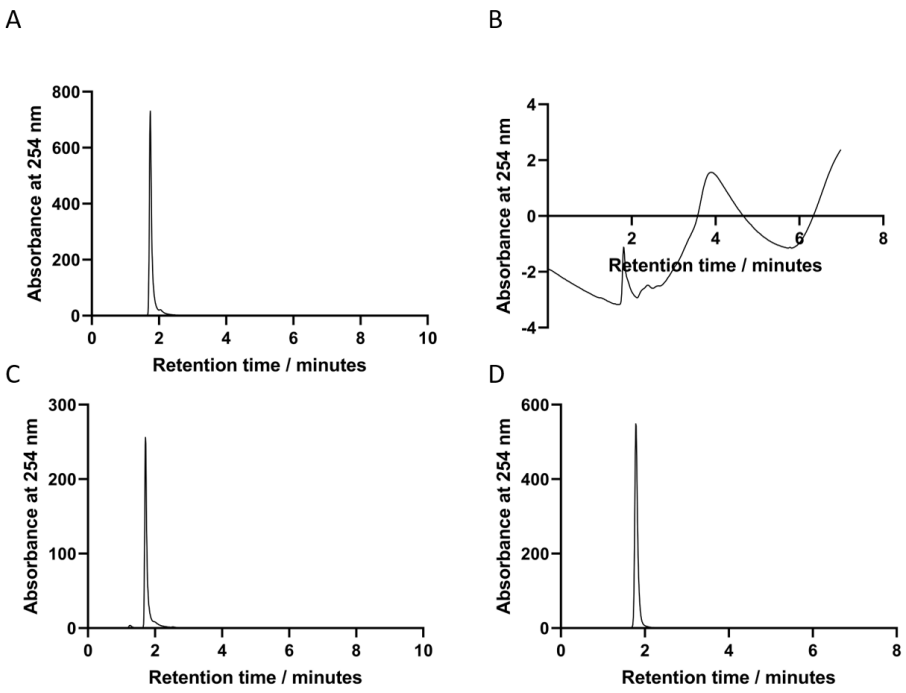

Figure S62. - The HPLC traces of H_2**A** with a mobile phase of 70 % water/30 % acetonitrile/0.1 % formic acid (A) and with 100 % acetonitrile (B), and H_2**A** and $Cu(OAc)_2$ with a mobile phase of 70 % water/30 % acetonitrile/0.1 % formic acid (C) and with 100 % acetonitrile (D).

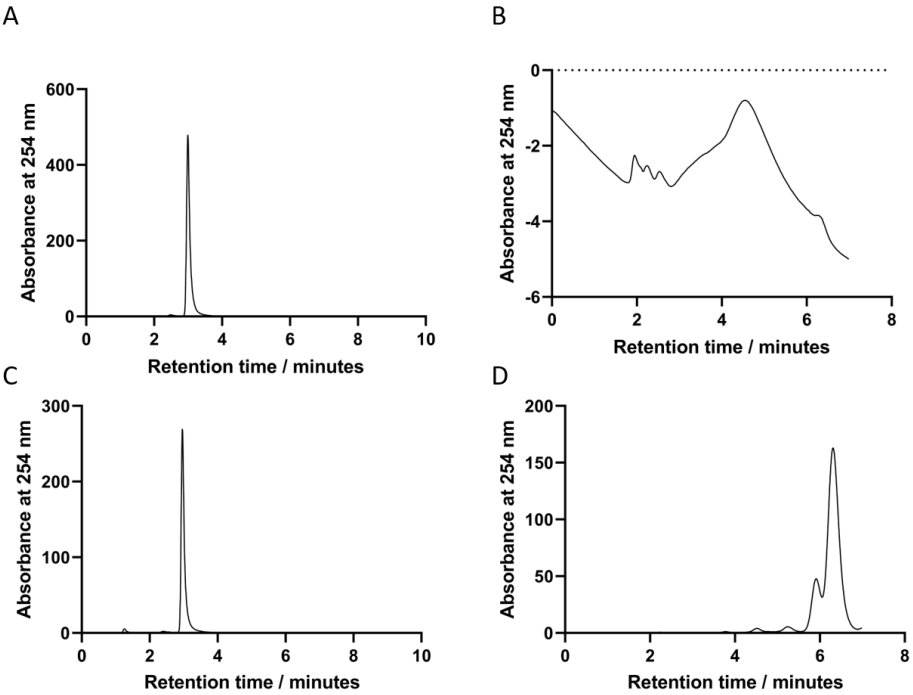

Figure S63. - The HPLC traces of H_2**L** with a mobile phase of 70 % water/30 % acetonitrile/0.1 % formic acid (A) and with 100 % acetonitrile (B), and H_2**L** and $Cu(OAc)_2$ with a mobile phase of 70 % water/30 % acetonitrile/0.1 % formic acid (C) and with 100 % acetonitrile (D).

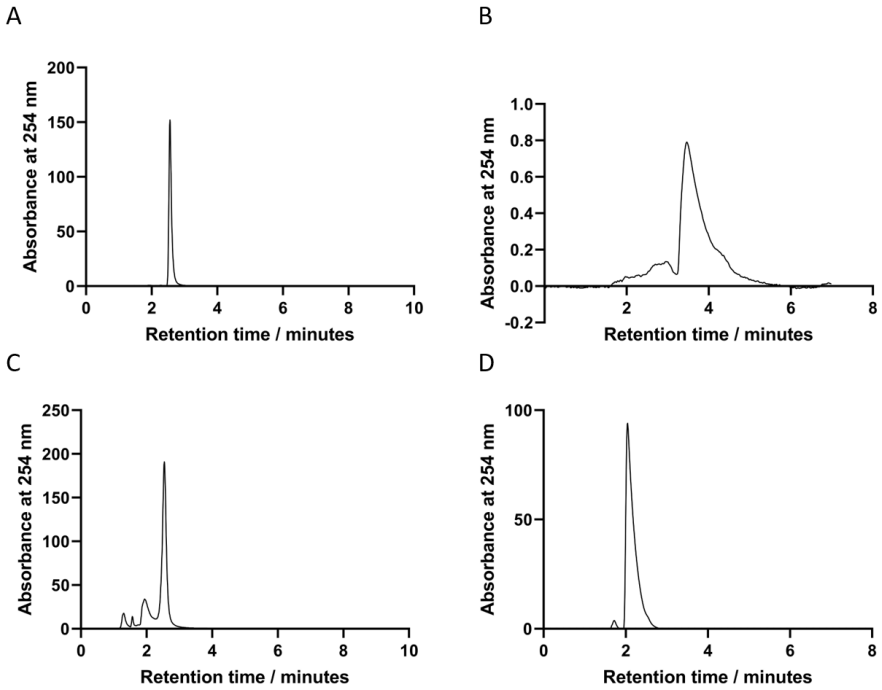

Figure S64. - The HPLC traces of H_2**V** with a mobile phase of 70 % water/30 % acetonitrile/0.1 % formic acid (A) and with 100 % acetonitrile (B), and H_2**V** and $Cu(OAc)_2$ with a mobile phase of 70 % water/30 % acetonitrile/0.1 % formic acid (C) and with 100 % acetonitrile (D).

Heteroleptic coordination cage redistribution

The mixed cage system is prepared as previously detailed. 50 µL of the resulting solution is injected into the HPLC column and the mixture of complexes separated using a C_{18} column with an eluent system of 100% acetonitrile at a flow rate of 0.3 mL/min. Collection of the elute between 4.2-4.6 minutes, 5.0-5.4 minutes and 6.6-7.0 minutes yielded pure $\mathbf{A_3L_1}$, $\mathbf{A_2L_2}$, and $\mathbf{A_1L_3}$ respectively. While the elute is pure at time of initial separation on the column, disproportionation of the complexes to a mixture of species occurs rapidly. As such, fresh samples must be obtained each time when observing the kinetics of the redistribution of these species.

After purification of each of $\mathbf{A_3L_1}$, $\mathbf{A_2L_2}$, and $\mathbf{A_1L_3}$, the sample was diluted to 1 mL with acetonitrile and analysed by UV-HPLC with an eluent system of 30% water + 0.1% formic acid in acetonitrile. The area under each signal was then integrated and the ratio between the area of each signal calculated to give the ratio between the two ligands in each species (Figure **S65**).

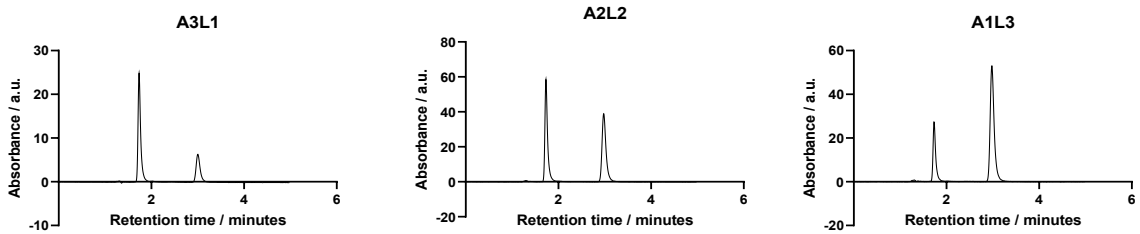

Figure S65. Absorption response at 254 nm of the free ligands after decomplexation of $\mathbf{A_3L_1}$ (left), $\mathbf{A_2L_2}$ (centre), and $\mathbf{A_1L_3}$ (right). The ratio of ligands is consistent with that expected from these complexes (3:1, 1:1 and 1:3, respectively).

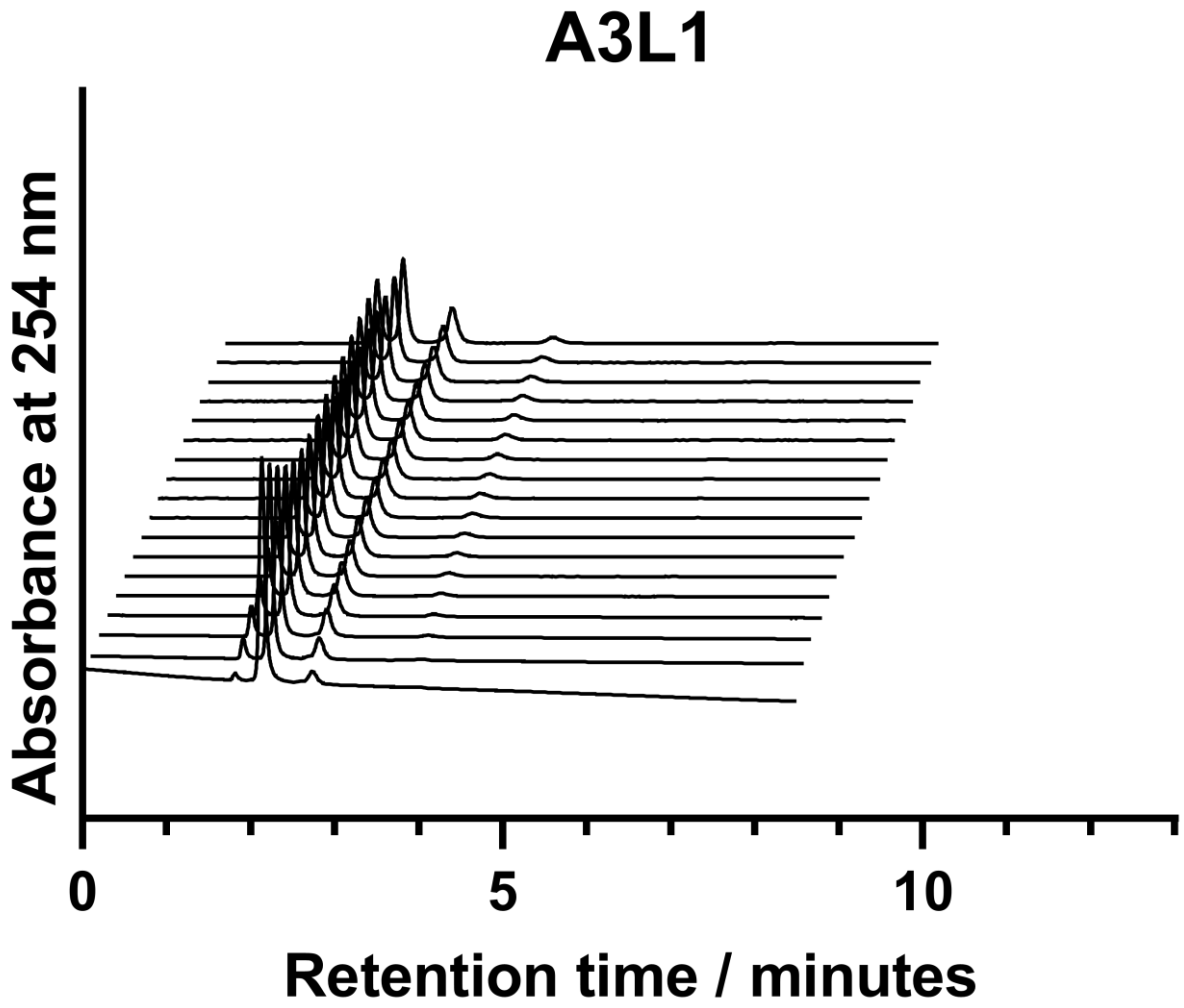

Figure S66. – Stack plot of raw HPLC data of the redistribution of A_3L_1 to a statistical mixture.

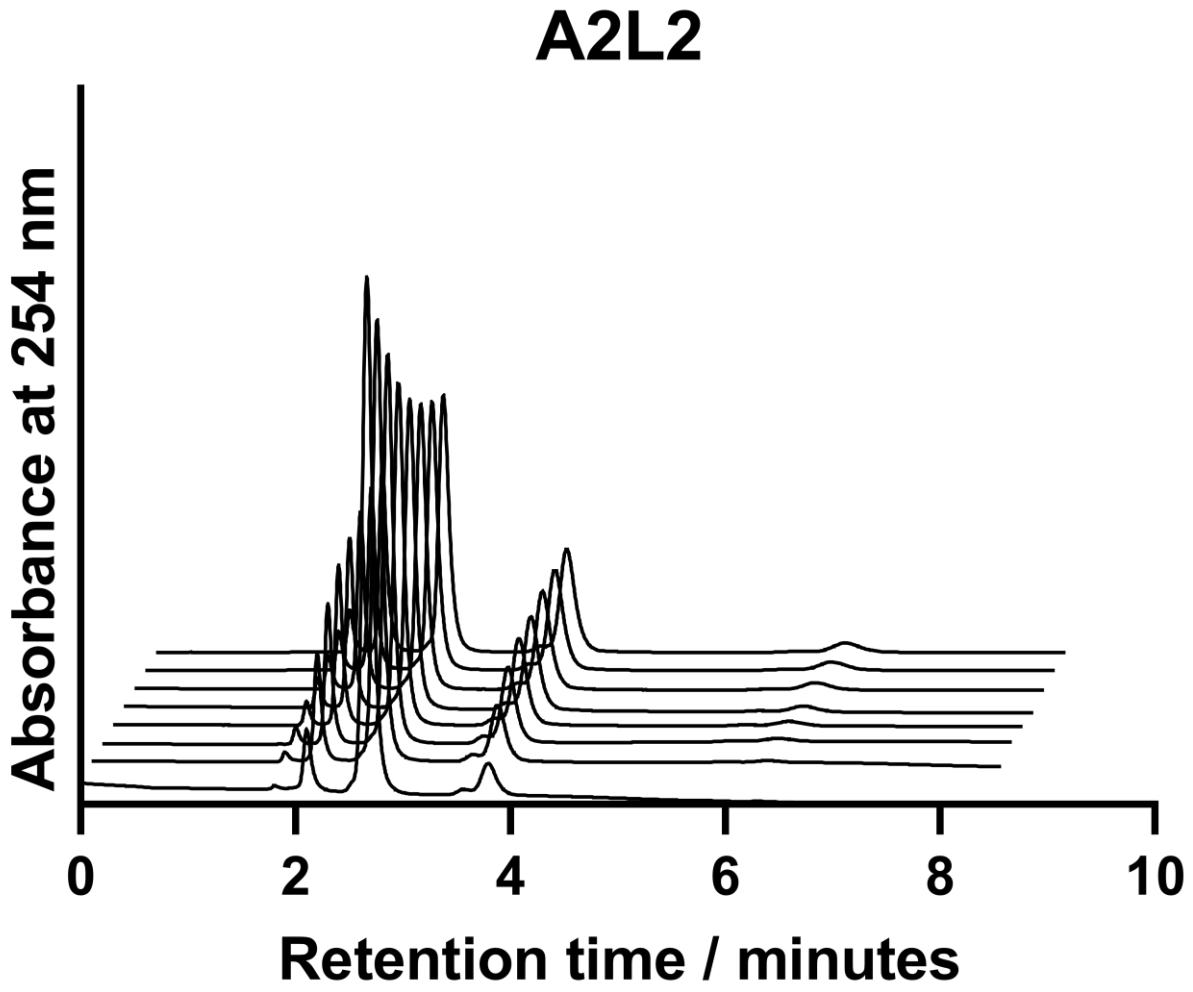

Figure S67. – Stack plot of raw HPLC data of the redistribution of $\mathbf{A_2L_2}$ to a statistical mixture.

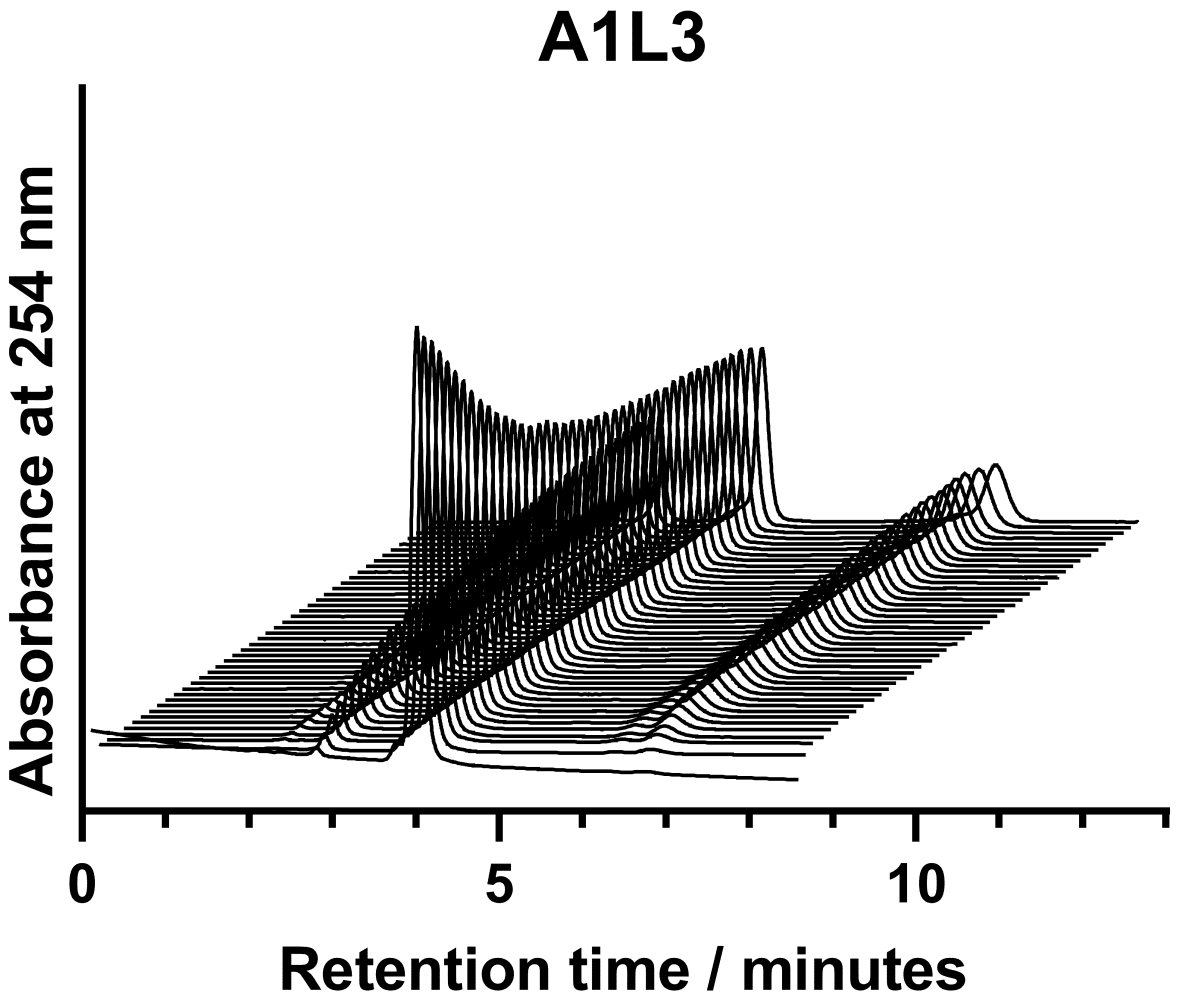

Figure S68. - Stack plot of raw HPLC data of the redistribution of $\mathbf{A_1L_3}$ to a statistical mixture.

Redistribution of $\mathbf{A_3L_1}$, $\mathbf{A_2L_2}$, and $\mathbf{A_1L_3}$ is observed by, immediately after purification, diluting the sample to 1 mL with acetonitrile and analysing by HPLC every 10 minutes. An eluent system of 100% acetonitrile at a flow rate of 1 mL/min is used, with UV-Vis spectroscopic analysis being conducted at 254 nm. Preparation of equimolar solutions of these species as it elutes from the HPLC instrument is not possible, and so three solutions of differing concentrations were made up through rough dilutions and back calculated from the total area under the curve using the gradients from the calibration curves for both $\mathbf{A_4}$ and $\mathbf{L_4}$, which encompass the range in which the redistribution experiment was run in order to determine whether concentration of the isolated complex plays a significant role in determining the rate of redistribution. As seen in Figure **S69**, the rate does not change considerably, especially compared to the change in rate observed between redistribution of $\mathbf{A_3L_1}$ and $\mathbf{A_1L_3}$.

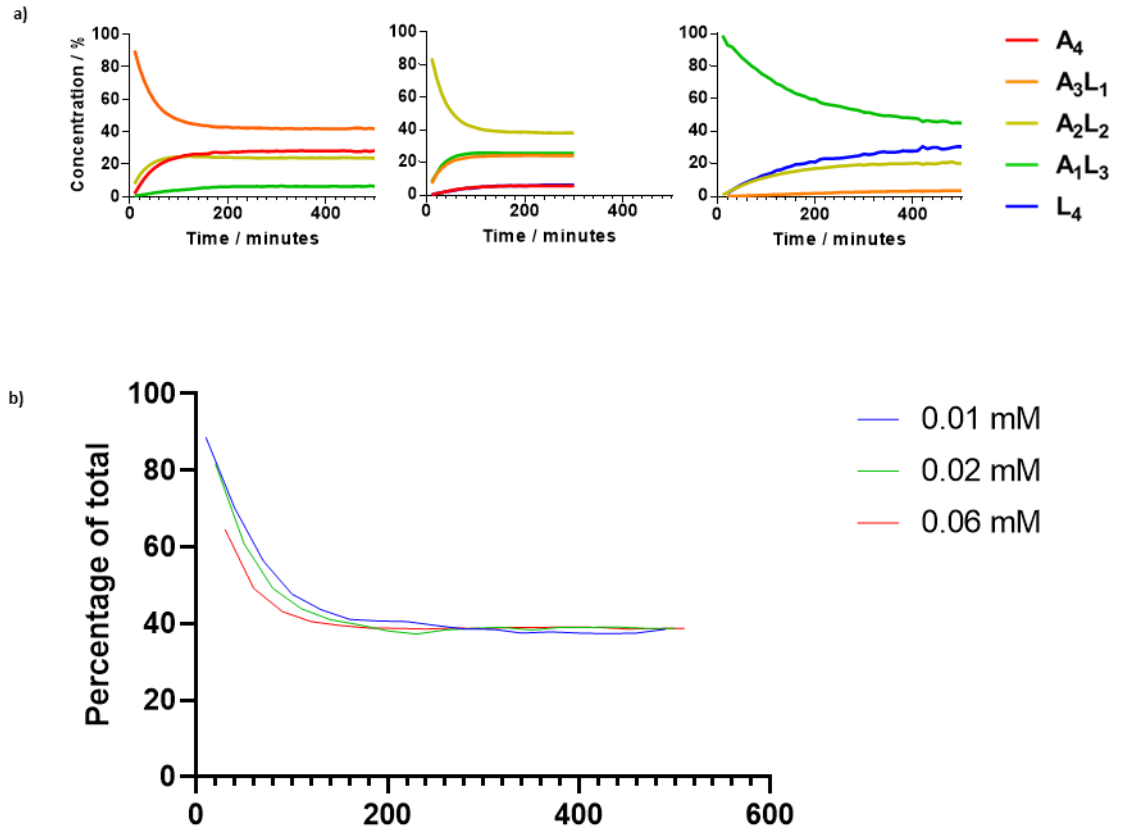

Figure S69. – **(a)** $\mathbf{A_3L_1}$ (left), $\mathbf{A_2L_2}$ (middle) and $\mathbf{A_1L_3}$ were purified by preparative HPLC and the redistribution of the ligands through ligand exchange to binomial distributions was followed over time by HPLC analysis every 10 minutes. **(b)** The time taken for the redistribution of $\mathbf{A_3L_1}$ to a statistical mixture followed by analysis of the signal of $\mathbf{A_3L_1}$ over time at a range of concentrations. Concentrations were calculated using the calibration curves of $\mathbf{A_4}$ and $\mathbf{L_4}$.

Monoimide carboxylate self-sorting experiment

To a 1 mL acetonitrile solution of N-Ala-4-bromophthalimide (40.9 mg, 137 µmol) and N-Leu-4-bromophthalimide (46.7 mg, 137 µmol) was added $Cu(OAc)_2$ (49.8 mg, 274 µmol). The solution was diluted to 0.1 mM and ESI-MS showed formation of the three $[Cu_2L_4]$ heteroleptic complexes and the homoleptic $[Cu_2(N\text{-}Ala\text{-}4\text{-}bromophthalimide)_4]$ and $[Cu_2(N\text{-}Leu\text{-}4\text{-}bromophthalimide)_4]$ complexes (Figure S70).

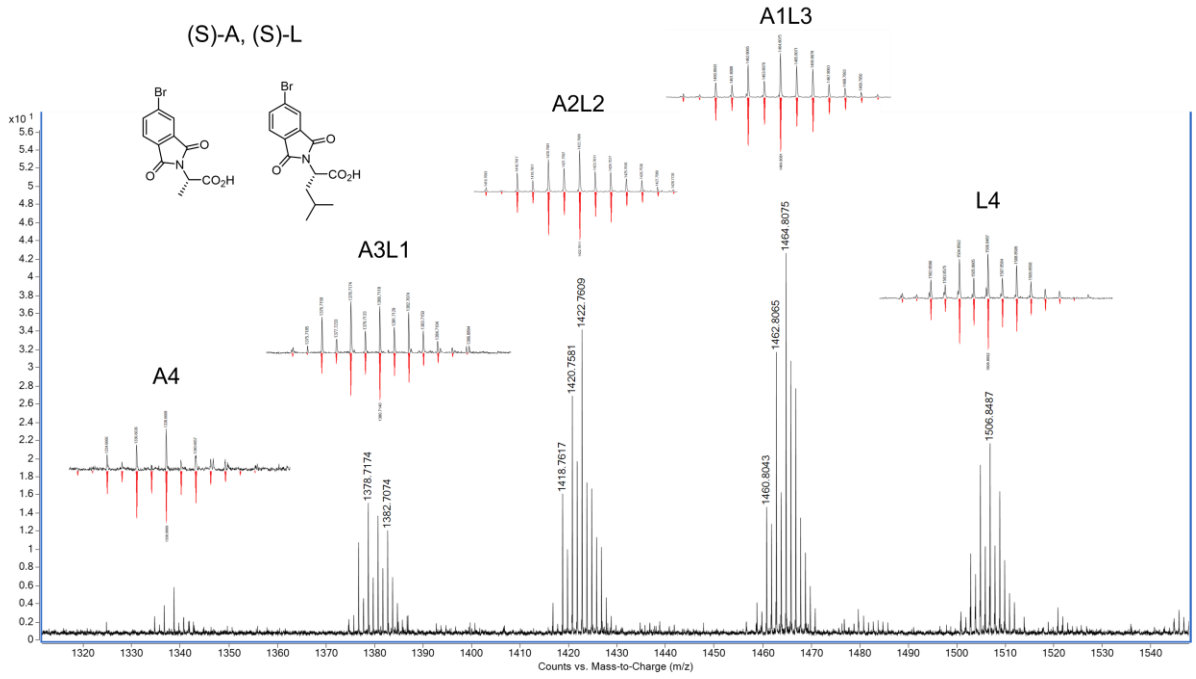

Figure S70. – Reaction between alanine-substituted and leucine-substitued bromophthalimides leads to statistical sorting during the formation of $[Cu_2L_4]$ complexes with formation of all five possible species, confirmed by the observation of signals arising from these complexes in the mass spectrometry analysis.

To a 1 mL acetonitrile solution of N-(*S*)-Ala-4-bromophthalimide (40.9 mg, 137 µmol) and N-(*R*)-Leu-4-bromophthalimide (46.7 mg, 137 µmol) was added $Cu(OAc)_2$ (49.8 mg, 274 µmol). The solution was diluted to 0.1 mM and ESI-MS showed formation of the three $[Cu_2L_4]$ heteroleptic complexes and the homoleptic $[Cu_2$(N-Leu-4-bromophthalimide)$_4]$ complex (Figure S71).

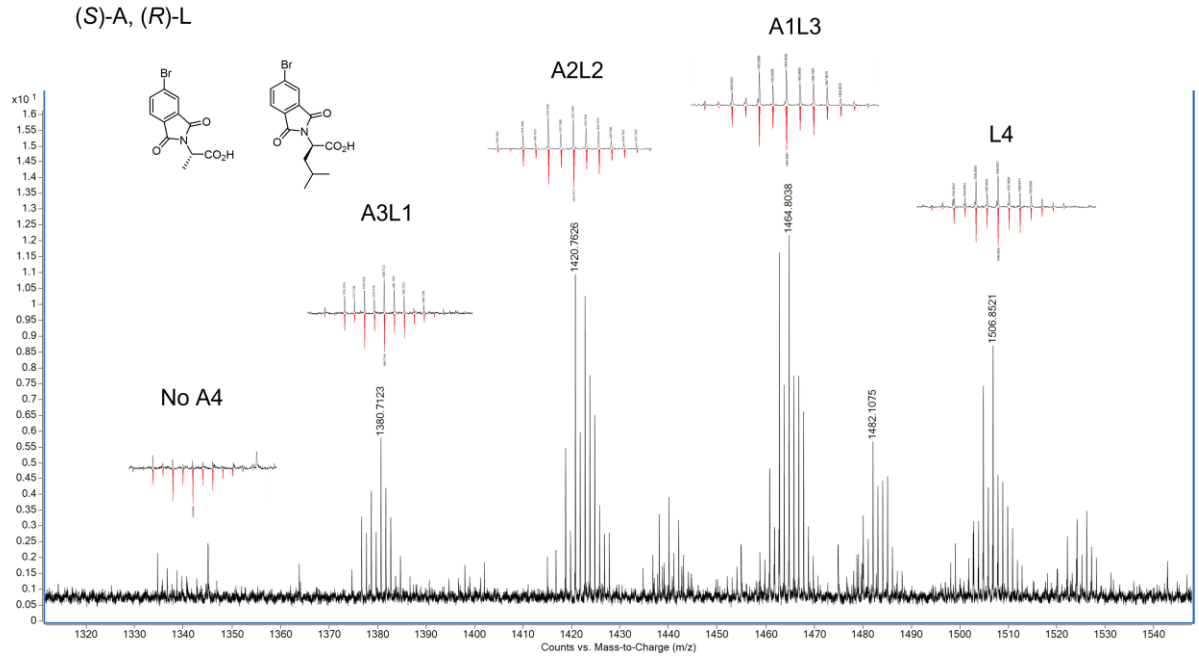

Figure S71. – Reaction between (S)-alanine-substituted and (*R*)-leucine-substitued bromophthalimides leads to statistical sorting during the formation of $[Cu_2L_4]$ complexes with formation of all three possible heteroleptic species as well as one of the homoleptic species, confirmed by the observation of signals arising from these complexes in the mass spectrometry analysis.

To a 1 mL acetonitrile solution of N-Iba-4-bromophthalimide (42.9 mg, 137 µmol) and N-Leu-4-bromophthalimide (46.7 mg, 137 µmol) was added $Cu(OAc)_2$ (49.8 mg, 274 µmol). The solution was diluted to 0.1 mM and ESI-MS showed formation of the three $[Cu_2L_4]$ heteroleptic complexes and the homoleptic $[Cu_2(N\text{-}Leu\text{-}4\text{-}bromophthalimide)_4]$ complex (Figure S72).

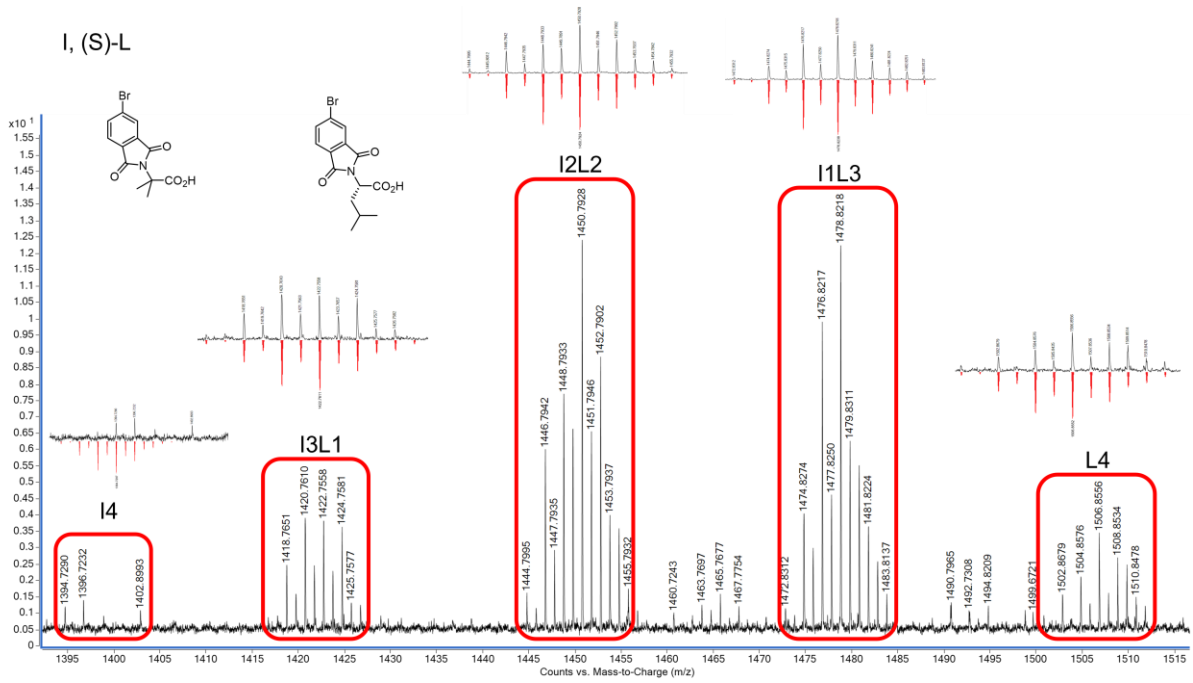

Figure S72. – Reaction between (2-aminoisobutyric acid)-substituted and (*R*)-leucine-substitued bromophthalimides leads to statistical sorting during the formation of $[Cu_2L_4]$ complexes with formation of all three possible heteroleptic species as well as one of the homoleptic species, confirmed by the observation of signals arising from these complexes in the mass spectrometry analysis.

To a 1 mL acetonitrile solution of N-Gly-4-bromophthalimide (39 mg, 137 µmol) and N-Iba-4-bromophthalimide (42.9 mg, 137 µmol) was added $Cu(OAc)_2$ (49.8 mg, 274 µmol). The solution was diluted to 0.1 mM and ESI-MS showed formation of the three $[Cu_2L_4]$ heteroleptic complexes and the homoleptic $[Cu_2(N\text{-Iba-4-bromophthalimide})_4]$ complex (Figure S73).

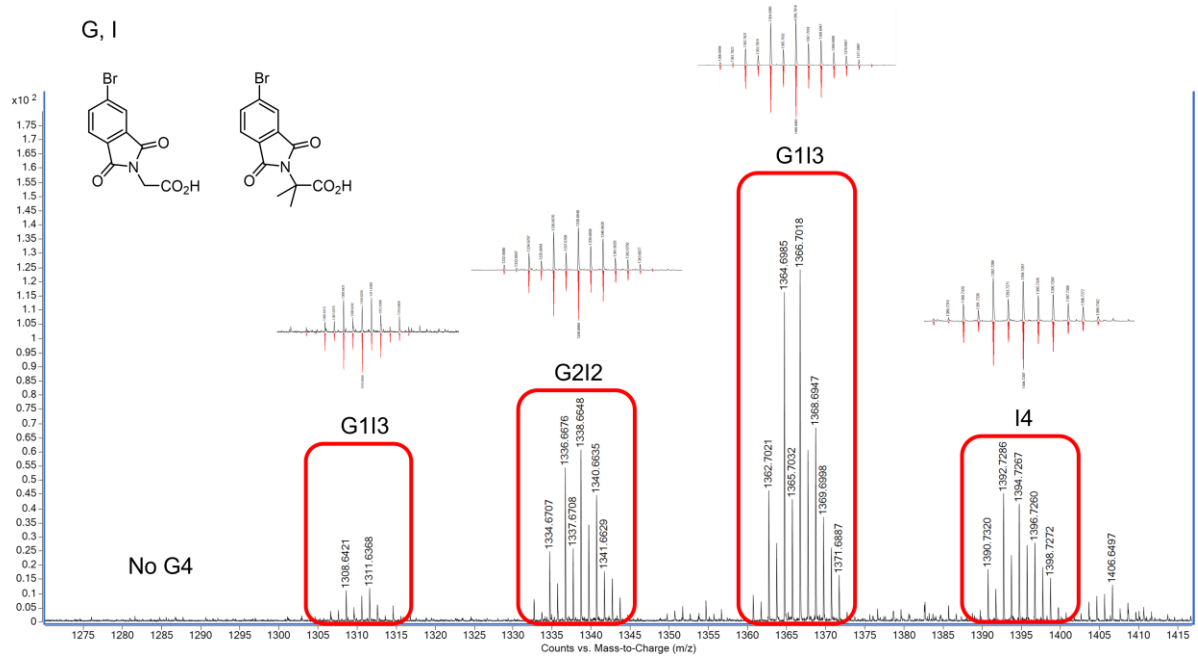

Figure S73. – Reaction between (S)-alanine-substituted and (*R*)-leucine-substitued bromophthalimides leads to statistical sorting during the formation of $[Cu_2L_4]$ complexes with formation of all three possible heteroleptic species as well as one of the homoleptic species, confirmed by the observation of signals arising from these complexes in the mass spectrometry analysis.

Circular dichroism measurements

***L*$_4$** *Concentration Dependant Control Experiment*

Standard solutions were prepared of H_2**L** (87.6 mg, 150 μmol) in N,N-dimethylacetamide (1 mL) and copper(II) acetate (27.3 mg, 150 μmol) in acetonitrile (1 mL). Aliquots of these solutions were mixed in 1:1 ratios and diluted to a total volume of 6 mL with 50:50 acetonitrile:N,N-dimethylacetamide and left for 24 hours at room temperature. A total of 8 solutions were formed with concentrations of H_2**L** in the range 0.01 – 0.8 mM. CD spectra were collected of solutions in which 0.1 mL of each reaction solution was diluted to 5 mL with acetonitrile (final solutions are over the **L**$_4$ concentration range 2.5 μM – 20 μM). The anticipated linear response as a function of concentration was observed, see Figure S74.

G*:*L *Ratio Dependant Experiment*

Standard solutions were prepared of copper(II) acetate (43.4 mg, 240 μmol) in acetonitrile (30 mL), H_2**L** (87.6 mg, 150 μmol) in N,N-dimethylacetamide (1 mL), and H_2**G** (70.8 mg, 150 μmol) in N,N-dimethylacetamide (1 mL). The reaction solutions were prepared by adding a total of 160 μL of the diacid standard solutions (in ratios ranging 8:0 to 0:8) with an additional 2.84 mL of DMA (3 mL total) to the copper(II) acetate standard solution (3 mL). The solutions were left to sit at room temperature for 24 hours. CD spectra were collected of solutions in which 0.1 mL of each reaction solution was diluted to 5 mL with acetonitrile (giving a final combined cage concentration of 20 μM in all cases), Figure S75.

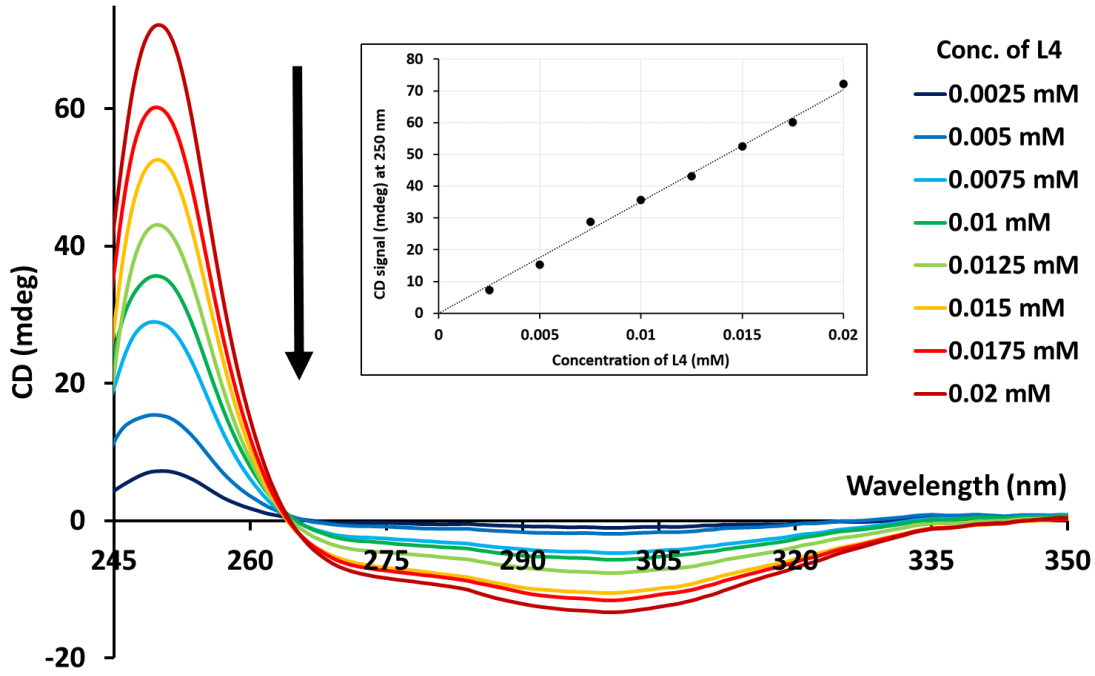

Figure S74. - Circular dichroism (CD) response as a function of **L**$_4$ concentration over the range 2.5 – 20 µM, showing a proportional linear decrease in signal (inset).

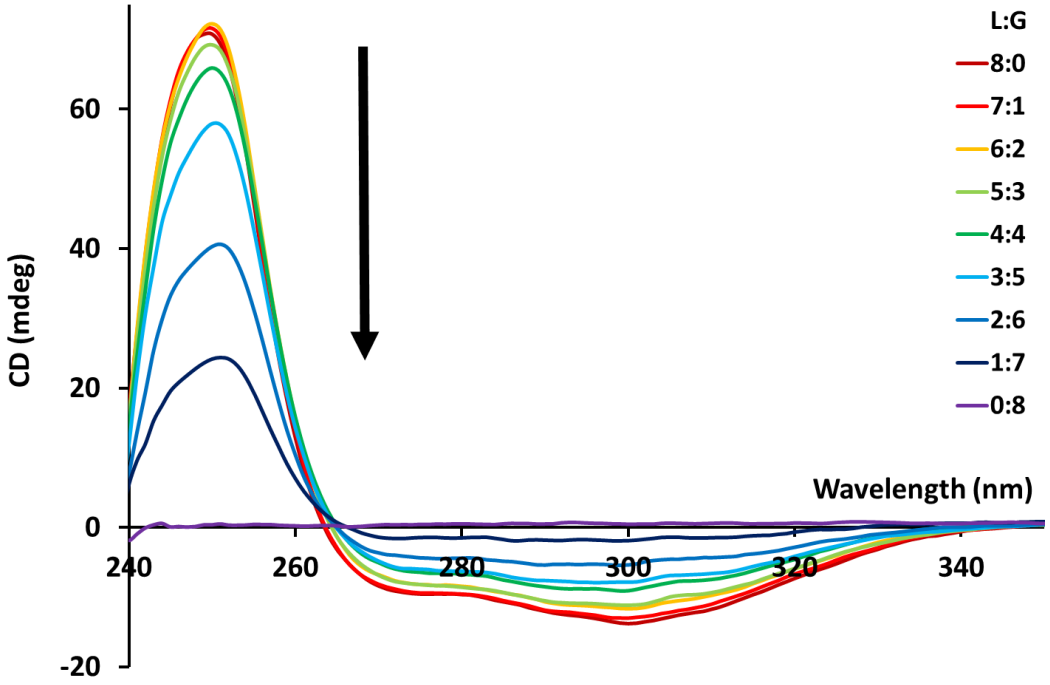

Figure S75. - Circular dichroism (CD) response as a function of different **L**:**G** ratios, showing a non-linear decrease as the proportion of **G** increases and a slight red shift.

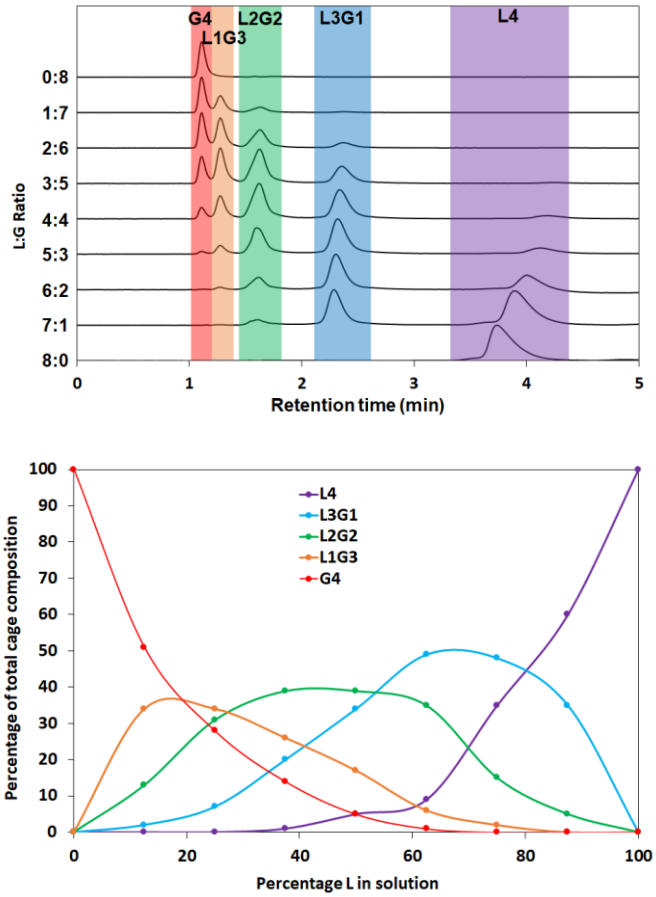

Figure S76. - HPLC traces (top) of mixed **L**:**G** solutions in the presence of $Cu(NO_3)_2$ showing elution of the five cage complexes and speciation plot (bottom) showing the changing cage ratios against increasing **L**. The speciation is slightly skewed towards **L** due to complex $\mathbf{G}_4$ crystallising over the course of the timed experiment, resulting in a shift in the equilibrium towards **L**-containing complexes.

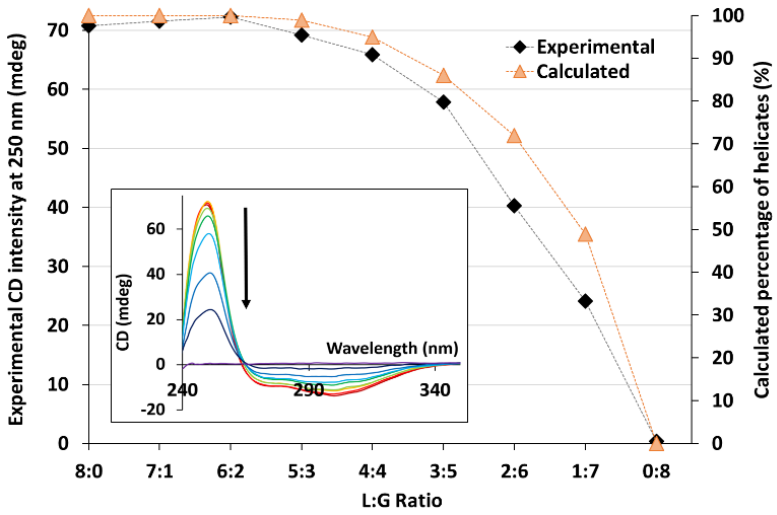

Figure S77. - (Main) Comparison of experimental circular dichroism spectra, plotted as maximum signal value, *vs.* the percentage of helicate present if all cages bar $\mathbf{G}_4$ are helical (calculated from HPLC results); lines are for a visual guide and are not fitted. (Inset) Reduction in CD signal with increasing proportion of **G**.

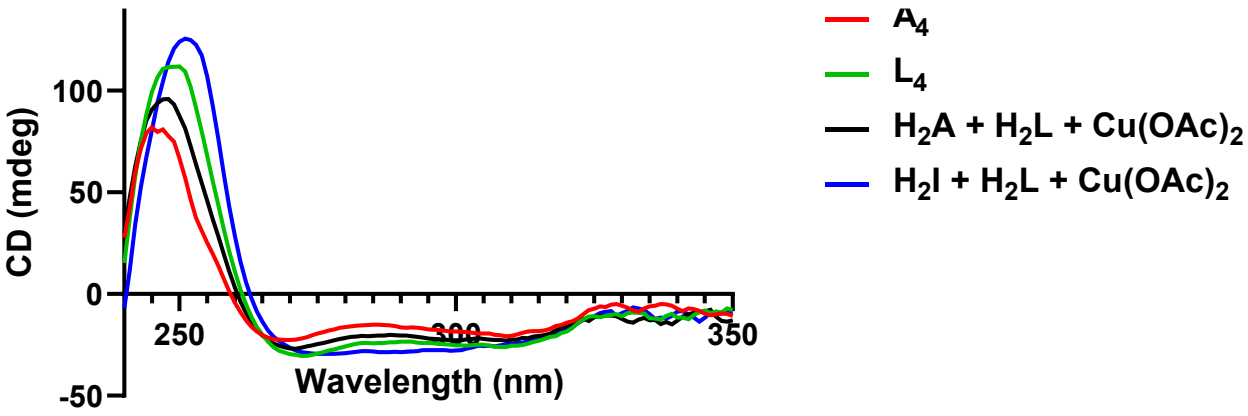

Figure S78. - Circular dichroism of the homoleptic cages $\mathbf{A_4}$ and $\mathbf{L_4}$, and the heteroleptic dynamic systems incorporating H_2**A**:H_2**L**, H_2**A**:H_2**I** and H_2**L**:H_2**I**, measured at 0.4 mM cumulative concentration of all cage species.

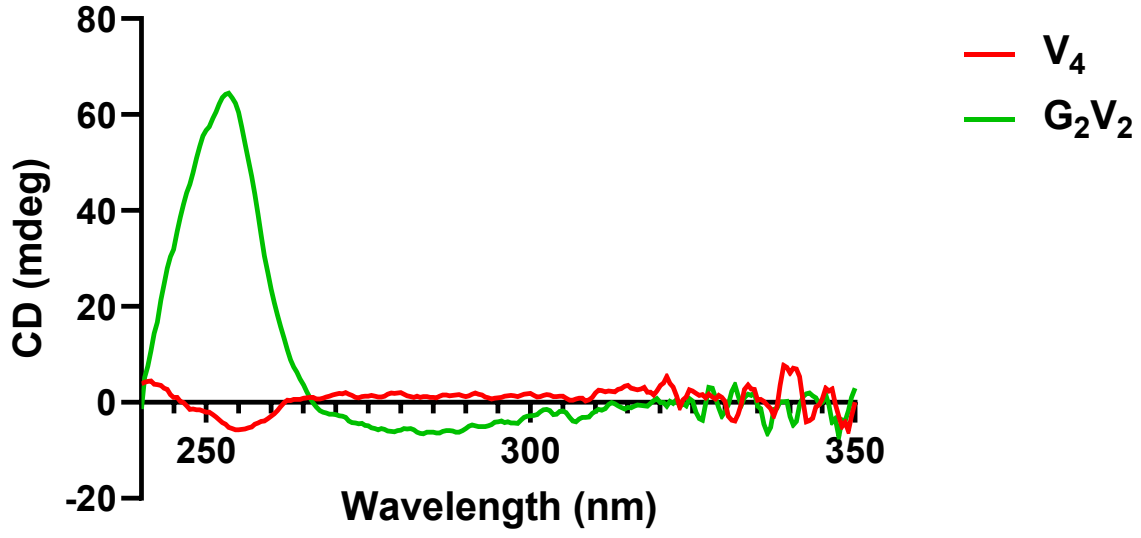

Figure S79. – Circular dichroism spectra of $\mathbf{G_2V_2}$ showing strong cotton effect, indicative of helicate formation. In contrast, the sample containing only ligand H_2**V** with $Cu(OAc)_2$ shows no signal, and therefore that $\mathbf{V_4}$ is forming in only very small concentrations and the bulk of the molecules in solution do not form large chiral structures.

Crystallographic Details

Diffraction data were collected using either a Rigaku SynergyS diffractometer or the MX2 beamline at the Australian Synchrotron, part of ANSTO.[2] The SynergyS operated using a microfocus sealed X-ray tube (Cu-Kα, λ = 1.54184 Å) with sample temperatures maintained at 123 K using an open-flow N_2 cryostream. Data processing was conducted using CrysAlisPro. The MX2 beamline operated at 17.4 keV (λ = 0.7108 Å) with sample temperatures maintained at 100 K using an open-flow N_2 cryostream. Data collections were controlled using the in-house control systems. The diffraction data were indexed and integrated using the XDS software suite.[3] Anomalous dispersion corrections for the nonstandard wavelength were made in the final refinement using Brennan and Cowan data. All datasets were solved using SHELXT and refined against F^2 by full matrix least-squares procedures with SHELXL-2018 within Olex2.[4] Non-hydrogen atoms were refined with anisotropic displacement parameters while hydrogen atoms attached to carbon were included in calculated positions with isotropic displacement parameters 1.2 or 1.5 times their carrier atoms. See Table S1 below.

Data for I_4 is of slightly lower quality than the other two compounds but represents the best that we were able to obtain from repeated efforts. The gross structure is unambiguous.

Table S1. – Crystallography tables for the SC-XRD experiments run on crystalline samples of **A_4**, **G_2I_2** and **I_4**.

Identification code	**A_4**	**G_2I_2**	**I_4**
Empirical formula	$C_{97.67}H_{73}Cu_4N_{11}O_{45.67}S_4$	$C_{125.67}H_{148.5}Cu_4N_{17.17}O_{54.67}S_4$	$C_{106.25}H_{96.5}Cu_4N_{10.75}O_{44}S_4$
Formula weight	2513.76	3156.54	2610.34
Temperature/K	373.15	123.00(10)	123.00(13)
Crystal system	tetragonal	monoclinic	monoclinic
Space group	$P4_32_12$	I2/a	P2/n
a/Å	17.438(3)	32.2388(4)	14.2290(4)
b/Å	17.438(3)	19.0842(2)	24.2010(5)
c/Å	41.986(8)	28.2540(4)	19.7403(5)
α/°	90	90	90
β/°	90	118.549(2)	94.244(3)
γ/°	90	90	90
Volume/Å^3	12767(4)	15269.7(4)	6779.1(3)
Z	4	4	2
ρ_{calc}g/cm^3	1.308	1.373	1.279
μ/mm^{-1}	0.806	1.906	1.965
F(000)	5125.0	6560.0	2682.0
Crystal size/mm^3	0.1 × 0.1 × 0.05	0.2 × 0.2 × 0.1	0.1 x 0.1 x 0.05
Radiation	Synchrotron (λ = 0.710915)	Cu Kα (λ = 1.54184)	Cu Kα (λ = 1.54184)
2Θ range for data collection/°	2.53 to 64.542	7.124 to 154.694	7.222 to 155.378°
Index ranges	$-26 \le h \le 26, -24 \le k \le 24, -60 \le l \le 60$	$-40 \le h \le 38, -24 \le k \le 24, -35 \le l \le 35$	$-17 \le h \le 17, -20 \le k \le 30, -23 \le l \le 24$
Reflections collected	225176	115511	73060
Independent reflections	21123 [R_{int} = 0.0725, R_{sigma} = 0.0350]	16053 [R_{int} = 0.0326, R_{sigma} = 0.0198]	14156 [R_{int} = 0.0870, R_{sigma} = 0.0471]
Data/restraints/parameters	21123/42/791	16053/48/989	14156/36/853
Goodness-of-fit on F^2	0.959	1.023	1.288
Final R indexes [I>=2σ (I)]	R_1 = 0.0967, wR_2 = 0.2479	R_1 = 0.0698, wR_2 = 0.2041	R_1 = 0.1135, wR_2 = 0.3257
Final R indexes [all data]	R_1 = 0.1322, wR_2 = 0.2879	R_1 = 0.0732, wR_2 = 0.2079	R_1 = 0.1401, wR_2 = 0.354
CCDC Deposition Number	2101252	2101259	2101260

Computational Methods

Geometry optimisations where carried out utilising the PBE0 functional and the 6-31G* basis-set.[5] This model chemistry was selected due to its performance on similar systems throughout the literature, including those involving similar di-copper nodes. Optimisations were initiated from the corresponding experimental crystal structure and geometric minima were determined through frequency analysis and noted by the presence of positive curvature over each degree of freedom. The effect of spin-state selection was investigated through the analysis of the G4 structure in the singlet, triplet and quintet states; it was noted that the thermodynamics were almost independent of the spin state, therefore the computationally more reliable quintet state was selected for the modelling of the other cages. Additionally, calculations were carried out in the presence of the SMD solvent model for acetonitrile. All calculations were carried out using Gaussian09 and relevant visualisations were conducted using GaussView5. Relative binding energies were determined through comparison of the energies of a formed neutral cage, calculated at the lowest lying quintet state, with individual calculations of their component ligands and metal ions; energies were then plotted relative to the homoleptic cage with the lower molecular weight R-group on the α-carbon.

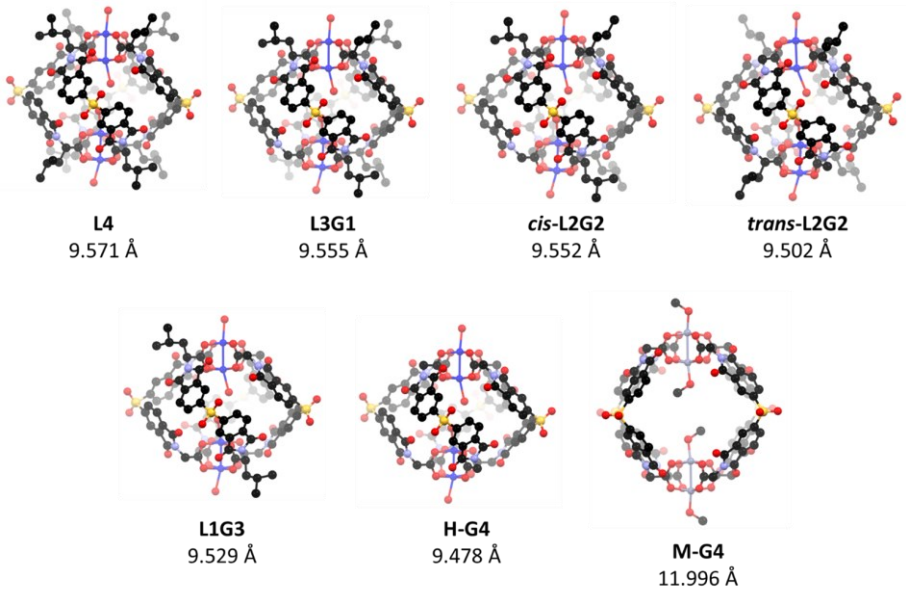

Figure S80. - The minimised structures of the six possible helical cage complexes from ligands H_2**G** and H_2**L** and the non-helical isomer of **G**$_4$, and their helical pitch (measured by distance between paddlewheel midpoints) for each.

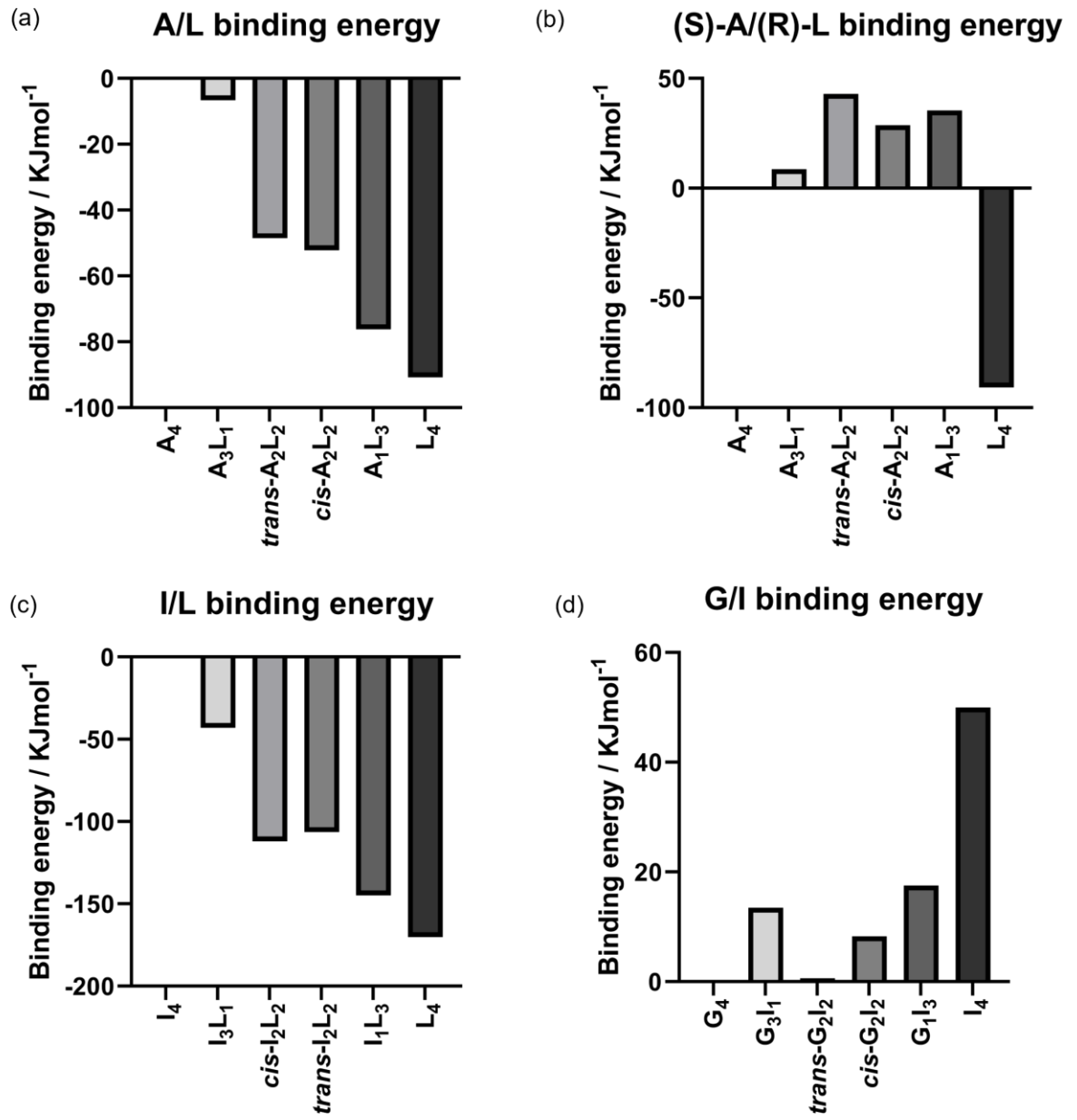

Figure S81. – The binding energies for each of the cage species possible from a 1:1 mixture of: (a) H_2**A** and H_2**L**, relative to the binding energy of $\mathbf{A_4}$. (b) (*S*)-H_2**A** and (*R*)-H_2**L** relative to the value of $\mathbf{A_4}$. (c) H_2**I** and H_2**L**, relative to the binding energy of $\mathbf{I_4}$. (d) H_2**G** and H_2**I**, relative to the binding energy of $\mathbf{G_4}$.

References

1 S. A. Boer and D. R. Turner, *Chem. Commun.*, 2015, **51**, 17375-17378.

2 D. Aragao, J. Aishima, H. Cherukuvada, R. Clarken, M. Clift, N. P. Cowieson, D. J. Ericsson, C. L. Gee, S. Macedo, N. Mudie, S. Panjikar, J. R. Price, A. Riboldi-Tunnicliffe, R. Rostan, R. Williamson and T. T. Caradoc-Davies, *Journal of Synchrotron Radiation*, 2018, **25**, 885-891.

3 W. Kabsch, *Journal of Applied Crystallography*, 1993, **26**, 795-800.

4 (a) G. M. Sheldrick, *Acta Crystallogr., Sect. C*, 2015, **71**, 3-8; (b)G. M. Sheldrick, *Acta Crystallogr., Sect. A*, 2015, **71**, 3-8; (c) O. V. Dolomanov, L. J. Bourhis, R. J. Gildea, J. A. K. Howard and H. Puschmann, *Journal of Applied Crystallography*, 2009, **42**, 339-341.

5 (a) J. P. Perdew, K. Burke and M. Ernzerhof, *Physical Review Letters*, 1996, **77**, 3865-3868; (b) J. P. Perdew, K. Burke and M. Ernzerhof, *Physical Review Letters*, 1997, **78**, 1396-1396; (c) M. J. Frisch, G. W. Trucks, H. B. Schlegel, G. E. Scuseria, M. A. Robb, J. R. Cheeseman, G. Scalmani, V. Barone, G. A. Petersson, H. Nakatsuji, X. Li, M. Caricato, A. Marenich, J. Bloino, B. G. Janesko, R. Gomperts, B. Mennucci, H. P. Hratchian, J. V. Ortiz, A. F. Izmaylov, J. L. Sonnenberg, D. Williams-Young, F. Ding, F. Lipparini, F. Egidi, J. Goings, B. Peng, A. Petrone, T. Henderson, D. Ranasinghe, V. G. Zakrzewski, J. Gao, N. Rega, G. Zheng, W. Liang, M. Hada, M. Ehara, K. Toyota, R. Fukuda, J. Hasegawa, M. Ishida, T. Nakajima, Y. Honda, O. Kitao, H. Nakai, T. Vreven, K. Throssell, J. J. A. Montgomery, J. E. Peralta, F. Ogliaro, M. Bearpark, J. J. Heyd, E. Brothers, K. N. Kudin, V. N. Staroverov, T. Keith, R. Kobayashi, J. Normand, K. Raghavachari, A. Rendell, J. C. Burant, S. S. Iyengar, J. Tomasi, M. Cossi, J. M. Millam, M. Klene, C. Adamo, R. Cammi, J. W. Ochterski, R. L. Martin, K. Morokuma, O. Farkas, J. B. Foresman and D. J. Fox, *Gaussian 09, Revision A.02,*, Gaussian, Inc., Wallingford CT, 2016; (d) C. Adamo and V. Barone, *The Journal of Chemical Physics*, 1999, **110**, 6158-6170; (e) R. Ditchfield, W. J. Hehre and J. A. Pople, *The Journal of Chemical Physics*, 1971, **54**, 724-728; (f) P. C. Hariharan and J. A. Pople, *Theoretica chimica acta*, 1973, **28**, 213-222; (g) W. J. Hehre, R. Ditchfield and J. A. Pople, *The Journal of Chemical Physics*, 1972, **56**, 2257-2261; (h) V. A. Rassolov, J. A. Pople, M. A. Ratner and T. L. Windus, *The Journal of Chemical Physics*, 1998, **109**, 1223-1229; (i) A. V. Marenich, C. J. Cramer and D. G. Truhlar, *The Journal of Physical Chemistry B*, 2009, **113**, 6378-6396; (j) R. Dennington, T. A. Keith and J. M. Millam, *GaussView5*, SemichemInc.: Shawnee Mission, KS, 2009.